TÜBİTAK

Turkish Journal of Earth Sciences

http://journals.tubitak.gov.tr/earth/

Research Article

Turkish J Earth Sci
(2015) 24: 399-460
© TÜBİTAK
doi:10.3906/yer-1504-20

Present state of knowledge and new geochemical constraints on the central part of the Mexican Volcanic Belt and comparison with the Central American Volcanic Arc in terms of near and far trench magmas

Surendra P. VERMA*
Renewable Energy Institute, National Autonomous University of Mexico, Temixco, Morelos, Mexico

Received: 14.04.2015 • **Accepted/Published Online:** 09.07.2015 • **Printed:** 04.09.2015

Abstract: A brief critical review is presented of the geological, geophysical, geochemical, and plate tectonic evidence for the origin and evolution of the central part of the Mexican Volcanic Belt (C-MVB). Databases were constructed for the C-MVB from new and published data as well as for the Central American Volcanic Arc (CAVA), other continental and island arcs, continental rifts or extensional areas, and collision zones. Conventional procedures as well as statistical techniques of multidimensional tectonic discrimination diagrams and significance tests were used to interpret the data. A subdivision of the databases for the C-MVB and CAVA into near the trench or front-arc and far from the trench or back-arc magmas helped to demonstrate the lack of slab input for the C-MVB and the presence of a classic arc-trench system for the CAVA. The use of software IgRoCS, DODESSYS, UDASYS, TecD, and TecDIA provided the following conclusions: 1) basic magmas in the C-MVB that originated in the mantle without the involvement of the subducted slab represent a continental rift setting; 2) C-MVB acid and intermediate magmas that originated, respectively, from the crust and mixed mantle-crustal sources do not show a clear influence of the present subducted slab and represent the tectonic setting of the older crustal and mixed mantle-crustal source rocks; and 3) all rocks in the CAVA were derived from the involvement of the subducted slab and represent a classical continental arc system related to the subduction of the Cocos plate beneath the Caribbean plate, whereas CAVA back-arc rocks originated mainly in the mantle, probably with much less involvement of the subducted slab. Reinterpretation of the Sr, Nd, Pb, and Hf isotopic data supports these inferences. I propose a new tectono-petrogenetic model based on the continuation of the extensional tectonics related to the triple rift system in the western part of the MVB.

Key words: Southern Mexico, Central America, log-ratio transformations, significance tests, extension or rift, subduction

1. Introduction

The Mexican Volcanic Belt (MVB), also known as the Trans-Mexican Volcanic Belt, a major geological province in central Mexico, extends approximately east-west from Veracruz (V) to Puerto Vallarta (Pu; Figure 1). This Miocene to Recent province, more than 1000 km long and about 200–500 km wide, houses more than 8000 volcanoes (some being active) and two prominent geothermal fields already producing electricity. The origin of the MVB has been highly debated (e.g., Ferrari and Rosas-Elguera, 1999; Márquez et al., 1999a, 1999b; Sheth et al., 2000; Blatter et al., 2001; Ferrari et al., 2001, 2002; Torres-Alvarado et al., 2002; Verma, 2002; Torres-Alvarado and Verma, 2003; Gómez-Tuena et al., 2007a), which makes its study important from various perspectives.

The central part of the MVB (C-MVB) has been shown to be a key area for understanding the complex tectonomagmatic processes of this volcanic province (e.g., Márquez et al., 1999c; Verma, 1999, 2000a; Wallace and Carmichael, 1999; Velasco-Tapia and Verma, 2001a, 2001b, 2013). The volcanism in the C-MVB is limited to the Neogene (mainly Pliocene to Holocene, with some older outcrops of Miocene age), including historic eruptions and the presently active volcano Popocatépetl. In this part of the belt the origin of magmas has also been highly debated (e.g., Márquez et al., 1999c, 2001; Wallace and Carmichael, 1999; Velasco-Tapia and Verma, 2001b, 2013; Verma, 2002, 2004, 2009; Martínez-Serrano et al., 2004; Siebe et al., 2004; Schaaf et al., 2005; Gómez-Tuena et al., 2007b; Torres-Alvarado et al., 2011; Cai et al., 2014). In summary,

* Correspondence: spv@ier.unam.mx

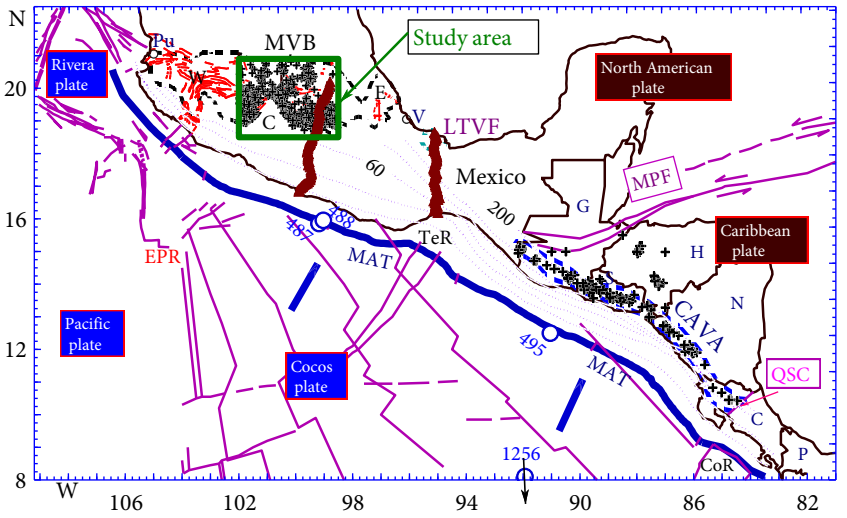

Figure 1. Location of the Mexican Volcanic Belt (MVB) and Central American Volcanic Arc (CAVA) along with the three oceanic plates (Pacific, Cocos, and Rivera) and two continental plates (North American and Caribbean; figure was modified after Verma, 2002, 2015a); the abbreviation are: Pu–Puerto Vallarta; V–Veracruz; W–western; C–central; E–eastern; G–Guatemala; S–El Salvador; H–Honduras; N–Nicaragua; C–Costa Rica; and P–Panama; schematic locations of samples are shown by small crosses; the numbers 487, 488, 495, and 1256 are Deep Sea Drilling Project Sites in the Cocos plate; the numbers 60 and 200 represent the approximate depth in km of the subducted slab; QSC–Quesada Sharp Contortion in Costa Rica defines the southern limit of the CAVA; the two transects for the dense seismic network in southern Mexico used by the UNAM-Cal Tech collaborative project (Pérez-Campos et al., 2008; Pacheco and Singh, 2010; Kim et al., 2011) are also shown schematically by thick irregular curves.

however, no clear distinction among the different magma types from the C-MVB can be made in space and time.

Recently, the geochemical data for the eastern part of the MVB (E-MVB) were interpreted from conventional multielement normalized and new multidimensional discrimination diagrams and discordancy and significance tests to decipher the origin, evolution, and tectonic setting (Verma, 2015a). A likely continental rift setting was inferred for the E-MVB. Further, as documented by Verma (2015a), to the south of Mexico in most of Central America, the Central American Volcanic Arc (CAVA) from Guatemala to northwestern Costa Rica, located in the Caribbean plate, presumably originated from the subduction of the same Cocos plate beneath the Caribbean plate (Figure 1). In fact, the CAVA, a continental arc subparallel to the Middle America Trench (MAT; see the orientations of CAVA and MAT in Figure 1), has been considered a classic arc-trench system (e.g., Carr et al., 1982, 2007; Carr and Rose, 1986; Walker et al., 2009; Heydolph et al., 2012).

The deepest trace of the slab is only about 60 km at about 250 km horizontal distance from the MAT (Figures 1 and 2; Pacheco and Singh, 2010) and still away from the volcanic front of the C-MVB. There are practically no deep earthquakes beneath the C-MVB (Figure 1; Pacheco and Singh, 2010). On the other hand, in Central America this depth contour of 60 km lies totally in the Pacific Ocean, and most of the front-arc volcanoes in Central America are located above the area where the subducted slab reaches depths of 100 to 200 km (Figure 1).

A critical review of the present state of knowledge and controversies related to the C-MVB could well be a worthwhile exercise at this stage. An unbiased comparison of the C-MVB and CAVA could then throw further light on the origin and evolution of this complex geological province (MVB), for which recently developed highly efficient and appropriate computational tools, such as DODESSYS (Verma and Díaz-González, 2012) and UDASYS (Díaz-González and Cruz-Huicochea, 2013; Verma et al., 2013a) for applying discordancy and significance tests, are available (Barnett and Lewis, 1994; Jensen et al., 1997; Miller and Miller, 2005; Verma, 2005). The application of discordancy tests prior to the significance tests is recommended in order to comply with the basic assumption of normally distributed variables (Jensen et al., 1997; Miller and Miller, 2005; Verma, 2005). The statistical inference from these computer programs is made through the new highly precise and accurate critical values obtained from Monte Carlo simulations (Verma

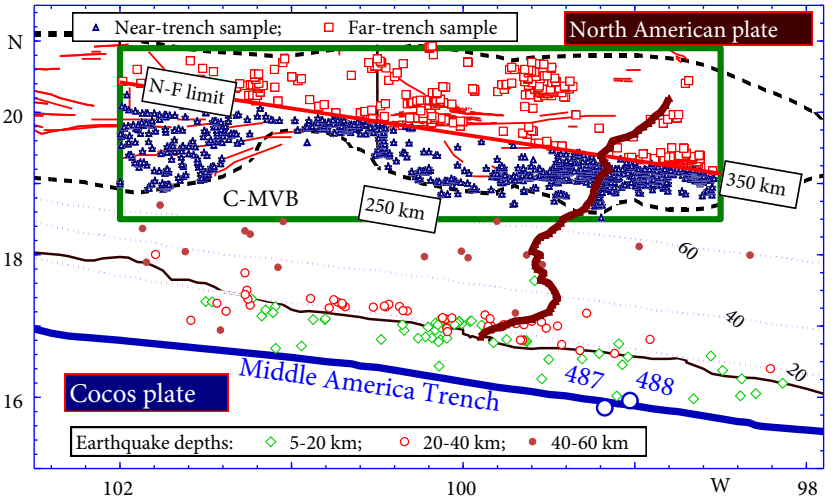

Figure 2. Location of samples in the central part of the Mexican Volcanic Belt (C-MVB) in terms of the near the trench (Near-trench) and far from the trench (Far-trench) subdivision used for testing different hypotheses; the numbers 487 and 488 are the Deep Sea Drilling Project Sites in the Cocos plate; the approximate depths of the earthquakes (5–20, 20–40, and 40–60 km) from Pacheco and Singh (2010) are also shown resulting from the subduction of the Cocos plate beneath the North American plate; note that practically no deep earthquakes are registered beneath the C-MVB because the depth contours of only 20–60 km can be traced (see dotted curves marked by 20, 40, and 60); 250 km and 350 km are the horizontal distances from the MAT; one transect for the dense seismic network in southern Mexico used by the UNAM-Cal Tech collaborative project (Pérez-Campos et al., 2008; Pacheco and Singh, 2010) is also shown schematically by a thick irregular curve.

and Quiroz-Ruiz, 2008, 2011; Verma et al., 2008; Cruz-Huicochea and Verma, 2013; Verma and Cruz-Huicochea, 2013).

Recently (2006–2013), natural logarithm-ratios of three sets of subcompositions of igneous rocks from different tectonic settings (arc, rift, ocean island, and mid-ocean ridge for basic rocks; island arc, continental arc, within-plate, and collision for intermediate and acid rocks) have been used in conjunction with linear discriminant analysis (LDA). Thus, 50 new multidimensional tectonic discrimination diagrams are available for all kinds of magmas (Verma et al., 2006, 2012, 2013b; Agrawal et al., 2008; Verma and Agrawal, 2011; Verma SP and Verma SK, 2013). Although the traditional additive log-ratio (alr) transformation of Aitchison (1986), instead of the more recent and mathematically more appropriate isometric log-ratio (ilr) transformation of Egozcue et al. (2003), was used, LDA renders the discriminant functions DF1-DF2 practically the same for both alr and ilr (Verma, 2015b).

These 50 diagrams were grouped into three sets of five diagrams each for basic and ultrabasic rocks (Verma et al., 2006; Agrawal et al., 2008; Verma and Agrawal, 2011), three sets for intermediate rocks (Verma SP and Verma SK, 2013), and four sets for acid rocks (Verma et al., 2012, 2013b). The conventional approach of using compositional variables in bivariate or ternary diagrams has already been shown to perform less well (Verma, 2010, 2012a, 2015b; Verma et al., 2012; Verma and Armstrong-Altrin, 2013). To facilitate the application of the complex multidimensional equations, two computer programs are now available (TecD by Verma and Rivera-Gómez, 2013a; TecDIA by Verma SP et al., 2015a).

My aim is as follows: 1) to review all pertinent geological, geophysical, geochemical, and plate tectonic information from the C-MVB; 2) to evaluate geochemical and isotopic data from both the C-MVB and CAVA; 3) to illustrate the use of the new geochemical tools of multidimensional tectonomagmatic diagrams, log-ratio transformed variables, and discordancy and significance tests and thus provide further constraints on the origin and tectonic setting of the C-MVB and compare this subprovince with the CAVA; and 4) for evaluating the possible contribution from the subducted slab, to statistically compare the compositions of near the trench and far from the trench C-MVB magmas, with emphasis on critical combinations of slab-sensitive components (Carr et al., 1990, 2007; Tatsumi et al., 1992; Walker et al., 2001; Verma, 2002, 2006). For the latter comparison,

the same procedure was also adopted for the subdivision of the CAVA rocks into main volcanic arc (volcanic front or front-arc) and behind the volcanic front or back-arc rocks. This work should thus reinforce new guidelines in geological and geochemical research.

2. Present state of knowledge of the Mexican Volcanic Belt (MVB)

2.1. Geological evidence

There is a well-defined fore-arc basin in Central America corresponding to the CAVA, but no such basin exists in the Pacific of southern Mexico (Figure 1; also see maps of Mexico and Central America, or Google Earth). Thus, the MAT shows a break near the Mexico-Guatemala border (von Huene, 1989); to the north of the Tehuantepec ridge (TeR in Figure 1) the continental shelf is narrow and the continental margin is a steep continental slope, whereas, to the south of this ridge, the continental shelf is underlain by a wide fore-arc basin presenting a classic arc-trench relationship between the CAVA and MAT. Other important observations are that the CAVA is subparallel to the MAT, the MVB makes an angle of about 15°–20° with it (Figure 1; Molnar and Sykes, 1969), and the CAVA has a well-defined width of the front-arc volcanoes whereas the MVB is diffuse with a varying width from west to east (Figures 1–3).

The C-MVB is characterized by extensive fracture and fault systems. In fact, in the western part of the MVB a well-defined triple junction with three intersecting rifts has been proposed (Tepic-Zacoalco rift, Colima rift, and Chapala rift; e.g., Luhr et al., 1985; Allan, 1986; Garduño-Monroy et al., 1993; Frey et al., 2007), which is widely accepted by all researchers. In the remaining parts of the MVB (the C-MVB and the eastern part of the MVB–E-MVB; Figure 1) also, such extensional features have been documented in numerous studies (Negendank et al., 1985; Johnson and Harrison, 1989, 1990; Ferrari et al., 1990; Suter et al., 1992, 1995a, 1995b, 2001; Mooser et al., 1996; Alaniz-Álvarez et al., 1998; García-Palomo et al., 2000, 2002a, 2002b; Anguita et al., 2001; Márquez et al., 2001; Wassmer et al., 2004; Norini et al., 2006; Campos-Enríquez et al., 2013, 2014). Suter et al. (2001) called these extensional features intra-arc extension, assuming that the MVB is an arc, which has been questioned, for example, by Verma (2002, 2004, 2009, 2015a). To call these features of intra-arc, it is an implicit assumption that the MVB is an arc, which is questionable (e.g., Verma, 2015a and references therein; see also the geochemical constraints presented in this work).

Further, dominantly east-west extension in the C-MVB has also been inferred from the orientation and distribution of more than 200 monogenetic volcanoes in

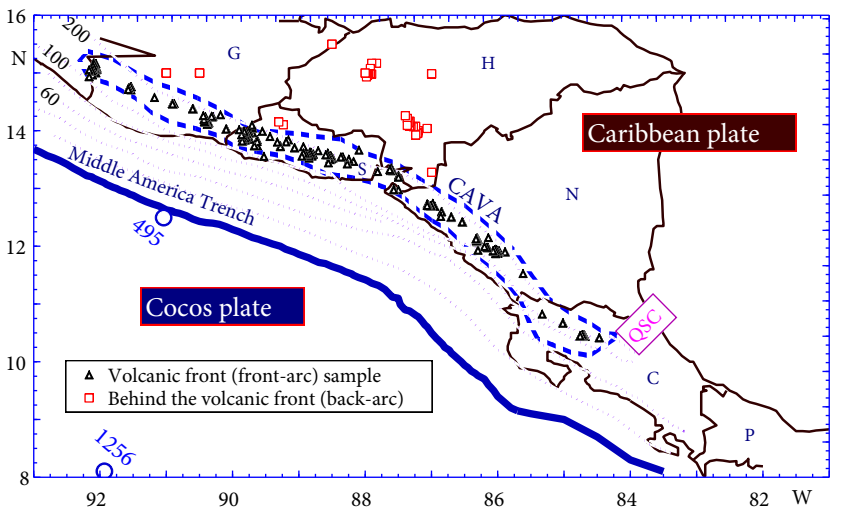

Figure 3. Location of samples in the Central American Volcanic Arc (CAVA) as a result of the subduction of the Cocos plate beneath the Caribbean plate in terms of the volcanic front (main-arc or front-arc) and behind the volcanic front (back-arc) subdivision used for testing and characterizing the subduction process; the abbreviation are: G–Guatemala; S–El Salvador; H–Honduras; N–Nicaragua; C–Costa Rica; and P–Panama; the numbers 495 and 1256 are the Deep Sea Drilling Project Sites in the Cocos plate; the numbers 60, 100, and 200 represent the approximate depth in km of the subducted slab; most of the volcanoes in Central America lie where the subducted slab reaches depths of 100 to 200 km; QSC–Quesada Sharp Contortion in Costa Rica defines the southern limit of the CAVA.

the Sierra de Chichinautzin area (Márquez et al., 1999c). In the C-MVB, in fact, seven different graben systems (Ajacuba, Pachuca, Zempoala, Tlalli-Santa Catarina, Chichinautzin-Izta-Malinche, Ciudad de México, and Acambay) have actually been mapped and documented (Mooser et al., 1996; Velasco-Tapia and Verma, 2001a); most of these grabens run approximately east-west, being subparallel to the MVB, and their presence is consistent with dominantly north-south extension.

Extensional features and fault structures are not limited to the MVB but have been mapped throughout the area between the C-MVB and the Mexican Pacific coast (e.g., Alaniz-Álvarez et al., 2007; Morán-Zenteno et al., 2007). Such extensional characteristics have also been long documented from seismic evidence (e.g., Jiménez and Ponce, 1978; Singh and Pardo, 1993; Pardo and Suárez, 1995; Pacheco and Singh, 2010; also Section 2.2). These observations provide important geological constraints against a simple arc-trench relationship for the MVB-MAT system.

2.2. Geophysical evidence

2.2.1. Seismic evidence

From earthquake data, the reconstruction of the trace of the subducted slab in Central America has been a typical textbook type example for the subduction tectonics (Figure 1; Burbach et al., 1984). The slab can be traced to more than 200 km in depth, and the depth contours are subparallel to the trench, as is the case of the main arc (CAVA). The CAVA lies at about 100 to 200 km depth above the slab (Figure 1).

The southern Mexico situation is anomalous because only the shallow part of the subducted slab up to a maximum of about 60 km depth can be interpreted from seismicity and that too only in front of the MVB (not beneath it); these shallow depth contours (up to 60 km) lie away from its volcanic front toward the trench (Figure 2). Surprisingly, the deeper contours of 80 to 100 km (if any, in southern Mexico) corresponding to the subduction of the Cocos plate (Figure 1) suddenly terminate between the volcanic front of the E-MVB and the Los Tuxtlas volcanic field (LTVF). The inference of the depth contours from the seismic data close to the LTVF (Figure 1) has been criticized; from geochemical evidence, the LTVF is shown to have a solely extension-related origin (Verma, 2006). No deep earthquakes (>60 km depth) have ever been recorded beneath the C-MVB (Figure 2), nor beneath the E-MVB (Figure 1). Although the horizontal distance of the study area of the C-MVB is between about 250 and 500 km, the subducted slab can only be traced seismically to about 60 km in depth (or even less) at about 230 km in horizontal distance from the MAT and no deeper (Figure 2; Pacheco and Singh, 2010).

Under a joint UNAM-Caltech (Universidad Nacional Autónoma de México, Mexico and California Institute of Technology, USA) multimillion dollar seismic study of southern Mexico, a dense seismic network was established (Figures 1 and 2), which complemented the existing seismic stations. The results were published in several papers (Pérez-Campos et al., 2008; Pacheco and Singh, 2010; Kim et al., 2011). Even these most recent seismic studies of the C-MVB do not show any conclusive evidence concerning the location of the subducted slab beneath this belt. Pérez-Campos et al. (2008) suggested that the subducted slab becomes "horizontal" (not "subhorizontal"), gets "attached" to the lower part of the continental crust, and then "continues" several tens of kilometers of horizontal distance without any seismic evidence (see lack of earthquakes in Pacheco and Singh (2010) because Pérez-Campos et al. (2008) did not present this information explicitly), and finally speculated it to suddenly "steeply" dip into the mantle, again without any seismic evidence. Pacheco and Singh (2010), on the other hand, continued to imagine the plate as subhorizontal, also without any seismicity. It is noteworthy that Pérez-Campos et al. (2008) made such speculations without any seismic evidence; no deep earthquakes have ever been recorded, neither at the volcanic front of the C-MVB nor beneath this belt (Figure 2; Pacheco and Singh, 2010). Pérez-Campos et al. (2008) were probably inspired by an earlier work (Pardo and Suárez, 1995) that has already been criticized by Verma (2000b, 2001a, 2009).

Because it would be impossible to generate magmas from the interaction of such a shallow slab (about 40–60 km deep), Pérez-Campos et al. (2008), unlike Pacheco and Singh (2010), proposed a steep turn in slab geometry. Their interpretation of the low-velocity zone and tomography with a few percent contrasts in these physical parameters is also questionable, because the model uncertainties were never stated by Pérez-Campos et al. (2008). After all, the seismic data should have much more than a few percent uncertainties on which this interpretation is based (see in this section my error estimates from the seismic data presented by Pacheco and Singh, 2010).

I suggest that some of the pending questions from Pérez-Campos et al. (2008) are as follows: 1) "What makes the slab continue to be subhorizontal for several tens of kilometers without generating any seismicity when it does generate shallow-level seismicity closer to the Middle America Trench?"; 2) "What causes the slab to make such a steep turn of 90°?" or "What would be the physical mechanism for such a drastic change in the subduction angle at such a shallow depth of only 40 km?"; 3) "Can dehydration of an oceanic crust take place at such shallow depths of 40–60 km?"; 4) "What is the physical evidence for the model of Pérez-Campos et al. (2008) to be valid?"; and 5) "From local shallow seismic evidence (mostly <60

km deep), how can much deeper mantle characteristics (60–700 km deep) be inferred?" These authors, of course, did not provide any answers to these questions.

The slab must become surprisingly denser to make such a right turn of about 90° as envisioned by Pérez-Campos et al. (2008) at only about 40–60 km in depth. It has been suggested to take place at much greater depths of 60–120 km (Bjørnerud and Austrheim, 2004 and references therein). Similarly, the higher-density eclogite formation from lower-density basalt and gabbro cannot be achieved at such shallow depths of 40 to 60 km (Bjørnerud and Austrheim, 2004).

Pérez-Campos et al. (2008) interpreted the presence of a low-velocity zone, which is supposed to prove the presence of subduction fluids beneath the C-MVB. This is certainly not true in the light of the interpretation of the geochemical data presented in this paper (Section 6.3) because if these subduction fluids were being contributed to the C-MVB, the near-trench magmas should show them more clearly as compared to the magmas far from the trench. In fact, the low-velocity zone can be readily and more appropriately explained in the rifting or extensional scenario of the MVB (Márquez et al., 1999c, 2001; Sheth et al., 2000; Verma, 2002, 2015a). The continental rift setting of the C-MVB would be consistent with all the seismic evidence available to date (e.g., Pérez-Campos et al., 2008; Pacheco and Singh, 2010) and with the statistical interpretation of the geochemical data documented in the present paper (Sections 5 and 6).

A histogram of centroid depths of all earthquakes (128 events) processed by Pacheco and Singh (2010) is shown in Figure 4a; importantly, no earthquake showed greater than 60 km depth. Very shallow earthquakes are commonly observed beneath the study area of the C-MVB, e.g., the 1995 earthquake of Milpa Alta at only about 12 km depth (UNAM and CENAPRED Seismology Group, 1995). These shallow earthquakes, in fact, constitute excellent evidence for the ongoing extensional or rifting processes within the MVB. Almost all earthquakes deeper than about 40 km related to the Mexican subduction zone (subduction of the Cocos plate beneath the North American plate) are of extensional type rather than compression, and the subduction is subhorizontal with an angle of only about 15° or even less (Suarez and Singh, 1986; Singh and Pardo, 1993; Pardo and Suárez, 1995; Ego and Ansan, 2002; Pérez-Campos et al., 2008; Pacheco and Singh, 2010). Transtensive deformation in the C-MVB has been attributed to the oblique convergence and slip partitioning at the MAT (Ego and Ansan, 2002).

To reconcile the anomalous situation of the lack of deep earthquakes beneath the MVB known to the geoscientific community for several decades and to continue to conform to the conventional subduction-related models, Pardo and Suárez (1995) used the deep earthquakes, probably corresponding to the Rivera plate, in Jalisco State of the western part of the MVB (Singh et al., 1985; Pardo and Suárez, 1993). They imagined the existence of the Cocos

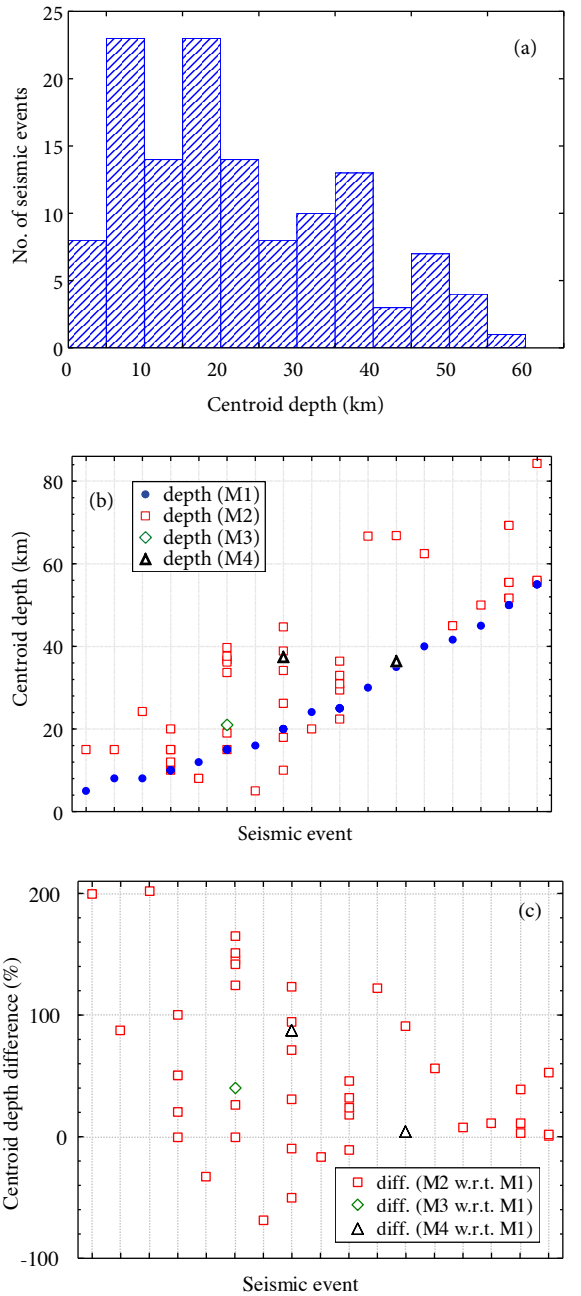

Figure 4. Centroid depths of earthquake from the dense seismic network in southern Mexico (Pacheco and Singh, 2010) and their uncertainties. **(a)** Histogram of centroid depths (km) processed by Pacheco and Singh (2010); **(b)** comparison of centroid depths for the same earthquakes obtained from different methods (M1 to M4; see text for the explanation of methods); and **(c)** percent differences of centroid depths representing method uncertainties (M2 to M4 with respect to M1).

subducted slab somewhat deeper beneath the central and eastern parts of the MVB (note that they projected these inferred depth contours as dashed curves in their paper). It is not clear why, for the proposal of depth contours in this seismic study (Pardo and Suárez, 1995), the two plates (Rivera and Cocos) were considered as though they were a single plate.

After all, the existence of the small Rivera plate has been established as independent of the Cocos plate (DeMets and Stein, 1990; DeMets and Wilson, 1997). On the other hand, it is also not clear how the subducted Rivera plate passes through the triple rift system (Figure 1; see, e.g., Luhr et al., 1985) to generate such deep earthquakes. The Rivera plate seismicity was, however, interpreted by Yang et al. (2009) to conclude that the subducted Rivera plate lies far away from the volcanic front of the western MVB towards the trench, which is again an unusual conclusion if the volcanism in the western MVB were to be related to the subduction of this plate beneath Mexico. Their interpretation does not support the earlier study of Pardo and Suárez (1995).

The rather subjective interpretation by Pardo and Suárez (1995) has already been criticized by Verma (2000b, 2001a, 2009), but the scientific community has paid little attention to this controversy. Instead, numerous researchers (e.g., Schaaf et al., 2005; Blatter et al., 2007; Gómez-Tuena et al., 2007b; Mukasa et al., 2007; Pérez-Campos et al., 2008; Cai et al., 2014) have taken it for granted that the hypothetical contours, drawn by Pardo and Suárez (1995) as dashed curves without any "deep" seismic evidence (see the paper and new interpretation by Pacheco and Singh, 2010), actually exist and have made them a fact by simply repeating in their papers.

One of the greatest problems with the seismic interpretations is that the experimental uncertainties inevitably present in the calculated centroid depths of earthquake locations are not taken into account in any seismic study. After all, the hypocenters and slab depth contours are experimentally determined parameters and are not absolute locations within the earth. Hence, their uncertainties must be evaluated and taken into account in any model reconstruction (Bevington and Robinson, 2003; Miller and Miller, 2005; Verma, 2005). In this connection, although Pacheco and Singh (2010) did not explicitly state that they are dealing with depth uncertainties, they presented four different estimates of earthquake hypocenter depths: Method 1 (M1) focal mechanism, Mw, and centroid/constraint depth from their study; Method 2 (M2) focal mechanism, Mw, and centroid depth from the global Centroid Moment Tensor (CMT) catalogue; Method 3 (M3) focal mechanism, Mw, and depth from Pacheco and Singh (1998); and Method 4 (M4) focal mechanism, Mw, and depth from Singh et al. (2007). Figures 4b and 4c clearly show extremely large uncertainties associated with the different methods (M2–M4) as compared to Method M1. The probably most precise method (M1) of Pacheco and Singh (2010) was used as a reference in Figure 4c. Note that this more precise method also provided all centroid depths as <60 km (Figures 4a and 4b).

I estimated the percentage differences among these different depth estimates for the same earthquakes, assuming Pacheco and Singh´s (2010) work, i.e. Method M1, as the reference. Forty values of the estimates for Method M2 showed differences from about –70% to +200% with respect to M1. Only one estimate for Method M3 presented by these authors showed +40% difference and two estimates for Method M4 resulted in about +4% and +88% differences. Therefore, such large differences (or errors in earthquake depth estimates) should not be ignored in any model based on such data. These positive as well as negative differences and significantly different hypocenter depth values also imply that the errors are not homoscedastic, nor are they systematic; they are random errors associated to the different methods. Certainly, therefore, the small contrasts of only a few percentages, interpreted by Pérez-Campos et al. (2008) in their models for deeper levels of up to about 700 km, have to be viewed with caution when the information is available on only very shallow earthquakes up to about 60 km that have large uncertainties of about –70% to +200%.

2.2.2. Magneto-telluric evidence

Magneto-telluric data acquired along the transect from the Pacific coast through the C-MVB and to the north (Jording et al., 2000) showed a low-resistivity zone beneath the C-MVB, which was interpreted by the authors as due to subduction fluids. The magneto-telluric data may well be consistent with the continental rift or extensional setting for the MVB proposed by Márquez et al. (1999c, 2001), Sheth et al. (2000), and Verma (2002, 2004, 2009). Similarly, the interpretation by Jödicke et al. (2006) is characterized by the same ambiguity. Furthermore, if the subducted slab can only be traced to several tens of kilometers before the C-MVB volcanic front and is only at most about 60 km deep (Pacheco and Singh, 2010), it cannot melt, nor dehydrate, to contribute any substance to the C-MVB.

2.2.3. Gravimetric evidence

Gravimetric studies (Campos-Enríquez and Sánchez-Zamora, 2000; Campos-Enríquez et al., 2003) have shown that partial melts exist in the lower crust beneath the MVB, making crustal involvement a feasible process in the genesis of magmas (e.g., Verma, 1999, 2015a; Schaaf et al., 2005; Ortega-Gutiérrez et al., 2008; Velasco-Tapia and Verma, 2013; Velasco-Tapia et al., 2013; Velasco-Tapia, 2014). The gravity data will be consistent with the

presence of either subduction fluids in an arc environment or mantle fluids in an extensional setting. No distinction can be made from the gravity method, nor can it be done from any other geophysical method. Only precise and accurate geochemical and isotopic data might clarify it in the future.

2.2.4. Thermal modeling

Thermal modeling of the combined Cocos and North American plates has been carried out (Manea et al., 2005) and used by other researchers as a valid argument in favor of the subduction-related origin of the MVB. Although, in this modeling work, there might be several objections and probable misinterpretations of the tectonics of this complex area, the main objection lies in the starting conceptual tectonic model that these authors (Manea et al., 2005) had used, i.e. that the subducted plate or slab is supposed to exist not only beneath the MVB but also far beyond through NW Mexico up to the state of Louisiana or Texas in the United States (see their figure presenting their starting model) – an absurd scenario indeed. More recently, in a combined seismic and thermal modeling study of the C-MVB, Pérez-Campos et al. (2008) interpreted the existence of a low-velocity shallow zone attributed to the presence of subduction fluids. Such fluids would be better interpreted as a result of rift-related partial melting upwelling zone, which is also consistent with the interpretation of the gravity data (Campos-Enríquez and Sánchez-Zamora, 2000) and shallow level seismicity recorded beneath the C-MVB (UNAM and CENAPRED Seismology Group, 1995; Pacheco and Singh, 2010) as well as with the quantitative statistical interpretation of the geochemical data documented by Verma (2009) and in the present paper (Section 6). Similarly, the schematic model presented by Blatter et al. (2007) relies on the hypothetical presence of the subducted slab beneath and beyond the C-MVB, which is simply not true, not even from the recent seismic evidence (Pacheco and Singh, 2010).

2.3. Geochemical evidence

The failure of generalized arc-models for the MVB has been long recognized (Verma and Aguilar-Y-Vargas, 1988). Based on major- and trace-elements and radiogenic isotopes, I, either alone (Verma, 1983, 1999, 2000a, 2000b, 2001a, 2001b, 2001c, 2002, 2003, 2004, 2009, 2015a) or with colleagues (Verma et al., 1991; Márquez et al., 1999c; Sheth et al., 2000, 2002; Velasco-Tapia and Verma, 2001a, 2001b; Torres-Alvarado and Verma, 2003; Verma and Carrasco-Núñez, 2003; Verma and Hasenaka, 2004; Verma and Luhr, 2010), published a series of papers on the origin and evolution of the MVB; some of them also included petrogenetic modeling. As far back as in 1983 (Verma, 1983) for the Los Humeros caldera, in 1988 (Verma and Aguilar-Y-Vargas, 1988) for the MVB, and in 1999 (Márquez et al., 1999c; Verma, 1999) for the Sierra de Chichinautzin in the C-MVB (located in the area near the trench or at the volcanic front area), these studies showed that the MVB is atypical, and its origin can be best explained from the ongoing rifting or extensional processes rather than the ongoing subduction. In fact, in one of my earlier papers (Verma, 2002) I summarized the geoscientific information for the entire southern Mexico and Central America from Guatemala to northwestern Costa Rica and affirmed the Mexican case as unique on the earth on the basis of quantitative arguments from seismology (depth to Wadati-Benioff zone), trace element geochemistry (Ba/La, La/Yb, Ba/Zr, and Be/Ce ratios), and radiogenic isotopes ($^{87}Sr/^{86}Sr$, $^{143}Nd/^{144}Nd$, $^{206}Pb/^{204}Pb$, and $^{207}Pb/^{204}Pb$ ratios and, above all, a new ratio parameter $\varepsilon_{Nd}/\varepsilon_{Sr}$). The uniqueness lies in the inference that, in spite of the ongoing subduction of the Cocos plate beneath the North American plate, there is no arc volcanism associated with this process in southern Mexico, whereas the subduction of the same oceanic plate beneath the Caribbean plate does give rise to an active arc: the Central American Volcanic Arc. The paper by Verma (2002) was never criticized by anyone but was mostly ignored because no arguments have thus far existed to prove it wrong.

The presence of disequilibrium phenocryst assemblages is a common characteristic in several volcanoes of the C-MVB, which has been interpreted as mixing or mingling of magmas in crustal reservoirs (Nixon, 1988a, 1988b; Aguirre-Díaz, 2001; Márquez and De Ignacio, 2002; Witter et al., 2005; Velasco-Tapia et al., 2013; Velasco-Tapia, 2014). It is, therefore, indispensable to take into account shallow-level processes before inferring about the deeper mantle and subduction processes. In fact, through the study of differentiated volcanic products of stratovolcanoes, such as Iztaccíhuatl (Nixon, 1988a, 1988b), Popocatépetl (Robin, 1984; Boudal, 1985; Siebe et al., 1999; Straub and Martin del Pozzo, 2001; Schaaf et al., 2005; Torres-Alvarado et al., 2011), or Nevado de Toluca (Martínez-Serrano et al., 2004), it would be almost impossible to unequivocally infer the deeper mantle processes, because the (continental) crustal processes can generally account for all observations and constraints. There will be no objective way to separate the effects of processes taking place at shallower crustal depths from the deeper mantle.

Similar problems may reside with the interpretation of deeper processes from the study of melt inclusions in minerals that have been reequilibrated at shallow, crustal depths (e.g., Cervantes and Wallace, 2003); in such cases, the inference being made might refer to shallow processes and not to deep-seated mantle sources.

Therefore, contrary to the views expressed in such studies of evolved magmas and melt inclusions, inferences about the deeper processes, such as the involvement

of subduction fluids or melts, cannot be easily and unequivocally made. The study of primitive or at least basic or ultrabasic magmas is a fundamental requirement if one wishes to conclude about the deeper mantle sources and processes (e.g., Verma, 2006; Luhr, 2007).

Some authors (Delgado et al., 1998) have used a simplistic and erroneous approach, already criticized by Sheth et al. (2002), whereby the mere presence of calc-alkaline magmas (should better be called subalkaline according to the TAS diagram and CIPW norm calculations; Verma et al., 2002, 2003) was interpreted to prove their origin in an arc environment.

On the other hand, the apparently systematic variations of geochemical parameters with distance from the trench documented by Blatter et al. (2007) are illusive because they can well be explained by the systematically more differentiated rock-types being sampled in their database as the MVB-MAT distance increases. These authors (Blatter et al., 2007) should have examined the variations of element concentrations, or more appropriately their ratios with the distance from the trench at a given SiO_2 level or for a given rock-type. Their interpretation was criticized by Torres-Alvarado et al. (2011).

Finally, for the unusual basic magmas from the MVB the nomenclature of ocean island basalt used by some authors (OIB, e.g., Márquez et al., 1999a, 1999b; Sheth et al., 2000; Ferrari, 2004) seems to be incorrect and should be abandoned, because such magmas are shown to belong to the continental rift rather than the OIB setting (Verma, 2009, 2015a; Verma and Luhr, 2010; Verma et al., 2011; Velasco-Tapia and Verma, 2013; Section 5.5). The new discriminant function-based tectonic discrimination diagrams (Verma et al., 2006; Agrawal et al., 2008; Verma and Agrawal, 2011) can actually distinguish between OIB and continental rift settings. This distinction was simply not possible before 2006 and might explain the use of this term for the MVB magmas prior to 2006.

2.3.1. Inverse modeling of geochemical data for primitive magmas from southern Mexico

Inverse modeling of geochemical data is a powerful quantitative technique (Hofmann and Feigenson, 1983; Hofmann et al., 1984; McKenzie and O'Nions, 1991; Ormerod et al., 1991; Feigenson and Carr, 1993; Maaløe, 1994; Velasco-Tapia and Verma, 2001a, 2013; Feigenson et al., 2003; Verma, 2004, 2006). Basic magmas with characteristics of primitive, little-differentiated magmas are present throughout the MVB (e.g., Luhr et al., 1989; Luhr, 1997; Wallace and Carmichael, 1999; Verma, 2000a, 2002, 2004), as well as in the LTVF (Verma et al., 1993a; Nelson et al., 1995; Verma, 2006). The geochemical data from the MVB have been subjected to inverse modeling. Specifically, the basic rock data from the Sierra de Chichinautzin in the C-MVB were modeled by Velasco-Tapia and Verma (2001a, 2013); these authors concluded that the primitive magmas represented partial melts from the underlying mantle without the involvement of the subducted slab. This work was extended to the west-central to eastern MVB (Verma, 2004) and to the LTVF (Verma, 2006), ascertaining the same conclusion for these regions as for the Sierra de Chichinautzin. Thus, a quantitative interpretation of the chemistry of primitive magmas from the MVB in terms of inverse modeling also confirms the inferences from other statistical arguments outlined in this paper. Velasco-Tapia and Verma (2013) also documented from inverse modeling that the CAVA represents the classic example of an arc setting wherein the HFSE and REE are decoupled from the LILE, indicating good functioning of the inversion procedure.

2.3.2. Sr, Nd, Pb, Os, Be, and Hf isotopes

Isotopic compositions have proved to be extremely useful in petrogenetic studies of volcanic provinces (e.g., Best and Christiansen, 2001; Faure, 2001; McBirney, 2007), and the MVB has been no exception. Numerous studies have been published on the Sr, Nd, and Pb isotopes from the MVB (Verma, 1983, 1999, 2000a, 2000b, 2001a, 2001b, 2001c, 2002, 2003, 2015a; Boudal, 1985; Verma and Nelson, 1989; Verma et al., 1991; Nakagawa et al., 1998; Siebe et al., 1999, 2004; Blatter et al., 2001, 2007; Velasco-Tapia and Verma, 2001a, 2013; Aguirre-Díaz et al., 2002; Verma and Carrasco-Núñez, 2003; Martínez-Serrano et al., 2004; Verma and Hasenaka, 2004; Schaaf et al., 2005; Verma et al., 2005; Gómez-Tuena et al., 2007b; Mukasa et al., 2007; Meriggi et al., 2008; García Tovar, 2009; Agustín-Flores et al., 2011; Torres-Alvarado et al., 2011; Arce et al., 2013; Koloskov and Khubunaya, 2013; Velasco-Tapia et al., 2013; Cai et al., 2014), including the present work. The shift to the right of the mantle array (Verma, 2006), towards and beyond the mean composition of subducted slab (Verma, 2000a, 2002), commonly observed in all arcs around the world, has not been documented in the MVB, which makes this volcanic province atypical for it to be an arc. An important point to mention here is that the Sr and Nd isotopic data should be adjusted to given reference values for the standards used for estimating mass spectrometric bias, as has been done in all studies on the MVB published by our group (Verma and Nelson, 1989; Verma et al., 1991; Verma, 1992, 1999, 2000a, 2000b, 2001a, 2001b, 2001c, 2002, 2003, 2015a; Velasco-Tapia and Verma, 2001a, 2013; Verma and Carrasco-Núñez, 2003; Verma and Hasenaka, 2004; Verma et al., 2005; Torres-Alvarado et al., 2011; Velasco-Tapia and Verma, 2013). Most other scholars studying the MVB have unfortunately not followed this convention (e.g., Boudal, 1985; Nakagawa et al., 1998; Siebe et al., 1999, 2004; Blatter et al., 2001, 2007; Aguirre-Díaz et al., 2002; Martínez-Serrano et al., 2004; Schaaf et al., 2005; Mukasa et al., 2007; García-Tovar, 2009; Agustín-Flores et

al., 2011; Arce et al., 2013; Koloskov and Khubunaya, 2013; Cai et al., 2014).

The studies (e.g., Martínez-Serrano et al., 2004) reporting isotopic compositions of the so-called adakitic rocks from the MVB have not confirmed the true adakitic nature of the studied rocks because their isotopic compositions are different from the subducting Cocos plate (Martínez-Serrano et al., 2004; Verma, 2009). Other geochemical characteristics of these "adakites" also cannot be obtained from the partial melting of subducting Cocos plate, being a requisite to call a rock an adakite. Similarly, models involving slab melts for the genesis of some MVB magmas (Gómez-Tuena et al., 2003, 2007b) are neither consistent with the composition of the subducting slab (Verma, 2000a, 2002), nor with the recent seismic evidence (Pacheco and Singh, 2010).

The osmium isotopic compositions of the MVB magmas (Lassiter and Luhr, 2001; Chesley et al., 2002) have not provided any convincing evidence in support of the subduction-related origin, although these authors have tried to explain their results in terms of such arc-trench models, downplaying the influence of the relatively thick (about 40 km) continental crust beneath the C-MVB.

A worldwide study of beryllium isotopes (Tera et al., 1986) also included samples from the MVB and CAVA. The MVB samples showed practically negligible contents of ^{10}Be in the MVB magmas (0.3×10^6 to 0.5×10^6 atoms g^{-1}; n = 3), which were similar to the ocean island and rift volcanoes (0.1×10^6 to 0.7×10^6 atoms g^{-1}; n = 15), MORB (0.1×10^6 to 0.9×10^6 atoms g^{-1}; n = 5), or flood basalt (0.2×10^6 to 0.7×10^6 atoms g^{-1}; n = 4), but significantly lower than the arc values (Tera et al., 1986). These authors argued that the uppermost layer of Cocos plate sediments is scraped off in the Mexican subduction zone but, because the CAVA rocks did have very high ^{10}Be contents (0.6×10^6 to 24×10^6 atoms g^{-1}; n = 17), this process was not required in the Central American segment of the same MAT (Figure 1). In fact, the range of ^{10}Be for the CAVA samples (0.6×10^6 to 24×10^6 atoms g^{-1}) is so wide that it includes all ranges of ^{10}Be values for other arcs (Tera et al., 1986). In spite of the adverse evidence for the MVB, the general subduction-related model was maintained. In this context, one may ask the following questions: 1) "What would be the reason for the sediments to be scraped off from the Mexican MAT, but not from the Central American MAT?"; and 2) "Why can the MVB not represent a continental rift setting?" If the MVB does represent a rift setting, the ^{10}Be data would be easily explained.

The most recent Hf isotope study by Cai et al. (2014), supposedly to have proved the involvement of slab melts in the genesis of the C-MVB magmas, will be discussed in greater detail in Section 6.4. These authors start with the hypothesis that the MVB is an arc. If a working hypothesis is taken as an established fact and all the adverse geological, geochemical, statistical, and geophysical evidence accumulated over three decades is ignored, nothing can cope with this kind of "science". Nevertheless, I propose some of the shortcomings of this work as follows: 1) Pardo and Suárez's (1995) interpolation of depth contours and Pérez-Campos et al.'s (2008) speculative 90° turn in the subducted slab, on which their work relies, are biased interpretations (Verma, 2002, 2009; this work); 2) Pacheco and Singh's (2010) interpretation of the same seismic data as Pérez-Campos et al. (2008) was not even mentioned, probably because it will not allow the presence of a mantle wedge, nor would the subducted slab be at appropriate depths for it to melt; 3) the current interpretation of the combined Nd and Hf isotopic data is biased and probably incorrect, as shown in Section 6.4; 4) the uncertainties in all modeled parameters, inevitably present, are neither stated nor taken into account while deriving inferences from different diagrams, and alternative extension-related models were not even evaluated.

2.3.3. Study of basic magmas as a prerequisite for arriving at a better-constrained petrogenetic model

Crustal contamination has been invoked in several studies of evolved magmas from the MVB (McBirney et al., 1987; Verma et al., 1991; Besch et al., 1995; Verma, 1999, 2000b, 2001a, 2001b, 2001c, 2003, 2015a; Torres-Alvarado and Verma, 2003; Verma and Carrasco-Núñez, 2003; Siebe et al., 2004; Schaaf et al., 2005; Velasco-Tapia and Verma, 2013). Further, the alternative lower or upper crustal reservoir is likely to impart similar signatures as those from the subducted slab to intermediate and acid magmas in the MVB (Section 6.3) and, therefore, the controversy concerning the origin of this province cannot be resolved from the study of such evolved magmas. These dual possibilities – subducted slab versus lower crust – for the origin of intermediate and acid magmas will have to be taken into account, and the origin of basic, primitive magmas will have to play a central role in such decisions.

2.4. Plate tectonic evidence

In an attempt to explain the origin of "continental rift-like" basic magmas of the MVB and presumably "arc-like" intermediate and acid magmas, Ferrari (2004) proposed a plate tectonic model, according to which the subducted slab broke during the late Miocene. Ferrari (2004) stated that "the trace of the detachment is expressed by a short (2–3 m.y.), eastward-migrating pulse of mafic volcanism that took place from ca. 11.5 to ca. 6 Ma to the north of the Pliocene–Quaternary volcanic arc, as hot, subslab material flowing into the slab gap produced a transitory thermal anomaly in the mantle wedge." I would say that there are several pending questions that must be answered before this suggestion should be considered acceptable: 1)

"How could the breakage of a 1000-km-long segment of the subducted slab be achieved?"; 2) "What could be the physical cause for this process?"; 3) "At what approximate depth did the detachment take place?"; 4) "If the slab detachment took place sometime during the late Miocene (neither the exact timing nor the depth of detachment are known or stated), the attached (integral) part of the subducted slab should have advanced at least 100 km or more downwards and must be traceable by the recent dense seismic network (Figure 1) especially designed for this purpose (Pacheco and Singh, 2010)"; 5) "Why is there widespread "continental rift-type" volcanism throughout the MVB during the Quaternary?" – according to Ferrari's model and my fourth question, there should simply be no such volcanism anywhere in the C-MVB; and 6) "Why does any rock type (basic, intermediate, or acid) from near the trench not show a greater subduction signal in all parameters than those from far from the trench?" No such differences are discernible from the compiled data (Section 6). Therefore, I conclude that the validity of this hypothesis is not ascertained from any of the available geochemical or geophysical evidence.

Kim et al. (2011), mainly from the data for the LTVF dense seismic array transect (the southern transect in Figure 1), suggested the collision of the Yucatán block with southern Mexico at about 12 Ma, which caused the breakage of the Cocos plate about 4 m.y. ago. Although it may apparently provide a mechanism for the slab break-up for Ferrari's model (Ferrari, 2004), there are even more difficulties with the proposal of Kim et al. (2011), as follows: 1) "Where is the arc or collision type volcanism from 25 Ma to the Holocene age (see Figure 10 of Kim et al., 2011), associated with the subduction of the now disappeared oceanic plate to which the Yucatán block was supposed to be attached?"; 2) "Where is the volcanism or plutonism associated with this middle Miocene collision event in southern Mexico?" – it is certainly not in the LTVF (Figure 1) because this Neogene volcanism is not of an arc-type (Verma, 2006); 3) as suggested by Kim et al. (2011), the Chiapas fold and thrust belt could be taken as the product of this collision provided there were evidence of the syncollision and postcollision igneous activity, which is not known; 4) even when volcanism is documented from the Chiapas belt, it must be shown to be of collision type; 5) these authors themselves admit that they have no paleomagnetic evidence to support their model; 6) "Why did the oceanic slab attached to the Yucatán block continue to grow even after this collision (see their Figure 10)?"; 7) the horizontal and vertical scales in their Figure 10 are not provided, and irrespective of this shortcoming the proportions of different geological identities seem to be incorrect; 8) "Why did the subducted slab corresponding to the Yucatán block remain intact but cause the Cocos slab to break off?"; and 9) "If the Cocos plate did break at about 4 Ma, it should be seismically traceable now at >60 km depth after its advancement during the 4 m.y. of additional subduction". Even more questions can be similarly posed. In fact, the plate tectonic model proposed by these authors is far from clear. Therefore, this work should best be considered as an unproved working hypothesis only. Thus, no workers (Ferrari, 2004; Kim et al., 2011) have been able to provide any satisfactory and well-tested plate tectonic model for the explanation of the anomalous and complex situation of the C-MVB, including the rest of southern Mexico (Verma, 2002, 2004, 2009, 2015a).

Furthermore, if the subducted slab is subhorizontal and shallow (<60 km deep), there should be no (or only subdued) volcanism associated to such a shallow slab (Kay et al., 1987, 1991; Verma, 2002; Ramos and Folguera, 2009). Yet there is abundant volcanism in the C-MVB (Figure 2).

3. New data from the central part of the Mexican Volcanic Belt (C-MVB)

Major and trace elements including the rare-earth elements and radiogenic isotopes were newly determined for 8 samples of Pliocene-Pleistocene volcanic rocks from the Cerro Jocotitlán area (approximate coordinates and results provided in Table 1), 38 samples from different areas of the C-MVB (Table 2), and 4 samples of upper crustal rocks (three of Eocene-Oligocene sedimentary rocks and one of granitic pluton) from the state of Michoacán (Table 3). All analyses were carried out at least in duplicate and only mean (rounded) values are presented in Tables 1–3.

Major and trace elements were determined from X-ray fluorescence spectrometry and rare-earth elements from high-performance liquid chromatography. The analytical details and accuracy estimates were given by Verma (1991a, 1991b) and Verma et al. (1992, 1993b). The Sr, Nd, and Pb isotopes ($^{87}Sr/^{86}Sr$, $^{143}Nd/^{144}Nd$, $^{206}Pb/^{204}Pb$, $^{207}Pb/^{204}Pb$, and $^{208}Pb/^{204}Pb$) were determined by thermal ionization mass spectrometry; the procedures and accuracy are similar to those summarized by Verma (1992). The $^{87}Sr/^{86}Sr$ ratios are normalized to $^{86}Sr/^{88}Sr$ = 0.11940 and adjusted to SRM987 $^{87}Sr/^{86}Sr$ of 0.710230. The $^{143}Nd/^{144}Nd$ are normalized to $^{146}Nd/^{144}Nd$ = 0.72190 and adjusted to La Jolla $^{143}Nd/^{144}Nd$ of 0.511860. The measured $^{87}Sr/^{86}Sr$ for the SRM987 standard was 0.710216 ± 11 (1s – one standard deviation; n = 36) and the measured $^{143}Nd/^{144}Nd$ for the La Jolla standard was 0.511833 ± 12 (1s; n = 82). Note that the measured isotopic ratios were adjusted following the convention of Mainz, Germany (Verma, 1992). The Pb isotopic ratios were corrected for fractionation estimated by running simultaneously the NBS982 standard and are relative to values of $^{206}Pb/^{204}Pb$ = 36.73845, $^{207}Pb/^{204}Pb$ = 17.15946, $^{208}Pb/^{204}Pb$ = 36.74432, and $^{207}Pb/^{206}Pb$ = 0.46707

Table 1. New geochemical and isotopic data for volcanic rock samples from Cerro Jocotitlán, State of Mexico, in the central part of the Mexican Volcanic Belt, Mexico.

Sample:	JO01	JO02	JO03	JO05	JO08	JO04	JO06	JO07
Long. (°W):	–99.6267	–99.6267	–99.6267	–99.6533	–99.618	–99.6267	–99.5919	–99.6005
Lat. (°N):	+19.6925	+19.6925	+19.6925	+19.7070	+19.792	+19.6925	+19.7360	+19.7423
Age	Pliocene–Pleistocene	Pliocene–Pleistocene	Pliocene–Pleistocene	Pliocene–Pleistocene	Pliocene–Pleistocene	Pliocene–Pleistocene	Pliocene–Pleistocene	Pliocene–Pleistocene
Magma type:	Intermediate	Intermediate	Intermediate	Intermediate	Intermediate	Acid	Acid	Acid
Rock type:	Andesite	Andesite	Andesite	Andesite	Andesite	Dacite	Dacite	Dacite
SiO_2	59.04	61.25	61.05	62.14	60.66	63.55	64.97	64.62
TiO_2	0.86	0.74	0.74	0.92	0.89	1.05	0.75	0.76
Al_2O_3	17.21	16.86	17.09	16.48	16.74	16.04	16.39	16.99
$Fe_2O_3^T$	6.05	5.2	5.16	5.33	5.6	4.84	4.22	4.37
MnO	0.099	0.089	0.09	0.088	0.094	0.08	0.071	0.076
MgO	4.31	3.63	3.45	3.23	3.68	1.59	2.23	2.36
CaO	5.5	5.18	5.17	5.14	5.64	4.01	4.04	4.33
Na_2O	3.27	3.49	3.48	3.74	3.46	4.07	3.7	3.84
K_2O	1.57	1.91	1.88	2.29	1.97	2.57	2.66	2.51
P_2O_5	0.162	0.133	0.12	0.222	0.187	0.226	0.169	0.175
LOI	2.19	1.67	1.95	0.56	0.8	2.07	0.72	0.37
Sum	100.26	100.15	100.18	100.14	99.72	100.10	99.92	100.40
$(SiO_2)_{adj}$	60.49	62.45	62.40	62.66	61.59	65.07	65.70	64.81
$(Na_2O + K_2O)_{adj}$	4.96	5.51	5.48	6.08	5.51	6.80	6.43	6.37
Q	14.24	15.81	16.07	15.16	14.59	18.79	20.59	18.95
Or	9.51	11.51	11.36	13.65	11.82	15.55	15.90	14.88
Ab	28.35	30.11	30.10	31.91	29.72	35.26	31.66	32.59
An	26.87	25.18	25.41	21.59	24.70	18.33	19.14	20.40
Di	0.00	0.11	0.00	2.15	2.00	0.43	0.00	0.00
Hy	16.29	13.70	13.29	11.39	13.04	7.16	8.75	9.14
Mt	2.15	1.84	1.83	1.87	1.97	1.90	1.64	1.68
Il	1.67	1.43	1.44	1.76	1.72	2.04	1.44	1.45
Ap	0.38	0.31	0.28	0.52	0.44	0.54	0.40	0.41
Mg#	64.98	64.52	63.53	61.22	63.12	46.95	58.74	59.27
FeO^T / MgO	1.26	1.29	1.35	1.48	1.37	2.74	1.70	1.67
La	25.4	16.5	21.0	24.9	20.9	18.5	22.2	30.2
Ce	45.0	29.6	40.3	49.1	43.7	44.5	40.6	58.0
Pr	5.8	4.1	4.9	5.9	5.0	4.4	5.1	6.6
Nd	23.0	16.7	19.9	23.6	20.5	17.5	19.6	24.7
Sm	4.6	3.4	4	4.8	4.1	3.6	4.0	4.9
Eu	1.27	0.95	1.05	1.25	1.11	0.82	0.94	1.14
Gd	4.5	3.1	3.6	4.6	3.8	3.3	3.9	4.9
Tb	0.78	0.62	0.69	0.79	0.68	0.61	0.72	0.89
Ho	0.79	0.53	0.56	0.68	0.63	0.60	0.60	0.80
Er	1.9	1.4	1.6	2.0	1.8	1.7	1.8	2.3
Tm	0.22	0.18	0.24	0.33	0.25	0.23	0.34	0.38
Yb	1.4	1.2	1.5	2.0	1.7	1.7	1.5	2.3
Lu	0.21	0.24	0.25	0.34	0.25	0.23	0.26	0.36
$(^{87}Sr / ^{86}Sr)_m$	0.704718	0.704761	0.704743	0.704918	0.704827	0.704700	0.705125	0.705112
$(^{143}Nd / ^{144}Nd)_m$	0.512656	0.512658	0.512642	0.512681	0.512657	0.512667	0.512604	0.512651

Abbreviations: The subscript adj refers to adjusted data (anhydrous 100% adjusted basis); Mg# = 100 Mg^{2+} / (Mg^{2+} + Fe^{2+}), atomic; FeO^T = total iron expressed as FeO (the computer program for adjustments and norm calculations is SINCLAS by Verma et al., 2002, or IgRoCS by Verma and Rivera-Gómez, 2013b). Replicate analyses of major elements were performed for most samples; n1 = number of analyses for major elements; n2 = number of analyses for trace elements; n3 = number of analyses for Sr isotopes; n4 = number of analyses for Nd isotopes. Rounded concentration values were reported; the sum may therefore be sometimes inconsistent. The $^{87Sr}/^{86}Sr$ ratios are normalized to $^{86}Sr/^{88}Sr$ = 0.11940 and adjusted to SRM987 $^{87}Sr/^{86}Sr$ of 0.710230. The $^{143}Nd/^{144}Nd$ are normalized to $^{146}Nd/^{144}Nd$ = 0.72190 and adjusted to La Jolla $^{143}Nd/^{144}Nd$ of 0.511860. The measured $^{87}Sr/^{86}Sr$ for the SRM987 standard was 0.710216 ± 11 (1s; n = 36) and the measured $^{143}Nd/^{144}Nd$ for the La Jolla standard was 0.511833 ± 12 (1s; n = 82). Note that the measured isotopic ratios were adjusted following the convention of Mainz (see Verma, 1992, 2002, 2006).

Table 2. Additional new geochemical and isotopic data for volcanic rock samples from the central part of the Mexican Volcanic Belt, Mexico.

Sample:	SC01	SC02	OX01	OX02	SMN01	SG01	VT01	VT02
Long. (°W):	–99.4000	–99.4583	–99.5917	–99.6267	–99.8017	–99.8944	–99.6417	–99.7083
Lat. (°N):	+19.3167	+19.3083	+19.3361	+19.6925	+19.3450	+19.5917	+19.3750	+19.5417
Area	Sierra de las Cruces	Sierra de las Cruces	Valle de Toluca	Valle de Toluca	Valle de Toluca	Valle de Toluca	Valle de Toluca	Valle de Toluca
Age	Pliocene–Pleistocene	Pliocene–Pleistocene	Pliocene–Pleistocene	Pliocene–Pleistocene	Pliocene–Pleistocene	Pliocene–Pleistocene	Pliocene–Pleistocene	Pliocene–Pleistocene
Magma type:	Acid	Acid	Intermediate	Intermediate	Intermediate	Intermediate	Intermediate	Acid
Rock type:	Dacite	Dacite	Andesite	Trachyandesite, latite	Andesite	Basaltic andesite	Trachyandesite, latite	Dacite
SiO_2	64.69	64.72	58.75	60.92	60.81	51.86	55.75	67.57
TiO_2	0.65	0.67	0.99	1.14	0.84	1.94	1.07	0.5
Al_2O_3	16.15	15.83	17.25	16.99	15.81	16.93	15.60	15.65
$Fe_2O_3^T$	4.46	4.50	5.89	5.79	5.76	10.15	6.72	3.28
MnO	0.078	0.079	0.108	0.089	0.094	0.158	0.096	0.063
MgO	2.56	2.65	3.96	1.75	4.88	5.42	5.98	1.52
CaO	3.92	4.30	6.52	4.84	5.49	7.57	6.90	3.41
Na_2O	4.28	4.62	3.78	3.98	3.71	3.68	4.49	4.19
K_2O	2.01	2.04	1.85	2.86	2.13	1.07	2.59	2.56
P_2O_5	0.146	0.167	0.191	0.308	0.218	0.572	0.741	0.118
LOI	0.90	0.40	0.72	1.05	0.93	0.45	0.23	0.94
Sum	99.84	99.98	100.01	99.72	100.67	99.80	100.17	99.80
$(SiO_2)_{adj}$	65.60	65.21	59.44	62.01	61.24	52.62	56.06	68.52
$(Na_2O + K_2O)_{adj}$	6.38	6.71	5.70	6.96	5.88	4.82	7.12	6.84
Q	18.96	16.69	9.67	13.53	11.72	1.39	0.00	23.32
Or	12.05	12.15	11.06	17.20	12.68	6.42	15.39	15.34
Ab	36.72	39.39	32.36	34.28	31.61	31.60	38.21	35.95
An	18.75	16.56	24.93	20.41	20.34	26.91	14.84	16.37
Di	0.00	3.12	5.29	1.64	4.55	6.04	11.80	0.00
Hy	10.03	8.69	12.28	7.75	14.97	19.39	10.68	6.43
Ol	0.00	0.00	0.00	0.00	0.00	0.00	2.71	0.00
Mt	1.74	1.74	2.07	2.26	2.01	3.17	2.59	1.28
Il	1.25	1.28	1.90	2.20	1.61	3.74	2.04	0.96
Ap	0.34	0.39	0.45	0.73	0.51	1.34	1.73	0.28
Mg#	60.73	61.34	63.65	44.88	68.82	57.33	70.57	55.53
FeO^T / MgO	1.57	1.53	1.34	2.98	1.06	1.69	1.01	1.94
Ba	424	452	530	792	414	524	1096	512
Co	14	13	18	12	36	32	22	7.5
Cr	107	84	57	8	177	149	160	40
Cu	14	16	18	9	22	21	37	6
Nb	4.7	5.7	7.6	14.0	6.1	21.8	15.3	5.5
Ni	58	48	28	8	82	40	130	13
Rb	52.8	53.2	44.2	58.4	32.5	9.4	26.3	68.2
Sr	420	454	436	398	512	149	1715	384
V	54	80	93	44	112	150	123	46
Y	17.8	21.4	25.8	37.6	18.4	36.2	17.8	14.2
Zn	66	66	62	74	78	108	102	50
Zr	146.3	147.8	158.3	280.7	167.0	299.1	215.8	135.6
La	12.8	13.5	20.5	23.8	12.7	25.5	58	16.4
Ce	22.7	24.2	36.0	35.8	28.2	66	127	30.7
Pr	3.4	3.6	4.8	4.3	3.9	8.2	13.4	3.6
Nd	13.9	14.5	19.0	15.1	14.9	34.0	48.7	14.8
Sm	3.1	3.2	3.9	3.5	3.3	7.6	7.5	2.9
Eu	0.92	1.05	1.09	0.92	1.02	2.22	1.96	0.82
Gd	2.9	3.1	3.7	4.7	3.1	7.1	5.1	2.7
Tb	0.52	0.58	0.72	0.87	0.54	1.0	0.80	0.57
Ho	0.48	0.52	0.64	1.06	0.50	1.10	0.64	0.48
Er	1.3	1.3	1.8	2.9	1.4	2.6	1.6	1.2
Tm	0.18	0.19	0.21	0.49	0.16	0.39	0.19	0.14
Yb	1.2	1.2	1.1	2.1	1.3	2.6	1.4	1.1
Lu	0.15	0.18	0.15	0.36	0.23	0.33	0.22	0.13
$(^{87}Sr / ^{86}Sr)_m$	0.704170	0.704139	0.703929	0.704596	0.704106	0.703761	0.704171	0.704205
$(^{143}Nd / ^{144}Nd)_m$	0.512873	0.512876	0.512727	0.512656	0.512862	0.512759	0.512827	0.512834

Table 2. (Continued.)

Sample:	VT03	VA02	VA03	ATH01	LC01	TU01	SF02	AG01
Long. (°W):	–99.7667	–99.5116	–99.5275	–99.6194	–100.4583	–100.4750	–100.4625	–100.4750
Lat. (°N):	+19.7361	+20.51330	+20.51330	+20.5917	+19.5000	+19.5375	+19.6056	+19.4625
Area	Valle de Toluca	Hidalgo	Hidalgo	Hidalgo (Atopixco)	Zitácuaro	Zitácuaro	Zitácuaro	Zitácuaro
Age	Pliocene–Pleistocene	Pliocene–Pleistocene	Pliocene–Pleistocene	Pliocene–Pleistocene	Pliocene–Pleistocene	Pliocene–Pleistocene	Pliocene–Pleistocene	Pliocene–Pleistocene
Magma type:	Acid	Intermediate	Intermediate	Acid	Intermediate	Intermediate	Acid	Acid
Rock type:	Dacite	Basaltic andesite	Basaltic andesite	Rhyolite	Basaltic andesite	Basaltic andesite	Dacite	Dacite
SiO_2	62.88	54.50	54.54	74.96	54.95	55.65	65.20	66.32
TiO_2	0.84	1.43	1.41	0.24	1.29	1.36	0.55	0.58
Al_2O_3	16.39	17.80	17.75	12.84	16.68	17.63	16.78	15.93
$Fe_2O_3^T$	4.89	8.14	8.09	1.73	8.39	7.91	3.89	3.31
MnO	0.084	0.129	0.128	0.030	0.129	0.123	0.073	0.026
MgO	2.96	4.82	7.69	0.17	5.65	3.98	2.34	0.99
CaO	4.85	8.44	8.33	0.75	7.27	7.52	4.78	4.06
Na_2O	3.58	3.38	3.54	3.48	3.75	3.81	4.20	4.22
K_2O	2.53	1.03	0.98	5.60	1.56	1.65	1.68	2.74
P_2O_5	0.198	0.338	0.314	0.031	0.300	0.333	0.145	0.161
LOI	0.84	–0.05	0.20	0.38	0.27	0.09	0.37	1.97
Sum	100.04	99.96	102.97	100.21	100.24	100.06	100.01	100.31
$(SiO_2)_{adj}$	63.62	54.85	53.40	75.18	55.33	56.02	65.63	67.61
$(Na_2O + K_2O)_{adj}$	6.18	4.44	4.43	9.11	5.35	5.50	5.92	7.10
Q	17.01	5.42	0.64	31.20	2.76	4.91	19.91	21.46
Or	15.13	6.13	5.67	33.19	9.28	9.82	9.99	16.51
Ab	30.65	28.78	29.33	29.53	31.95	32.45	35.77	36.40
An	21.43	30.55	29.03	2.88	24.24	26.30	22.11	16.75
Di	1.30	7.62	7.57	0.55	8.20	7.41	0.65	2.25
Hy	10.51	15.46	21.99	1.33	17.80	13.28	8.67	3.84
Mt	1.90	2.52	2.44	0.78	2.60	2.45	1.50	1.29
Il	1.61	2.73	2.62	0.46	2.47	2.60	1.05	1.12
Ap	0.46	0.79	0.71	0.07	0.70	0.78	0.34	0.38
Mg#	61.99	59.83	70.51	22.01	62.88	55.87	61.84	44.62
FeO^T / MgO	1.49	1.52	0.95	9.16	1.34	1.79	1.50	3.01
Ba	639	406	418	273	364	398	404	756
Co	13	21	23	1	44	24	12	6
Cr	56	68	68	18	142	64	50	12
Cu	12	10	8	1	31	22	14	5.5
Nb	9.6	11.2	10.5	19.2	10.6	11.2	4.5	8.4
Ni	32	9	7.5	8	74	18.5	26	8
Rb	72.7	15.6	15.4	288.0	26.6	27.4	29.0	71.1
Sr	396	670	669	38	614	633	895	397
V	76	134	132	14	152	152	52	40
Y	23.0	25.4	25.3	44.2	24.0	25.2	12.6	26.9
Zn	66	83	85	38	92	88	56	54
Zr	201.1	221.4	216.3	216.0	178.1	191.0	115.7	226.1
La	25.3	11.7	17.8	18.7	19.9	19.7	12.5	19.5
Ce	52	27.3	39	31	45	43	20.7	33
Pr	5.9	4.8	5.2	4.8	5.4	5.3	3.1	3.9
Nd	24.6	12.6	22.1	17.9	23.2	21.3	12.1	15.5
Sm	4.7	2.9	4.9	3.6	5.0	4.6	2.5	3.4
Eu	1.15	1.08	1.61	0.29	1.54	1.44	0.81	0.75
Gd	4.2	3.7	4.9	3.4	4.8	4.3	2.2	4.1
Tb	0.74	0.64	0.75	0.68	0.81	0.74	0.44	0.70
Ho	0.72	0.74	0.86	0.85	0.82	0.69	0.34	0.80
Er	1.9	2.0	2.3	2.8	2.3	1.9	0.9	2.5
Tm	0.22	0.32	0.28	0.46	0.34	0.26	0.10	0.35
Yb	1.8	1.8	2.1	3.1	2.1	1.6	0.8	2.6
Lu	0.25	0.31	0.27	0.38	0.32	0.21	0.09	0.42
$(^{87}Sr / ^{86}Sr)_m$	0.704994	0.704100	0.704098	0.707654	0.703740	0.703796	0.703453	0.704453
$(^{143}Nd / ^{144}Nd)_m$	0.512622	0.512661	0.512662	0.512574	0.512970	0.512767	0.512796	0.512654

Table 2. (Continued.)

Sample:	AG02	AG03	SF01	LANO01	SLP01	ZIN01	PUR02	SFT01
Long. (°W):	−100.4750	−100.4750	−100.4750	−100.3533	−100.9200	−100.8208	−100.45278	−100.0167
Lat. (°N):	+19.4625	+19.4625	+19.4625	+19.8200	+19.7917	+19.8958	+20.1194	+19.8083
Area	Zitácuaro	Zitácuaro	Zitácuaro	MGVF (La Nopalera)	MGVF (San Lucas Pío)	MGVF	MGVF (Puraguita)	MGVF (San Fco. Tepeolulco)
Age	Pliocene–Pleistocene	Pliocene–Pleistocene	Pliocene–Pleistocene	Pliocene–Pleistocene	Pliocene–Pleistocene	Pliocene–Pleistocene	Pliocene–Pleistocene	Pliocene–Pleistocene
Magma type:	Acid	Acid	Acid	Intermediate	Intermediate	Intermediate	Acid	Acid
Rock type:	Dacite	Dacite	Dacite	Basaltic trachyandesite, mugearite	Basaltic trachyandesite, mugearite	Andesite	Rhyolite	Dacite
SiO_2	66.70	66.43	65.43	55.52	55.09	57.73	75.28	62.77
TiO_2	0.59	0.59	0.52	1.71	1.35	1.27	0.06	0.72
Al_2O_3	16.05	15.90	16.19	16.53	17.72	17.16	12.32	15.6
$Fe_2O_3^T$	3.39	3.67	3.65	9.23	8.25	7.41	1.03	4.84
MnO	0.025	0.051	0.062	0.147	0.129	0.118	0.022	0.082
MgO	0.95	0.95	2.19	4.35	4.35	3.16	0.03	3.73
CaO	3.61	3.56	4.36	6.64	7.36	6.19	0.44	4.65
Na_2O	4.28	4.27	4.27	4.11	4.27	3.66	3.50	3.93
K_2O	2.78	2.79	2.43	1.68	1.44	2.31	4.60	2.17
P_2O_5	0.163	0.163	0.146	0.51	0.404	0.32	0.011	0.187
LOI	1.79	1.87	0.61	0.09	0.00	0.79	2.71	1.23
Sum	100.33	100.24	99.86	100.52	100.36	100.12	100.00	99.91
$(SiO_2)_{adj}$	67.86	67.72	66.10	55.67	55.24	58.45	77.43	63.84
$(Na_2O + K_2O)_{adj}$	7.18	7.20	6.77	5.81	5.73	6.04	8.33	6.20
Q	21.83	21.61	18.58	4.34	2.49	9.01	37.00	15.87
Or	16.71	16.81	14.51	9.96	8.53	13.82	27.96	13.04
Ab	36.85	36.83	36.50	34.87	36.23	31.36	30.46	33.82
An	16.66	16.29	18.02	21.75	25.00	23.87	2.17	18.83
Di	0.40	0.54	2.33	6.48	7.31	4.19	0.00	2.73
Hy	4.70	4.97	7.30	14.94	14.06	11.95	0.95	11.98
Mt	1.32	1.44	1.41	3.21	2.87	2.61	0.48	1.89
Il	1.14	1.14	1.00	3.26	2.57	2.44	0.12	1.39
Ap	0.38	0.38	0.34	1.18	0.94	0.75	0.03	0.44
Mg#	43.02	41.09	61.78	55.11	57.87	52.63	7.72	67.49
FeO^T / MgO	3.21	3.48	1.50	1.91	1.71	2.11	30.89	1.17
Ba	732	742	516	490	416	560	1	458
Co	6	6	10	41	40	20	1	48
Cr	16	14	63	102	72	18	12	134
Cu	4	6	18	22	31.5	22	1	14
Nb	8.1	8.5	5.3	20.9	15.6	13.9	17.6	7.6
Ni	8	7	30	46	41	18	6	62
Rb	71.9	70.6	61.0	34.4	20.8	46.6	236.3	38.7
Sr	393	393	751	541	616	500	0.3	565
V	37	37	61	153	151	118	6	80
Y	23.1	22.3	11.1	39.0	25.4	127.8	55.1	17.7
Zn	56	54	54	101	91	94	53	71
Zr	225.8	223.2	115.2	281.6	206.7	221.4	89.6	170.7
La	12.0	18.4	10.1	35	16.8	74	17.6	16.8
Ce	16.5	33	18.5	65	37	57	51	29.2
Pr	2.4	4.1	3.2	8.6	5.0	17.4	5.9	3.9
Nd	9.3	13.2	10.9	36.2	19.0	64	25.1	15.2
Sm	2.2	3.1	2.2	7.5	4.2	14.1	7.6	3.3
Eu	0.59	0.80	0.71	2.08	1.32	2.59	0.18	0.99
Gd	2.7	3.3	1.7	7.5	4.0	17.1	8.4	2.8
Tb	0.54	0.58	0.28	1.1	0.62	2.3	1.4	0.48
Ho	0.47	0.50	0.25	1.28	0.70	3.2	1.9	0.43
Er	1.4	1.5	0.61	3.6	2	9.3	5.5	1.2
Tm	0.16	0.19	0.07	0.47	0.28	1.28	0.81	0.17
Yb	1.4	1.5	0.6	3.1	1.8	7.8	4.0	1.1
Lu	0.19	0.20	0.09	0.47	0.25	1.2	0.60	0.17
$(^{87}Sr / ^{86}Sr)_m$	0.704472	0.704454	0.703930	0.703704	0.703809	0.704081	0.744584	0.703891
$(^{143}Nd / ^{144}Nd)_m$	0.512650	0.512643	0.512714	0.512821	0.512863	0.512800	0.512681	0.512851

Table 2. (Continued.)

Sample:	ZIN02	CALA01	CALA02	DOCO01	AZ01	LA70–D
Long. (°W):	–100.7861	–100.5833	–100.5717	–100.5717	–100.7000	–100.6644
Lat. (°N):	+19.8667	+19.8903	+19.9117	+19.9117	+19.7639	+19.7869
Area	MGVF	North of Caldera Los Azufres (Santa Mónica)	North of Caldera Los Azufres (Santa Mónica)	North of Caldera de Los Azufres	Caldera de Los Azufres	Caldera Los Azufres
Age	Pliocene–Pleistocene	Pliocene–Pleistocene	Pliocene–Pleistocene	Pliocene–Pleistocene	Pliocene–Pleistocene	Pliocene–Pleistocene
Magma type:	Acid	Acid	Acid	Acid	Acid	Acid
Rock type:	Rhyolite	Dacite	Dacite	Rhyolite	Rhyolite	Rhyolite
SiO_2	74.26	63.09	62.75	76.88	72.55	71.5
TiO_2	0.07	0.77	0.77	0.06	0.21	0.16
Al_2O_3	12.79	16.54	16.52	12.75	13.49	13.7
$Fe_2O_3^T$	1.08	4.78	4.72	1.08	1.91	0.95
MnO	0.029	0.082	0.080	0.021	0.044	0.04
MgO	0.03	2.30	2.15	0.02	0.24	0.1
CaO	0.54	4.62	4.61	0.31	0.97	0.57
Na_2O	3.50	4.06	3.78	3.92	3.69	3.14
K_2O	4.65	2.78	2.92	4.45	4.46	4.66
P_2O_5	0.012	0.234	0.232	0.020	0.041	0.05
LOI	3.05	0.86	1.44	0.6	2.5	4.55
Sum	100.01	100.12	99.97	100.11	100.10	99.42
$(SiO_2)_{adj}$	76.65	63.79	63.91	77.32	74.43	75.42
$(Na_2O + K_2O)_{adj}$	8.41	6.92	6.82	8.42	8.36	8.02
Q	35.64	15.26	16.23	36.21	31.85	35.73
Or	28.36	16.61	17.58	26.45	27.04	29.05
Ab	30.57	34.74	32.58	33.36	32.03	28.03
An	2.68	18.90	19.84	1.42	4.66	2.64
Di	0.00	2.22	1.56	0.00	0.00	0.00
Hy	1.00	8.39	8.34	0.95	2.07	0.95
Mt	0.50	1.85	1.84	0.49	0.88	0.45
Il	0.14	1.48	1.49	0.11	0.41	0.32
Ap	0.03	0.55	0.55	0.05	0.10	0.12
Mg#	7.39	56.45	55.10	5.05	26.52	23.22
FeO^T / MgO	32.39	1.87	1.98	48.59	7.16	8.55
Ba	88	606	624	4	462	890
Co	1	24	30	2	4	
Cr	8	41	37	10	9	
Cu	4	8	8	1	5	
Nb	16.1	10.8	10.6	26.4	11.8	20
Ni	6	12	11	8	7	
Rb	151.4	70.2	70.6	242.4	149.3	147
Sr	11	452	453	2.1	84	62
V	5	69	70	6	14	10
Y	22.4	22.8	23.1	89.4	20.6	35
Zn	36	72	70	54		
Zr	97.7	224.1	218.8	107.4	146.6	208
La	9.3	23.0	30	4.5	25.0	
Ce	22.5	43	55	14.0	43	
Pr	2.9	5.5	7.5	2.2	5.4	
Nd	11.7	21.2	28.0	11.2	17.9	
Sm	2.9	4.1	5.5	4.8	3.3	
Eu	0.21	1.06	1.30	0.16	0.48	
Gd	2.9	3.7	4.9	6.9	2.9	
Tb	0.61	0.65	0.82	1.1	0.56	
Ho	0.62	0.62	0.84	1.65	0.66	
Er	1.9	1.8	2.3	5.4	1.8	
Tm	0.27	0.22	0.30	0.80	0.32	
Yb	1.9	1.6	2.1	5.2	1.9	
Lu	0.23	0.27	0.31	0.72	0.27	
$(^{87}Sr / ^{86}Sr)_m$	0.704967	0.704483	0.704435	0.723431	0.704288	0.704149
$(^{143}Nd / ^{144}Nd)_m$	0.512793	0.512738	0.512749	0.512689	0.512813	0.512830

Table 2. (Continued.)

Sample:	LA37	LA34	LA48	LA38	LA50	LA64	LA52	LA74
Long. (°W):	–100.6294	–100.6050	–100.6481	–100.6486	–100.6572	–100.6600	–100.7075	–100.7131
Lat. (°N):	+19.8069	+19.7922	+19.7711	+19.8092	+19.7725	+19.7853	+19.7947	+19.7203
Area	Caldera de Los Azufres	Caldera Los Azufres	Caldera Los Azufres	Caldera Los Azufres	Caldera Los Azufres	Caldera Los Azufres	Caldera Los Azufres	Caldera Los Azufres
Age	Pliocene–Pleistocene	Pliocene–Pleistocene	Pliocene–Pleistocene	Pliocene–Pleistocene	Pliocene–Pleistocene	Pliocene–Pleistocene	Pliocene–Pleistocene	Pliocene–Pleistocene
Magma type:	Intermediate	Acid	Acid	Acid	Acid	Acid	Acid	Acid
Rock type:	Andesite	Dacite	Rhyolite	Rhyolite	Rhyolite	Rhyolite	Rhyolite	Rhyolite
SiO_2	58.00	67.0	71.2	76.2	73.5	70.1	72.9	74.7
TiO_2	0.92	0.45	0.22	0.05	0.06	0.36	0.07	0.08
Al_2O_3	17.00	15.5	14.1	12.7	13.5	14.6	12.4	12.5
$Fe_2O_3^T$	6.27	3.44	2.24	1.01	1.6	3.02	1.25	1.17
MnO	0.130	0.07	0.05	0.03	0.05	0.08	0.04	0.04
MgO	4.51	1.09	0.4	0.1	0.1	0.35	0.15	0.13
CaO	6.73	2.8	1.31	0.34	0.54	1.08	0.53	0.52
Na_2O	3.68	3.71	3.86	3.62	4.39	3.83	3.32	3.44
K_2O	1.74	3.43	4.22	4.55	4.61	4.21	4.29	4.74
P_2O_5	0.240	0.13	0.07	0.05	0.05	0.05	0.05	0.05
LOI	0.14	1.91	1.11	0.89	0.26	1.74	4.07	2.02
Sum	99.36	99.53	98.78	99.54	98.66	99.42	99.07	99.39
$(SiO_2)_{adj}$	58.74	68.81	73.01	77.30	74.78	71.92	76.81	76.78
$(Na_2O + K_2O)_{adj}$	5.49	7.33	8.29	9.16	8.25	8.23	8.41	8.29
Q	8.67	24.4	29.34	37.13	29.01	28.73	37.37	35.91
Or	10.41	20.82	25.57	27.28	27.72	25.52	26.71	28.79
Ab	31.54	32.24	33.49	31.07	37.79	33.25	29.60	29.92
An	25.04	13.39	6.20	1.38	2.39	5.16	2.43	2.32
Di	5.81	0	0.00	0.00	0.00	0.00	0.00	0.00
Hy	14.00	5.68	2.77	1.13	1.68	3.17	1.51	1.34
Mt	2.20	1.36	1.03	0.46	0.73	1.39	0.59	0.54
Il	1.77	0.88	0.43	0.10	0.12	0.70	0.14	0.16
Ap	0.56	0.31	0.17	0.12	0.12	0.12	0.12	0.12
Mg#	65.20	46.05	33.90	22.14	15.22	24.97	25.63	24.19
FeO^T /MgO	1.25	2.84	5.04	9.09	14.40	7.76	7.50	8.10
Ba	490	660	820	20	580	800	140	120
Nb	10.0	13	17	21	22	19	18	21
Rb	46.0	100	140	169	136	134	188	219
Sr	651	327	141	12	23	120	31	27
V	120	39	11	10	10	21	10	10
Y	22	26	34	28	41	38	34	37
Zr	194	192	197	120	267	254	124	132

For more explanation see footnote of Table 1.

Table 3. Geochemical and isotopic data for crustal samples from the central part of the Mexican Volcanic Belt, Mexico.

Sample:	9463A	9593B	96341B	9490B	95142A	95142C	9490C	0401m
Long. (°W):	–98.70583	–98.61056	–98.81278	–98.64361	–98.62389	–98.62389	–98.64361	–98.61056
Lat. (°N):	+19.07528	+19.08917	+19.17583	+19.08694	+19.09278	+19.09278	+19.08694	+19.08694
Area:	East of San Pedro Nexapa	West of Buenavista	Cerro Chinconquiat	Paso de Cortés	East of Paso de Cortés	East of Paso de Cortés	Paso de Cortés	West of Buenavista
Reference:	Schaaf et al. (2005)	Schaaf et al. (2005)	Schaaf et al. (2005)	Schaaf et al. (2005)	Schaaf et al. (2005)	Schaaf et al. (2005)	Schaaf et al. (2005)	Schaaf et al. (2005)
Age of material:	?	?	?	?	?	?	?	?
Material:	Xenolith	Xenolith	Xenolith	Xenolith	Xenolith	Xenolith	Xenolith	Xenolith
Rock type (equivalent):	Ultrabasic	Ultrabasic	Intermediate	Intermediate	Intermediate	Acid	(Acid)	–––
SiO_2	37.59	41.21	56.12	60.29	61.83	63.26	81.74	
TiO_2	0.18	0.93	0.86	0.83	0.92	0.74	0.3	
Al_2O_3	20.37	10.21	18.24	16.12	11.81	16.35	7.65	
$Fe_2O_3^T$	3.19	3.15	7.52	5.9	6.11	5.1	2.14	
MnO	0.05	0.07	0.12	0.09	0.06	0.08	0.02	
MgO	22.27	31.89	4.04	5.15	3.39	3.79	1.15	
CaO	17.13	13.03	7.09	5.79	12.69	5.07	5.87	
Na_2O	0.02	0.01	3.95	4.16	2.51	4.39	0.97	
K_2O	0.01	0.01	1.47	1.54	1.49	1.79	0.63	
P_2O_5	0.01	0.01	0.17	0.19	0.14	0.18	0.06	
LOI	0.12	0.17	0.64	0.01	0.01	0.01	0.01	
Sum	100.94	100.69	100.22	100.07	100.96	100.76	100.54	
$(SiO_2)_{adj}$	37.39	41.11	56.69	60.53	61.53	63.02	81.43	
$(Na_2O + K_2O)_{adj}$	0.03	0.02	5.48	5.72	3.98	6.16	1.59	
Q	8.5	4.7	446.9	381.2	209.9	426.6	433.3	
Co	9.6	6.4	19.3	18.7	15.5	14.1	6.6	
Cr				194	115	98		
Cs	0.11	0.08	0.96	1.99	1.45	2.38	1.03	
Cu	9	9	56	6	12	3	4	
Ga	26	13	22	20	22	20	9	
Hf	0.22	1.25	2.98	4.28	11.6	4.38	2.57	
Nb	1.22	3.89	4.18	6.18	8.03	4.91	2.84	
Ni	14	16	26	124	38	86	13	
Pb			5	8		22	6	
Rb	1	1.3	34.7	45.2	37.4	49.1	21	
Sc	1	3	18	25	16	12	8	
Sr	27.4	20.5	526.6	451.9	500	430.8	222.5	274.9
Ta	0.21	1.17	0.31	0.36	0.5	0.33	0.24	
Th	3.43	18.65	0.95	4.74	6.13	4.65	2.65	
U	0.17	1.39	0.42	1.87	2.3	1.72	1.91	
V	14		190	109	152	91	48	
Y	5.5	9.0	15.2	18.4	24.9	15.8	10.1	
Zn	17	17	95	63	81	65	26	
Zr	11.2	17.2	115.9	159.6	483.4	169.1	99	
La	4.3	5.46	13.56	17.67	21.44	15.2	7.13	
Ce	18.64	24.79	30.5	36.71	43.36	31.66	14.34	
Pr	1.38	2.43	3.28	3.71	4.38	3.25	1.57	
Nd	6.78	12.15	14.99	17.26	20.67	15.16	7.72	0.54
Sm	1.37	2.61	3.2	3.87	4.32	3.35	1.59	
Eu	0.31	0.51	1.05	1.16	1.09	1.03	0.45	
Gd	1.24	2.19	3.31	4.39	4.85	3.28	1.7	
Tb	0.23	0.34	0.55	0.68	0.78	0.56	0.28	
Dy	0.87	1.58	2.69	3.51	4.06	2.58	1.69	
Ho	0.2	0.28	0.47	0.56	0.79	0.45	0.36	
Er	0.55	1.0	1.42	1.85	2.51	1.51	0.95	
Tm	0.08	0.14	0.15	0.29	0.37	0.18	0.12	
Yb	0.52	0.99	1.38	1.96	2.65	1.27	1.16	
Lu	0.084	0.161	0.194	0.243	0.43	0.229	0.155	
$(^{87}Sr / ^{86}Sr)_m$	0.706870		0.704208			0.704258	0.707439	0.707086
$(^{143}Nd / ^{144}Nd)_m$	0.512817		0.512798			0.512861	0.512596	0.512215

Table 3. (Continued.)

Sample:	TL–45–X2	TL–45–X5	TL47–X1	SC37A	SC49A	SC24A	SC49B	SC35A	SC57A
Long. (°W):	–98.75669	–98.75669	–98.75189	–99.48310	–99.42530	–99.27610	–99.42530	–99.37580	–99.26350
Lat. (°N):	+19.36175	+19.36175	+19.3296944	+19.4686	+19.5256	+19.2075	+19.5256	+19.2744	+19.252
Area	Telapón volcano	Telapón volcano	Telapón volcano	Sierra de Las Cruces	Sierra de Las Cruces	Sierra de Las Cruces	Sierra de Las Cruces	Sierra de Las Cruces	Sierra de Las Cruces
Reference	García Tovar (2009)	García Tovar (2009)	García Tovar (2009)	Velasco-Tapia et al. (2013)	Velasco-Tapia et al. (2013)	Velasco-Tapia et al. (2013)	Velasco-Tapia et al. (2013)	Velasco-Tapia et al. (2013)	Velasco-Tapia and Verma (2014)
Age	?	?	?	?	?	?	?	?	?
Material:	Xenolith	Xenolith	Xenolith	Xenolith	Xenolith	Xenolith	Xenolith	Xenolith	Xenolith
Rock type (equivalent):	Intermediate	Intermediate	Intermediate	Intermediate	Intermediate	Intermediate	Intermediate	Intermediate	Intermediate
SiO_2	54.4	55.17	53.18	54.93	58.24	58.35	58.96	59.33	56.64
TiO_2	1.35	1.25	1.13	1.044	0.701	0.976	0.689	0.765	0.792
Al_2O_3	17.68	17.6	17.98	16.05	15.42	17.02	15.02	16.83	17.12
$Fe_2O_3^T$	7.86	7.31	7.91	6.99	5.79	6.71	5.92	5.75	6.53
MnO	0.12	0.11	1.3	0.111	0.096	0.115	0.093	0.069	0.075
MgO	5.5	5.04	6.14	3.45	6.45	3.83	6.08	3.79	2.7
CaO	7.7	7.22	8.18	6.37	6.44	5.7	6.22	4.8	4.96
Na_2O	3.22	3.65	3.15	4.04	3.51	4.09	3.57	4.13	4.15
K_2O	0.97	1	0.91	1.41	1.43	1.4	1.41	1.54	1.9
P_2O_5	0.26	0.24	0.19	0.31	0.14	0.22	0.14	0.16	0.16
LOI	0	0	0	5.314	0.48	1.523	0.598	3.029	5.05
Sum	99.06	98.59	100.07	100.02	98.70	99.93	98.70	100.19	100.08
$(SiO_2)_{adj}$	55.26	56.29	53.48	58.34	59.58	59.60	60.38	61.36	59.92
$(Na_2O + K_2O)_{adj}$	4.26	4.74	4.08	5.78	5.02	5.61	5.09	5.82	6.40
Q	331	387	350	507	329	319	358	309	302
Co	25	26	33	26	22	20	22	17	16
Cr	286	238	321	220	280	120	230	240	290
Cs				1.3	1	0.6	1.1	1.1	1.6
Cu	22	27	18	50	10	40	20	30	50
Ga				18	18	20	17	19	22
Hf				3.9	2.9	3.4	2.9	3.2	3.6
Nb	8	7	4	3	3	4	3	3	13
Ni	44	40	75	90	80	70	100	80	50
Pb	6	5		11	9	9	7	10	13
Rb	20	21	19	31	29	27	31	35	49
Sc				21	18	15	18	15	18
Sr	522	538	540	813	474	496	458	453	481
Ta				0.3	0.2	0.3	0.3	0.3	0.3
Th	3	3	3	3.8	2.8	2	2.8	2.6	2.5
U				1.7	0.9	0.7	1.1	1.2	1.3
V	156	155	150	150	125	116	123	100	99
Y	18	19	19	24	18	19	22	14	13
Zn	72	69	81						
Zr	163	166	145	138	100	129	103	114	131
La				26.8	12.3	12.7	13.6	11.1	11.5
Ce				58.9	23.9	28.5	25.4	25	25.6
Pr				8.01	3.12	3.65	3.55	3.22	3.35
Nd				34.4	13.3	15.8	14.8	13.5	14.1
Sm				7	3.1	3.7	3.3	3.1	3
Eu				2.09	1.03	1.31	1.11	1.1	1.13
Gd				5.8	3.3	3.6	3.3	2.9	3
Tb				0.8	0.5	0.6	0.6	0.5	0.5
Dy				4.5	2.9	3.4	3.3	2.8	2.6
Ho				0.9	0.6	0.7	0.7	0.5	0.5
Er				2.4	1.7	1.9	2	1.5	1.4
Tm				0.34	0.25	0.28	0.29	0.23	0.2
Yb				2.3	1.6	1.8	1.9	1.5	1.3
Lu				0.36	0.24	0.26	0.28	0.23	0.2
$(^{87}Sr / ^{86}Sr)_m$	0.703793	0.703912	0.70379	0.70425				0.703899	
$(^{143}Nd / ^{144}Nd)_m$	0.51287	0.512829	0.512795	0.512826	0.512818			0.51287	
$(^{206}Pb / ^{204}Pb)_m$	18.689	18.71	18.698						
$(^{207}Pb / ^{204}Pb)_m$	15.5902	15.6234	15.5909						
$(^{207}Pb / ^{204}Pb)_m$	38.447	38.554	38.458						

Table 3. (Continued.)

Sample:	HP29	X– 10	X– 16	AGUI233a	P3DOB	P2DOB	P4DOB
Long. (°W):	–99.5514	–100.1000	–100.1000	–100.3333	–100.91	–100.91	–100.91
Lat. (°N):	+20.4750	+19.0200	+19.0200	+20.2500	+19.58	+19.58	+19.58
Area	North of Huichapan	Zitácuaro–Valle de Bravo	Zitácuaro–Valle de Bravo	Amealco	Michoacán	Michoacán	Michoacán
Reference	Verma (2001)	Mukasa et al. (2007)	Mukasa et al. (2007)	Aguirre–Díaz et al. (2002)	This work	This work	This work
Age	?	?	?	Precambrian	Eocene–Oligocene	Eocene–Oligocene	Eocene–Oligocene
Material:	Limestone	Cpx–megacryst	Cpx–megacryst	Xenolith	Conglomerate	Sandstone	Shale
Rock type (equivalent):				Acid	(Acid)	Acid	Acid
SiO_2				63.95	89.78	62.58	66.19
TiO_2				0.19	0.36	0.62	0.83
Al_2O_3				18.35	5.6	16.3	16.14
$Fe_2O_3^T$				2.55	0.91	4.8	7.42
MnO				0.05	0.01	0.05	0.01
MgO				1.39	0.1	2.6	0.5
CaO				4.51	0.09	1.33	0.1
Na_2O				4.64	0.12	6.08	0.23
K_2O				1.78	0.6	2.36	3.42
P_2O_5				0.16	0.04	0.11	0.11
LOI				0	1.77	2.71	4.43
Sum				97.29	99.38	99.54	99.38
$(SiO_2)_{adj}$				65.71	92.04	64.85	70.11
$(Na_2O + K_2O)_{adj}$				6.60	0.74	8.75	3.87
Q	6			675	203	1750	544
Co	1			7.3	1	14	9
Cr	4			6	46	137	110
Cs							
Cu	4				14	21	48
Ga							
Hf				9.5			
Nb	0.9				4.8	8	16.2
Ni	6				8	54	30
Pb							
Rb	2.1				24	45	153
Sc				5			
Sr	307			384	72	874	145
Ta							
Th				0.8			
U				0.8			
V	9			22	41	148	176
Y	2.6			8	9.8	17.4	35.6
Zn	10			44	7	56	120
Zr	7				108	177	197
La	0.32			26	6	9.8	9.1
Ce	0.49			42.5	18.8	16.8	22.0
Pr	0.1			5.3	1.3	2.5	2.6
Nd	0.2			18	4.2	9.7	10.7
Sm	0.09			3.4	1	2.2	2.3
Eu	0.03			1.6	0.24	0.6	0.5
Gd	0.1			2.24	0.7	2.1	2.0
Tb	0.02			0.36	0.12	0.34	0.33
Dy				1.66			
Ho	0.02			0.32	0.15	0.44	0.36
Er	0.06			0.96	0.54	1.3	1.1
Tm	0.01			0.21	0.09	0.18	0.16
Yb	0.04			1.13	0.60	1.26	1.34
Lu	0.01			0.16	0.10	0.22	0.25
$(^{87}Sr / ^{86}Sr)_m$	0.707329	0.703643	0.70339	0.705869	0.709884	0.705293	0.701645
$(^{143}Nd / ^{144}Nd)_m$	0.512556	0.512858	0.512833	0.512660	0.512342	0.512556	0.512096
$(^{206}Pb / ^{204}Pb)_m$	24.391	18.611	18.624		19.41	19.277	21.118
$(^{207}Pb / ^{204}Pb)_m$	15.918	15.578	15.565		15.692	15.657	15.798
$(^{207}Pb / ^{204}Pb)_m$	38.773	38.181	38.191		39.047	39.288	41.566

Table 3. (Continued.)

Sample:	Lu_LHG	LuJor23	LuJor24	LuJor38	LuJor21	1050–540G	LHG
Long. (°W):	–101.8150	–101.7505	–101.7492	–101.7295	–101.7547	–101.8141	–101.8141
Lat. (°N):	+19.0000	+18.9725	+18.9682	+18.9587	+18.9710	+18.9995	+18.9995
Area	Michacán	Michacán	Michacán	Michacán	Michacán	Michacán	Michacán
Reference	Luhr and Carmichael (1985)	Luhr and Carmichael (1985)	Luhr and Carmichael (1985)	Luhr and Carmichael (1985)	Luhr and Carmichael (1985)	Hasenaka (1992)	This work
Age	?	?	?	?	?	?	?
Material:	Pluton	Pluton	Pluton	Pluton	Pluton	Pluton	Pluton
Rock type:	Acid	Acid	Acid	Acid	Acid	Acid	Acid
SiO_2	67.2	63.54	64.84	65.37	75.99	64.1	
TiO_2	0.64	0.96	0.74	0.76	0.24	0.84	
Al_2O_3	14.05	15.45	15.47	14.57	12.17	16.18	
$Fe_2O_3^T$	5.05	6.15	4.85	4.96	0.92	5.07	
MnO	0.07	0.03	0.07	0.08	0.04	0.09	
MgO	1.74	3.19	2.45	2.27	0.05	2.78	
CaO	3.47	4.82	4.16	3.97	0.46	4.13	
Na_2O	3.04	3.62	3.53	3.32	2.73	3.5	
K_2O	4.1	0.21	3.46	3.95	5.95	3.34	
P_2O_5	0.11	0.18	0.17	0.13	0.03	0.18	
LOI	0	2.86	0.73	0.58	0.55	0	
Sum	99.47	101.01	100.47	99.96	99.13	100.21	
$(SiO_2)_{adj}$	68.13	65.01	65.04	65.81	77.13	63.87	
$(Na_2O + K_2O)_{adj}$	7.24	3.92	7.01	7.32	8.81	6.82	
Q	537	101	352	572	574		
Co							
Cr	26	12		14	44		
Cs	8.84						
Cu	43	15	62	176	52		
Ga	14	16	11	16	15		
Hf	8.54						
Nb	14	7	9	10	8		
Ni	2	26	4	16	21		
Pb							
Rb	204	15	406	158	158		
Sc	13.01						
Sr	135	233	54	154	218		
Ta							
Th	20.52						
U	6.19						
V	107						
Y	32	39	47	28	26		
Zn	59	31	32	51	54		
Zr	251	307	119	273	225		
La	22.2	37	45	16	20		
Ce	48.1	86	82	45	51		
Pr							
Nd	23						
Sm	4.83						
Eu	0.72						
Gd							
Tb	0.76						
Dy							
Ho							
Er							
Tm							
Yb	2.67						
Lu	0.396						
$(^{87}Sr / ^{86}Sr)_m$	0.70641					0.7055	0.706289
$(^{143}Nd / ^{144}Nd)_m$	0.512787						0.512772
$(^{206}Pb / ^{204}Pb)_m$	18.862						
$(^{207}Pb / ^{204}Pb)_m$	15.599						
$(^{207}Pb / ^{204}Pb)_m$	38.699						

Table 3. (Continued.)

Sample:	NT35PB	NT35PV	NT35EC	NT35EM	NT35EN	NT35PN
Long. (°W):	–99.7	–99.7	–99.7	–99.7	–99.7	–99.7
Lat. (°N):	+19.1	+19.1	+19.1	+19.1	+19.1	+19.1
Area	Nevado de Toluca	Nevado de Toluca	Nevado de Toluca	Nevado de Toluca	Nevado de Toluca	Nevado de Toluca
Reference	Martínez-Serrano et al. (2004)	Martínez-Serrano et al. (2004)	Martínez-Serrano et al. (2004)	Martínez-Serrano et al. (2004)	Martínez-Serrano et al. (2004)	Martínez-Serrano et al. (2004)
Age	?	?	?	?	?	?
Material:	Phyllite	Phyllite	Chlorite schist	Gneiss	Schist	Phyllite
Rock type:	Metamorphic	Metamorphic	Metamorphic	Metamorphic	Metamorphic	Metamorphic
Rb	111.71	115.72	31.88	89.66	124.88	125.28
Sr	54.7	113.9	199.5	40.95	57.89	90.17
Nd	25.24	15.64	12.76	18.9	25.18	30.42
Sm	4.57	3.28	3.04	3.47	4.53	5.73
$(^{87}Sr / ^{86}Sr)_m$	0.721094	0.716173	0.705727	0.721883	0.707108	0.715649
$(^{143}Nd / ^{144}Nd)_m$	0.512261	0.512331	0.512673	0.512248	0.512422	0.512259
$(^{206}Pb / ^{204}Pb)_m$	18.984	19.021	18.864	19.036	19.1	19.025
$(^{207}Pb / ^{204}Pb)_m$	15.631	15.69	15.632	15.694	15.679	15.675
$(^{207}Pb / ^{204}Pb)_m$	39.114	39.162	38.713	39.256	39.224	39.223

More explanation in the footnote of Table 1.

for this standard. Only the measured adjusted ratios were reported; the initial ratios could not be accurately estimated because precise radiometric age data for these Neogene (probably Pliocene to Pleistocene) samples are not individually available. The initial isotopic ratios for some samples, especially $^{87}Sr/^{86}Sr$ in the acid magma types, could be significantly affected by radiogenic in situ growth correction.

4. Databases and data processing methods

4.1. Central part of the Mexican Volcanic Belt (C-MVB) and Central American Volcanic Arc (CAVA)

Additional geochemical data from the C-MVB were compiled from the following sources (listed in alphabetical order): Aguirre-Diaz (2001); Aguirre-Diaz and López-Martínez (2009); Aguirre-Díaz and McDowell (1999), Aguirre-Díaz et al. (2002); Agustín-Flores et al. (2011); Arce et al. (2003, 2005, 2008, 2013); Blatter and Hammersley (2010); Blatter et al. (2001, 2007)**;** Bloomfield (1973, 1975); Boudal (1985); Cai et al. (2014); Capra et al. (1997); Carmichael et al. (2006); Cathelineau et al. (1987, 1991); Cavazos Tovar (2006); Chesley et al. (2002); D'Antonio (2008) including the compiled data therein; Delgado et al. (1998); Demant (1981); Dobson and Mahood (1985); Ferrari et al. (1994, 2000); García-Palomo et al. (2002a, 2002b); García Tovar (2009); Gómez-Tuena et al. (2007b); Guilbaud et al. (2009); Gunn and Mooser (1971); Hasenaka (1992); Hernández Rojas (2007); Koloskov and Khubunaya (2013); Larocque et al. (1998); Luhr and Carmichael (1985); Martin del Pozzo (1989); Martínez-Serrano et al. (2004); Meriggi et al. (2008); Mukasa et al. (2007); Negendank (1972); Nixon (1988a, 1989); Pérez et al. (1979); Pradal and Robin (1994); Robin (1984); Rueda et al. (2013); Schaaf et al. (2005); Siebe et al. (1999, 2004); Silva Mora (1988); Straub and Martin del Pozo (2001); Straub et al. (2008); Swinamer (1989); Torres-Alvarado et al. (2011); Velasco-Tapia (2014); Velasco-Tapia and Verma (2001a, 2013, 2014); Velasco-Tapia et al. (2013); Verma (1999, 2000a, 2001a, 2001b, 2002, 2003); Verma and Carrasco-Núñez (2003); Verma and Hasenaka (2004); Verma et al. (1991, 2005); and Wallace and Carmichael (1999).

The samples used for geochemical studies are seldom radiometrically dated, and no separation according to the age can, therefore, be easily done. Some of the Popocatépetl samples are as young as a few years. Nevertheless, most of the samples span a narrow range of less than 5 m.y. (Pliocene to Holocene), and all are treated together. There is no age-specific difference between the basic and evolved rocks; all magma types from basic to acid are considered contemporary. Furthermore, no geographic distinction can be made among the different magma types.

The CAVA data were compiled from the following sources: Agostini et al. (2006); Alvarado et al. (2006); Avellán et al. (2012); Bardintzeff and Deniel (1992); Bolge et al. (2006); Cameron et al. (2002); Carr (1984); Carr et al. (1990); Chan et al. (1999); Duffield et al. (1992); González Partida et al. (1997); Hazlett (1987); La Femina et al. (2004); Mora et al. (2004); Pardo et al. (2008); Patino et al. (1997, 2000); Rotolo and Castorina (1998); Ryder et al.

(2006); Singer et al. (2011); Sussman (1985); and Walker et al. (1990, 2000, 2001).

For the classification of fresh volcanic rocks, the well-known total alkalis versus silica (TAS) diagram (Le Bas et al., 1986; Le Bas, 2000; Le Maitre et al., 2002) proposed by the International Union of Geological Sciences (IUGS) is extensively used. For rock classification based on the IUGS scheme and CIPW norm computation, a new computer program, IgRoCS (Verma and Rivera-Gómez, 2013b), which supersedes SINCLAS (Verma et al., 2002, 2003), was used under the Middlemost option for Fe-oxidation ratio adjustment (Middlemost, 1989). This not only rendered a highly uniform treatment for the complete datasets but also made the rock nomenclature fully consistent with the IUGS.

To better understand and evaluate different petrogenetic models, the datasets for the C-MVB and CAVA were subdivided into two subsets each as follows: the nomenclature used for the C-MVB is near the trench and far from the trench samples (Figure 2) and for the CAVA it is the volcanic front or front-arc and behind the volcanic front or back-arc samples (Figure 3).

4.2. Other arcs, continental rifts or extensional areas, and collision zones

Major and trace element data for both continental and island arcs were compiled from relevant sources as follows: 1) Continental arc of the Andes in Chile (Davidson et al., 1988; Frey et al., 1984; Hickey et al., 1986; Gerlach et al., 1988; Hickey-Vargas et al., 1989; Tormey et al., 1991; Vergara et al., 1991, 2004; Trumbull et al., 1999; Mattioli et al., 2006; Rodríguez et al., 2007; Vezzoli et al., 2008); 2) Continental arc of the Andes in Peru (Lebti et al., 2006); 3) Continental arc of the Andes in Ecuador (Beate et al., 2001; Samaniego et al., 2005, 2011; Bryant et al., 2006; Hidalgo et al., 2007; Hoffer et al., 2008; Robin et al., 2009; Chiaradia et al., 2011); 4) Continental arc of the Andes in Colombia (Calvache and Williams, 1997); 5) Aleutian arc (Nye and Reid, 1986; Romick et al., 1990; Kay and Kay, 1994; Dreher et al., 2005; Finney et al., 2008); 6) Barren Island, Andaman Sea, Indian Ocean (Alam et al., 2004; Luhr and Haldar, 2006); 7) Fiji Islands (Rogers and Setterfield, 1994); 8) Hokkaido, Japan (Hoang et al., 2011; Takanashi et al., 2011; Ayabe et al., 2012; Feineman et al., 2013); 9) Izu-Bonin arc, Japan (Tamura et al., 2005; Shukuno et al., 2006; Kimura et al., 2010); 10) Japan arc (Sakuyama and Nesbitt, 1986; Tamura et al., 2003; Moriguti et al., 2004; Kimura and Yoshida, 2006; Tatsumi et al., 2008; Ohba et al., 2009); 11) Indonesia (Stolz et al., 1990; Tatsumi et al., 1991; van Bergen et al., 1992; Edwards et al., 1994; Hoogewerff et al., 1997; Turner and Foden, 2001; Gertisser and Keller, 2003; Chadwick et al., 2007; Handley et al., 2007; Sendjaja et al., 2009); 12) Lesser Antilles arc (Thirlwall and Graham, 1984; Thirlwall et al., 1996; Turner et al., 1996; Zellmer et al., 2003; Smith et al., 2004; Lindsay et al., 2005; Halama et al., 2006; Davidson and Wilson, 2011; Cassidy et al., 2012); 13) Kamchatka arc (Dorendorf et al., 2000; Churikova et al., 2001; Izbekov et al., 2004; Grib et al., 2009; Bindeman et al., 2010; Bryant et al., 2011); 14) Kermadec arc (Gamble et al., 1993, 1995; Haase et al., 2002; Smith et al., 2003, 2006); 15) Kurile arc (Martynov et al., 2010); 16) Mariana arc (Hole et al., 1984; Woodhead, 1988; Elliott et al., 1997; Wade et al., 2005); 17) Philippines arc (Bau and Knittel, 1993; Castillo and Newhall, 2004; DuFrane et al., 2006); 18) New Hebrides arc (Dupuy et al., 1982; Monzier et al., 1993, 1997); 19) North Island, New Zealand (Booden et al., 2011); 20) Ryukyu arc (Shinjo et al., 2000); 21) Taiwan (Lai et al., 2008); 22) Solomon Islands (Schuth et al., 2004; Chadwick et al., 2009; Petterson et al., 2011); 23) Tonga arc (Hergt and Woodhead, 2007); and 24) Vanuatu arc (Eggins, 1993; Peate et al., 1997; Raos and Crawford, 2004).

The continental rift setting was represented by well-developed rifts as well as extensional areas and postcollision extension zones as follows: 1) San Luis Potosí, Mexico – Neogene rocks (Aguillón-Robles et al., 2012, 2014); 2) Baja California, Mexico – Pliocene-Pleistocene as well as late Miocene (Calmus et al., 2003); 3) Mogollon-Datil volcanic field, New Mexico, USA (Davis and Hawkesworth, 1995); 4) NW Cerro del Rio, New Mexico, USA (Duncker et al., 1991); 5) Basin and Range, Nevada-Arizona, USA (Fitton et al., 1991; Feuerbach et al., 1993); 6) Rio Grande rift, New Mexico, USA (Gibson et al., 1992; McMillan et al., 2000); 7) San Juan volcanic field, Colorado, USA (Parat et al., 2005); 8) Hurricane volcanic field, Utah, USA (Smith et al., 1999); 9) Santa Rosa Calico volcanic field, Nevada, USA (Brueseke and Hart, 2009); 10) Western USA (Leat et al., 1989; Kempton et al., 1991); 11) Northwest Iran (Kheirkhah et al., 2009); 12) Eastern Iran (Pang et al., 2012); 13) Postcollision extensional Miocene-Holocene rocks from Western and Northwestern Anatolia, Turkey (Aldanmaz et al., 2000; Akal, 2003; Agostini et al., 2007, 2010); 14) Postcollision extensional Miocene-Holocene rocks from Eastern Anatolia, Turkey (Karsli et al., 2008; Varol and Alpaslan, 2012); 15) North and Northeast China (Zhang et al., 1995; Han et al., 1999); 16) Postcollision extensional Miocene rocks from the Lhasa terrane, Tibet (Chen et al., 2010); 17) Postcollision extensional Miocene-Pleistocene rocks from Central and Southern Tibet (Turner et al., 1993; Zhidan et al., 2001; Hou et al., 2004; Zhao et al., 2009); 18) Morocco and Mali, NW Africa (Bertrand, 1991); 19) Djibouti, Africa – negative Nb anomaly (Daoud et al., 2010); 20) Djibouti, Africa – positive Nb anomaly (Barrat et al., 1993); 21) Ethiopian rift, Africa – negative Nb anomaly (Class et al., 1994; Barrat et al. 2003; Beccaluva et al., 2009); 22) Ethiopian rift, Africa – positive Nb anomaly (Class et al., 1994; Barrat et al., 2003; Beccaluva et al., 2009); 23) Massif Central, France (Chauvel and Jahn, 1984); and 24) Saudi Arabia (Camp et al., 1991).

Finally, for representing collision zones, geochemical data were compiled for Cretaceous to Paleogene rocks from the following areas and sources: 1) Central Anatolia, Turkey (Ilbeyli et al., 2004); 2) Western Anatolia, Turkey (Koprubasi and Aldanmaz, 2004); 3) Ulubey, Turkey (Temizel et al., 2012); 4) Western Pontides, Turkey (Karsli et al., 2011); 5) Lesser Caucasus, Azerbaijan (Dilek et al., 2010); and 6) Himalayas and Tibet (Harris et al., 1988; Mo et al., 2007, 2008; Zheng et al., 2012).

Some localities such as Anatolia and Tibet represent time-related tectonic settings that were appropriately assigned. All compiled data were processed by IgRoCS (Verma and Rivera-Gómez, 2013b) in the same way as done for the C-MVB and CAVA. All databases were then handled by other computer programs, i.e. DODESSYS, TecD, and TecDIA. All these programs will be available from the website Tlaloc.

5. Results

5.1. Rock types

The TAS diagram is shown in Figure 5a for the C-MVB and Figure 5b for the CAVA. The near the trench and far from the trench rock types from the C-MVB are distinguished by using two different symbols, which show a considerable overlap for all kinds of magmas from basic to acid present in both segments (Figure 5a). In the CAVA, on the other hand, all kinds of magmas have been analyzed from the volcanic front or front-arc area but only basic and intermediate magmas from the back-arc region (Figure 5b). This contrasting observation is also confirmed from the synthesis of magma and rock types for these two volcanic provinces (Table 4). Full distribution of all rock types for 2140 and 725 samples, respectively, from the C-MVB and CAVA is presented in Table 4. Some rock samples from the C-MVB, whose coordinates could not be deduced from the original authors' descriptions, are not included in this synthesis.

5.2. Normalized Masuda–Coryell plots for the rare-earth elements

Average values of chondrite-normalized rare-earth elements (REEs) were used to schematically show the relationships of the patterns for basic to intermediate rocks from the C-MVB and CAVA in Figures 6a and 6b, respectively. The information on the number of samples used for each magma type is also included along with the average adjusted SiO_2 concentration (Figures 6a and 6b).

In the C-MVB, the concentrations of REEs do not increase in the sequence of basic, intermediate, and acid magmas (Figure 6a), which implies that these magma types are not likely to be related through a simple differentiation process, such as fractional crystallization without crustal assimilation. The concentrations of the REEs, being incompatible elements, are likely to increase in fractional crystallization from basic to intermediate to acid (e.g., Rollinson 1993; Torres-Alvarado et al., 2003), which is simply not observed. Crustal assimilation could,

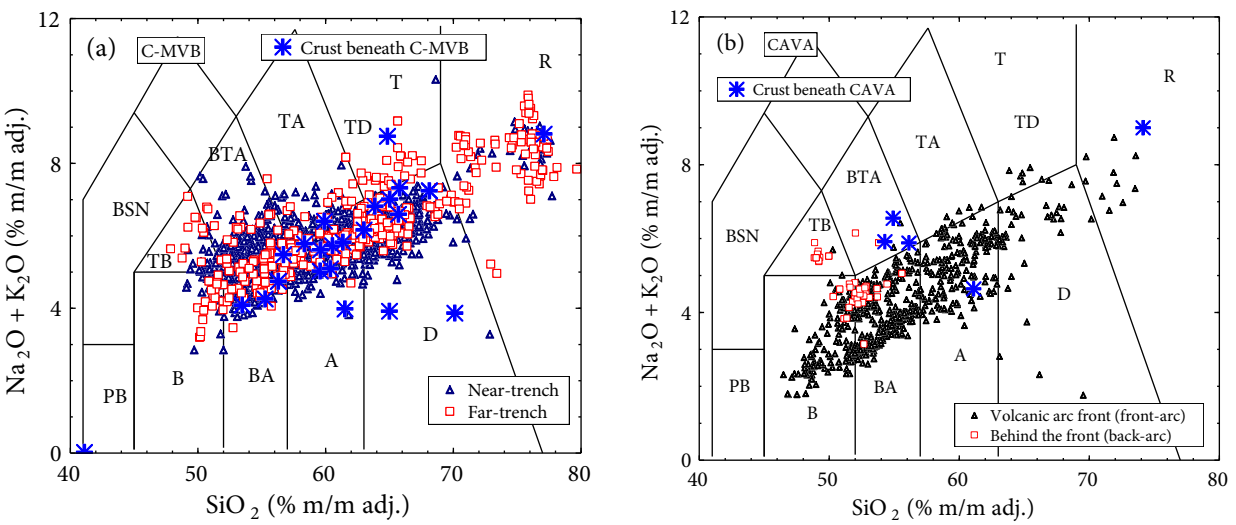

Figure 5. Total alkalis $(Na_2O + K_2O)_{adj}$ versus silica $(SiO_2)_{adj}$ (TAS) diagram (Le Bas et al., 1986) for igneous rocks of **(a)** the central part of the Mexican Volcanic Belt (C-MVB) and **(b)** the Central American Volcanic Arc (CAVA); %m/m is the recommended name of the wt.% unit and adj. refers to the adjusted concentrations from the SINCLAS program (Verma et al., 2002); the symbols used are shown as insets, crustal rocks represent xenolith and plutonic as well as sedimentary rocks. The rock names are: PB–picrobasalt; B–basalt; A–andesite; D–dacite; R–rhyolite; BSN–basanite; TB–trachybasalt; BTA–basaltic trachyandesite; TA–trachyandesite; TD–trachydacite; T–trachyte; the magma types are basic– <52% $(SiO_2)_{adj}$; intermediate– 52%–63% $(SiO_2)_{adj}$; acid– >63% $(SiO_2)_{adj}$.

Table 4. Rock and magma type distribution of compiled samples from the central part of the Mexican Volcanic Belt (C-MVB) and Central American Volcanic Arc (CAVA).

Magma and rock type	C-MVB			CAVA		
	Near trench	Far from the trench	Total	Main arc	Back arc	Total
Basic	75	32	107	154	29	183
Alkali basalt	4	–––	4	4	–––	4
Subalkali basalt	34	19	53	148	15	163
Basaltic trachyandesite, mugearite	11	2	13	–––	–––	–––
Basaltic trachyandesite, shoshonite	–––	2	2	–––	–––	–––
Trachybasalt, hawaiite	25	4	29	1	11	12
Potassic trachybasalt	1	5	6	1	3	4
Intermediate	1165	169	1334	468	20	488
Basaltic andesite	307	56	363	300	17	317
Andesite	635	77	712	155	–––	155
Basaltic trachyandesite, mugearite	142	9	151	2	1	3
Basaltic trachyandesite, shoshonite	23	7	30	–––	2	2
Trachyandesite, benmoreite	30	9	39	10	–––	10
Trachyandesite, latite	28	9	37	1	–––	1
Trachyte	–––	2	2	–––	–––	–––
Acid	513	186	699	54	–––	54
Dacite	475	86	561	38	–––	38
Rhyolite	37	78	115	10	–––	10
Trachydacite	–––	7	7	–––	–––	–––
Trachyte	1	15	16	6	–––	6
Total number of samples	1753	387	2140	676	49	725

therefore, be an important petrogenetic process in the C-MVB. The patterns for crustal rocks having generally lower normalized concentrations (Figure 6a) also indicate that the assimilation combined with fractional crystallization or mixing of magmas from mantle and crustal sources could be an appropriate petrogenetic process. The latter would be true if acid magmas represent crustal partial melts and intermediate types define hybrid melts from the combination of basic and acid magmas as originally suggested by Verma (1999, 2000a) for the Sierra de Chichinautzin at the volcanic front of the C-MVB and later confirmed by Velasco-Tapia and Verma (2013).

The REE patterns of average magmas in the CAVA (Figure 6b), on the other hand, seem to be more consistent with the fractional crystallization as the dominant differentiation process although, from quantitative estimates, crustal assimilation would also be required to a lesser degree than for the C-MVB.

The radiogenic Sr and Nd isotope data presented below confirm these statements for the C-MVB and CAVA.

5.3. Multielement normalized diagrams

Selected elements in basic to acid magmas from the C-MVB and CAVA are plotted in normalized diagrams of Figures 7a and 7b, respectively. The near the trench and far from the trench basic rocks from the C-MVB (Figure 7a) and front-arc and back-arc basic rocks from the CAVA (Figure 7b) show a contrasting behavior of the Nb anomaly with respect to a large-ion lithophile element Ba and a light rare-earth element La. The basic magmas from the C-MVB show a similar behavior for both near the trench and far from the trench areas, whereas the CAVA front-arc and back-arc rocks do not; the Nb anomaly is negative for the CAVA volcanic front, but it is positive, on the average, for the back-arc rocks.

A comparison of the C-MVB intermediate and acid magmas with the respective basic types shows that the concentrations of the incompatible high-field strength elements Nb and Ta are lower in the former. The evolved C-MVB rocks have larger negative Nb and Ta anomalies (Figure 7a). Again, this behavior is inconsistent with a simple fractional crystallization process for basic to acid magmas, and crustal assimilation will be required to explain them (Verma, 1999, 2000a, 2001b, 2015a; Velasco-Tapia and Verma, 2013). However, in the CAVA, the behavior of Nb and Ta seems to be more consistent with a simpler petrogenetic relationship among these magma types (Figure 7b) than in the C-MVB.

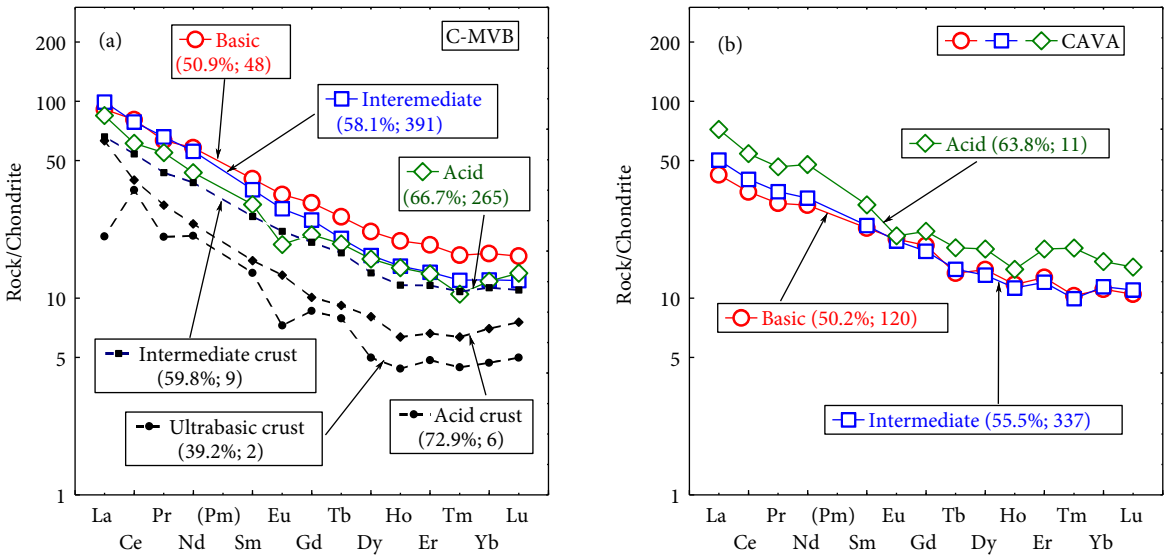

Figure 6. Masuda–Coryell normalized plots for rare-earth elements in basic to acid magmas from **(a)** the central part of the Mexican Volcanic Belt (C-MVB) and **(b)** the Central American Volcanic Arc (CAVA); the normalizing values are from McDonough and Sun (1995); for the C-MVB average values of different types of underlying continental crust area are also plotted in (a).

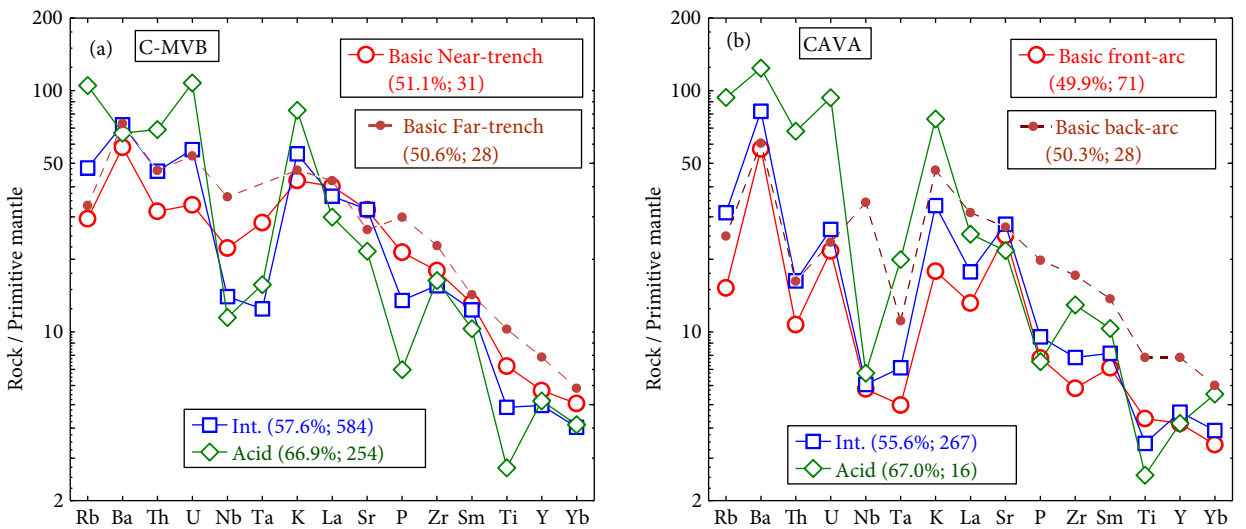

Figure 7. Multielement normalized diagrams for selected elements in basic to acid magmas from **(a)** the central part of the Mexican Volcanic Belt (C-MVB) and **(b)** the Central American Volcanic Arc (CAVA); the normalizing values are from Sun and McDonough (1989); for both provinces, the near the trench (Near-trench) and far from the trench (Far-trench) or volcanic front (front-arc) and behind the volcanic front (back-arc) basic magmas are separately plotted.

5.4. Radiogenic isotopes of Sr, Nd, and Pb

The average values of $^{87}Sr/^{86}Sr$ and $^{143}Nd/^{144}Nd$ for the three magma types (basic, intermediate, and acid) from the C-MVB and CAVA are plotted in Figure 8. The data for near the trench or front-arc and far from the trench or back-arc (Figure 3) are distinguished by different symbols. The data from the C-MVB plot within the "mantle array" whereas those from the CAVA, except for intermediate magmas from the back-arc region, show relatively higher $^{143}Nd/^{144}Nd$ than the C-MVB. The mean isotopic compositions for all three magma types from the CAVA front-arc as compared to the back-arc are shifted towards the composition of the downgoing slab. The mean isotopic composition of the CAVA intermediate magmas from the back-arc region overlap with the intermediate and acid magmas from near the trench region of the C-MVB.

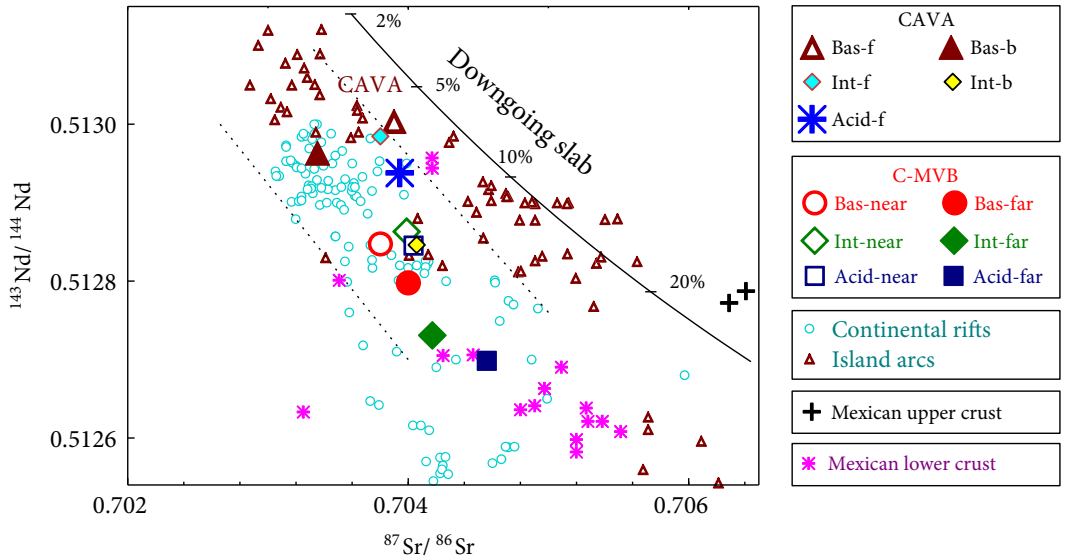

Figure 8. The $^{87}Sr/^{86}Sr$–$^{143}Nd/^{144}Nd$ diagram for the central part of the Mexican Volcanic Belt (C-MVB) and Central American Volcanic Arc (CAVA); for comparison are included compiled data from continental rifts, island arcs, and Mexican lower and upper crust as well as the trace of the mantle array (Faure, 1986) and mixing curve for MORB-sediments from the subducting Cocos plate (the 2% to 20% values on this curve represent the percentage of sediments in the mixture; Verma, 2000a); the symbols are shown in insets; the abbreviations are as follows: Bas–basic; Int–intermediate; for the C-MVB, near–near the trench and far–far from the trench; for the CAVA, f–volcanic front (front-arc) and b– behind the arc (back-arc).

Thus, the influence of the subducted slab seems to be clearly observed for the front-arc magmas of the CAVA. It is not so clear for the C-MVB because both sets of mean compositions from near and far from the trench plot well within the mantle array and away from the mixing curve for MORB and sediments from the Cocos plate. The worldwide continental rift and island arc data also support this distinction (Figure 8). Furthermore, the C-MVB mean isotopic data are similar to the crustal compositions, especially the Mexican lower crust (Figure 8).

Four bivariate plots of Sr, Nd, and Pb isotopic compositions of the C-MVB and CAVA magmas are also shown in Figures 8a–8d. The C-MVB samples show generally overlapping isotopic compositions, except for $^{143}Nd/^{144}Nd$. They also plot somewhat away from the mixing curves for the downgoing slab. The isotopic compositions of the crustal rocks beneath the C-MVB overlap mostly with the C-MVB magma compositions.

A simple examination of Figure 9 shows that the $^{143}Nd/^{144}Nd$ values of the C-MVB magmas would require about 10%–20% or more sediment to 90%–80% or less MORB mixture (Cocos plate; Verma, 2000a). The Pb isotopic ratios ($^{206}Pb/^{204}Pb$, $^{207}Pb/^{204}Pb$, and $^{208}Pb/^{204}Pb$), on the contrary, would be consistent with only about 1%–2% or less sediment to 99%–98% or more MORB proportions (Figures 9c and 9d). The $^{87}Sr/^{86}Sr$ of the C-MVB magmas (Figure 9a) would be significantly lower than the 10%–20% sediment contributions required by $^{143}Nd/^{144}Nd$ but significantly higher than the 1%–2% necessary for the Pb isotopes. Therefore, with such different proportions of sediments required in the altered MORB-sediment mixture, the involvement of the subducted slab cannot easily explain the combined Sr, Nd, and Pb isotope data (Figures 8 and 9). The CAVA isotopic data, on the other hand, require relatively small (about 1%–10% sediments in the MORB-sediment mixture representing the downgoing slab; Figures 8 and 9a–9d) and are internally consistent with derivation from the involvement of the subducted Cocos plate.

5.5. Tectonomagmatic discrimination diagrams

One hundred DF1-DF2 equations for three subcompositions of 50 diagrams were listed in the respective papers (Verma et al., 2006, 2012, 2013; Agrawal et al., 2008; Verma and Agrawal, 2011; Verma SP and Verma SK, 2013). They were also recently reproduced by Verma SP et al. (2015a, 2015b) in a supplementary data file. These subcompositions can be classified into three

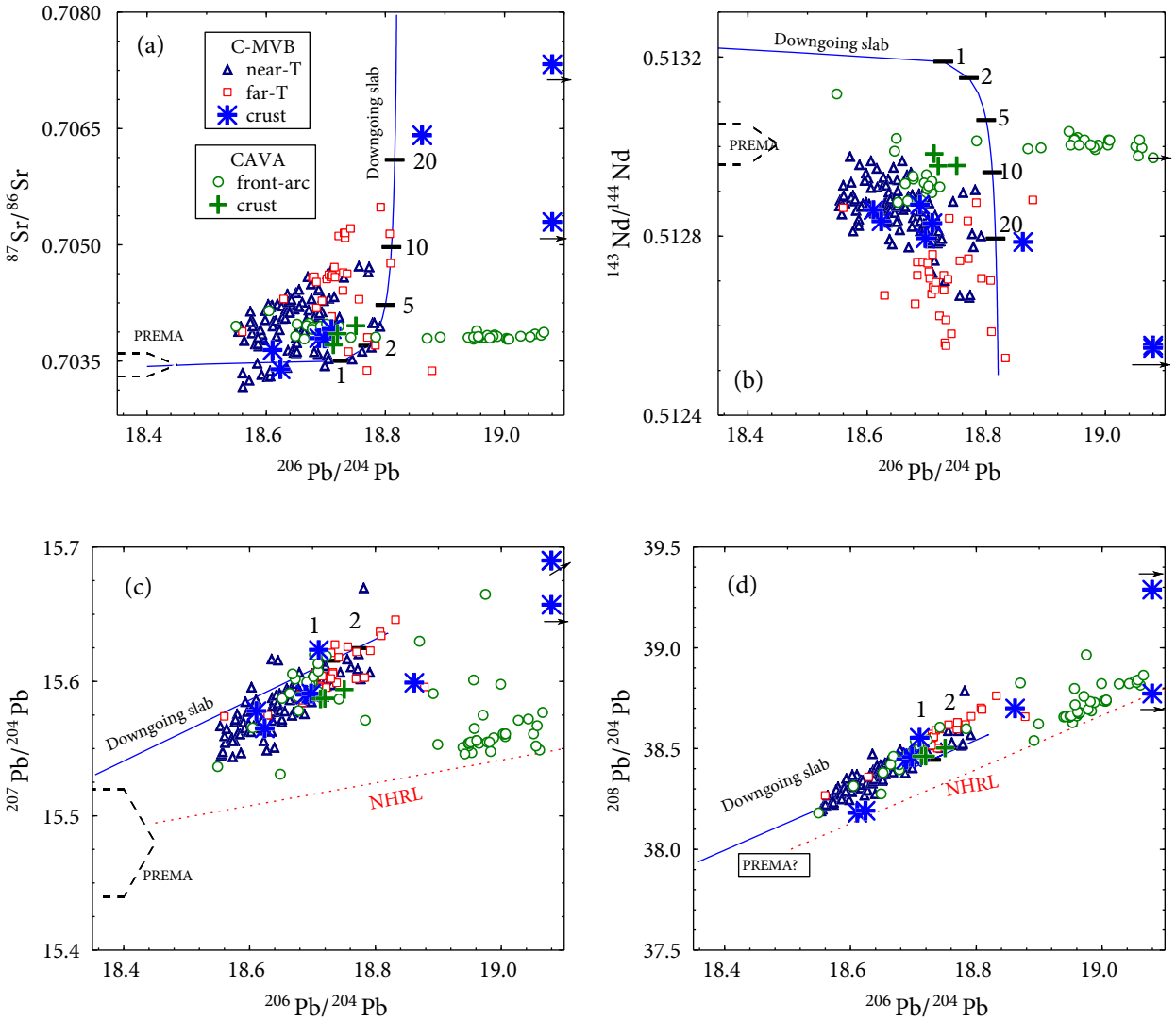

Figure 9. The Sr-Nd-Pb bivariate isotope diagrams for the central part of the Mexican Volcanic Belt (C-MVB) and Central American Volcanic Arc (CAVA). The symbols are shown as insets in (a); the downgoing slab composition is shown for MORB-sediment mixtures (Verma, 2000a); the tick marks are for 1%, 2%, 5%, 10%, and 20% sediment component; PREMA–prevalent mantle average composition; NHRL–northern hemisphere reference line from Hart (1984) included in Pb-Pb plots. **(a)** $^{206}Pb/^{204}Pb$–$^{87}Sr/^{86}Sr$; **(b)** $^{206}Pb/^{204}Pb$–$^{143}Nd/^{144}Nd$; **(c)** $^{206}Pb/^{204}Pb$–$^{207}Pb/^{204}Pb$; and **(d)** $^{206}Pb/^{204}Pb$–$^{208}Pb/^{204}Pb$.

groups: 1) all 11 major elements or oxides; 2) selected major and trace elements; and 3) selected trace elements. For sedimentary rocks as well, multidimensional tectonic discrimination diagrams are beginning to be proposed (Verma and Armstrong-Altrin, 2013) and used (e.g., Absar and Sreenivas, 2015; Armstrong, 2015; Bouyo et al., 2015; Zaid, 2015a, 2015b; Zaid and Gahtani, 2015; Zaid et al., 2015). The multidimensional diagrams for igneous rocks have been successfully tested and used by numerous researchers (e.g., Sheth, 2008; Pandarinath and Verma, 2013; Verma and Oliveira, 2013, 2015; Verma, 2013; Verma SK and Verma SP, 2013; Pandarinath, 2014a, 2014b; Bora and Kumar, 2015; Kaur et al., 2015; Rahman and Mondal, 2015; Srivastava et al., 2015; Verma SK et al., 2015).

The probability calculations are the same as those reported earlier (Verma and Agrawal, 2011; Verma, 2012b; Verma et al., 2012, 2013; Verma SP and Verma SK, 2013). To keep the presentation short and for illustration purposes, just two equations for the first diagram (IAB-CRB-OIB-MORB) of Verma et al. (2006), based on adjusted major-element natural log-ratios (where the subscript $_{adj}$ is eliminated for simplicity and the subscript $_{m2}$ represents the second set of adjusted major element-based diagrams), are:

$$DF1_{(IAB\text{-}CRB\text{-}OIB\text{-}MORB)_{m2}} = -4.676\times\ln(TiO_2/SiO_2) + 2.533\times\ln(Al_2O_3/SiO_2) - 0.388\times\ln(Fe_2O_3/SiO_2) + 3.969\times\ln(FeO/SiO_2) + 0.898\times\ln(MnO/SiO_2) - 0.583\times\ln(MgO/SiO_2) - 0.290\times\ln(CaO/SiO_2) - 0.270\times\ln(Na_2O/SiO_2) + 1.081\times\ln(K_2O/SiO_2) + 0.184\times\ln(P_2O_5/SiO_2) + 1.544, \quad (1)$$

$$DF2_{(IAB\text{-}CRB\text{-}OIB\text{-}MORB)_{m2}} = 0.675\times\ln(TiO_2/SiO_2) + 4.590\times\ln(Al_2O_3/SiO_2) + 2.090\times\ln(Fe_2O_3/SiO_2) + 0.851\times\ln(FeO/SiO_2) - 0.433\times\ln(MnO/SiO_2) + 1.483\times\ln(MgO/SiO_2) - 2.363\times\ln(CaO/SiO_2) - 1.656\times\ln(Na_2O/SiO_2) - 0.676\times\ln(K_2O/SiO_2) + 0.413\times\ln(P_2O_5/SiO_2) + 13.164. \quad (2)$$

After ascertaining the magma types as basic or ultrabasic, intermediate, and acid varieties, the appropriate tectonomagmatic discrimination diagrams were applied. The respective probabilities were calculated for intermediate and acid diagrams. For each diagram set for basic magmas, however, a synthesis of samples plotting in different tectonic fields was prepared for all five diagrams. The two computer programs, TecD for basic and ultrabasic and TecDIA for intermediate and acid magma types, are extremely useful for automatically computing these percent values and obtaining inferences and tables.

Because a given tectonic setting is absent from one of the five diagrams for basic and ultrabasic rocks, the maximum percent value can only be about 80% in case all samples plotted in that particular setting in the remaining four diagrams. For the diagram sets of intermediate and acid magmas, the synthesis of percent values are calculated for sample probabilities instead of the sample counting; the maximum percent probability value for a given tectonic setting could be more than 80% provided most samples plot well within this field and the remaining ones plot nearer the tectonic field boundary in other fields. Thus, because a synthesis of percent values can be computed for all five diagrams in a given set, it is not necessary to actually plot the samples in the various diagrams as recently confirmed by Verma (2012b) and Verma SP et al. (2015b). Therefore, only one set of diagrams will be presented (Figure 10) for illustration purposes.

5.5.1. Central part of the Mexican Volcanic Belt (C-MVB)

The five diagrams for basic rocks based on log-ratio transformation of adjusted major elements (Verma et al., 2006) are shown in Figures 10a–10e for such rocks from the C-MVB. The results are summarized in Table 5. This set will be described in greater detail. Out of 116 rock samples (equivalent to 100%), 95 samples (amounting to about 82%; Table 5) plotted in the CRB field in the first diagram of IAB-CRB-OIB-MORB (Figure 10a); the remaining 21 samples plotted in the other three fields. Note that it is difficult to actually count so many samples in a given diagram, most of which might be overlapping; therefore, as stated before, the computer program TecD is very useful for counting and preparing the synthesis presented in Table 5. The number of basic rock samples for the far from the trench region is considerably less (n = 33) than that for the near the trench region (n = 80). No attempt was made to separately consider them in this discussion although the conclusions will not change even if they were considered separately.

The by-chance probability of this particular diagram (Figure 10a) for a given field is only about 25%. For the CRB field only, the probability of samples (82%) plotting in this field far exceeded the by-chance probability of 25%; for the other three fields, the probability of samples (1% to 11%) was significantly less than this by-chance probability (Figure 10a; Table 5). It is pertinent to point out that equal by-chance probability values for each tectonic field were assumed during the proposal of multidimensional diagrams, which will amount to 25% when four tectonic fields are under consideration in a given diagram (Verma et al., 2006). The other four diagrams (Figures 10b to 10e) are for three fields at a time and complete all the combinations of these tectonic settings. In three of these four diagrams (Figures 10b, 10c, and 10e), the total probability of samples for the CRB field was very high (amounting to about 86% to 90%; Table 5). In the diagram that does not have this particular tectonic setting (Figure 10d), the samples were distributed among the other three tectonic settings (MORB with about 47%; IAB, which is actually the combined island and continental arc setting, with about 35%; and the OIB with about 18%; Table 5).

The overall synthesis, also computed from TecD, for all five diagrams (Figures 10a to 10e; Table 5) indicated that, out of the total of 580 points (equivalent to 100%), 404 of them plotted in the CRB field (equivalent to about 70%), with the remaining three fields with probabilities of about 4% to 14% amounting to significantly less than the by-chance probability of about 25% for the combination of all five diagrams discriminating four tectonic fields. Thus, all five diagrams based on log-ratios of adjusted major elements (Figures 10a–10e) clearly indicated a continental rift setting (CRB; Table 5) for basic magmas of the C-MVB.

Having described the use of these multidimensional

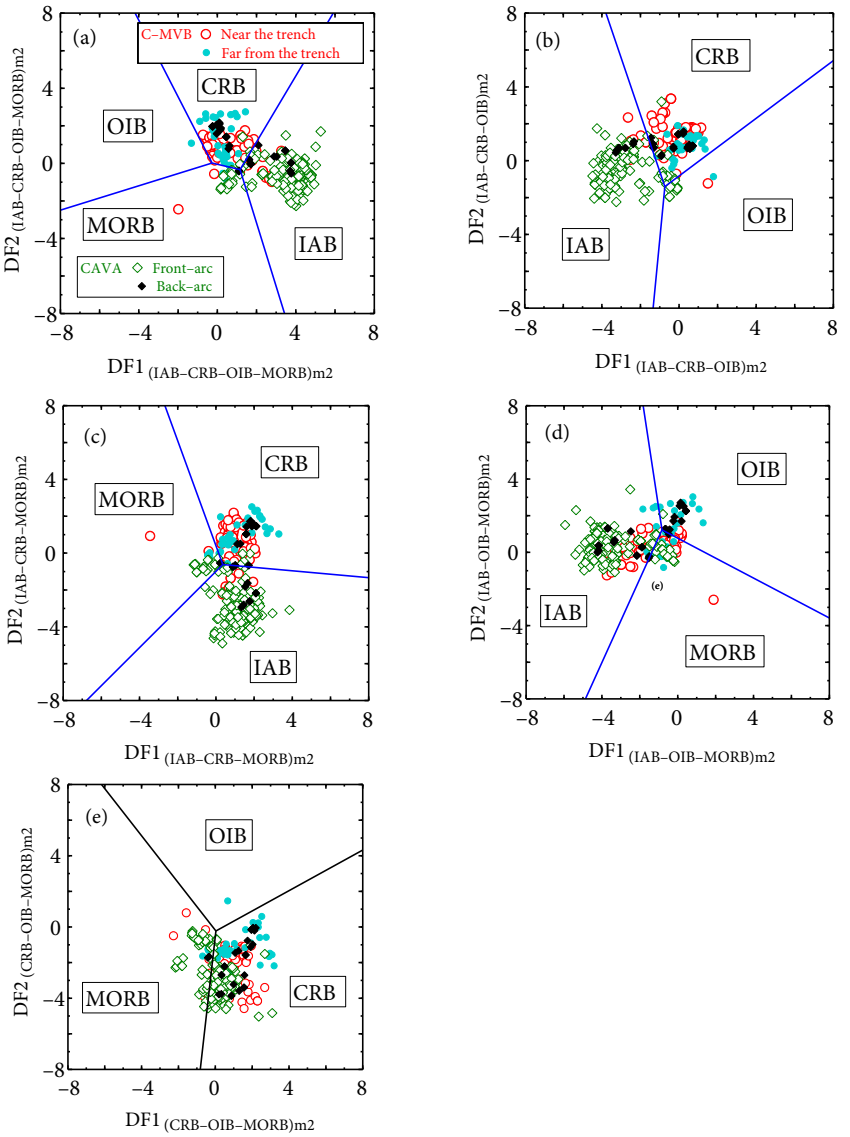

Figure 10. Multidimensional tectonomagmatic diagrams based on log-ratios of major elements (Verma et al., 2006) for the C-MVB and CAVA basic magmas. Note that the near the trench and far from the trench magmas from the C-MVB and the front-arc and back-arc magmas for the CAVA are distinguished in these plots. The four tectonic settings discriminated in these diagrams are: IAB–island (or continental) arc basic rocks; CRB–continental rift basic rocks; OIB–ocean island basic rocks; and MORB–mid-ocean ridge basic rocks. Note also that both sets of the C-MVB samples plot in the CRB field in all diagrams in which this setting is present, whereas the CAVA samples (especially the front-arc) confirm their arc setting in the diagrams in which IAB setting is included. **(a)** IAB-CRB-OIB-MORB; **(b)** IAB-CRB-OIB; **(c)** IAB-CRB-MORB; **(d)** IAB-OIB-MORB; and **(e)** CRB-OIB-MORB.

diagrams in great detail for the first set, the remaining results will only be briefly mentioned. The set of diagrams based on log-ratios of relatively immobile trace elements also supported this conclusion for basic magmas, because these diagrams indicated a CRB setting with total percent probability of about 71% (Table 5).

The third set of diagrams based on a combination of immobile major and trace elements also indicated a CRB setting but with a much lower percent probability of about 42%. Note that the next highest total percent probability value of about 26% was for the MORB setting, but this value is similar to the by-chance probability of 25% (Table 5).

Table 5. Application of multidimensional diagrams for deciphering tectonic setting of Neogene basic magmas from the central part of the Mexican Volcanic Belt (C-MVB).

Figure reference; figure type; figure no.	Discrimination diagram §	Total no. of samples (%)	Predicted tectonic affinity and number of discriminated samples (%)				
			IAB	CRB+OIB	CRB	OIB	MORB
Verma et al. (2006); log-ratios of major elements (m2); Figure 9	IAB–CRB–OIB–MORB	116 (100)	13 (11.2)	–––	95 (81.9)	1 (0.9)	7 (6)
	IAB–CRB–OIB	116 (100)	9 (7.8)	–––	105 (90.5)	2 (1.7)	–––
	IAB–CRB–MORB	116 (100)	9 (7.8)	–––	100 (86.2)	–––	7 (6)
	IAB–OIB–MORB	116 (100)	40 (34.5)	–––	–––	21 (18.1)	55 (47.4)
	CRB–OIB–MORB	116 (100)	–––	–––	104 (89.7)	1 (0.9)	11 (9.5)
C-MVB: Synthesis of all five diagrams of Verma et al. (2006)		580 (100)	71 (12.2)	–––	404 (69.7)	25 (4.3)	80 (13.8)
Agrawal et al. (2008); log–ratios of immobile trace elements (t1); no figure	IAB–CRB+OIB–MORB	21 (100)	0 (0)	19 (90)	–––	–––	2 (10)
	IAB–CRB–OIB	21 (100)	0 (0)	–––	20 (95)	1 (5)	–––
	IAB–CRB+ MORB	21 (100)	0 (0)	–––	20 (95)	–––	1 (5)
	IAB–OIB–MORB	21 (100)	0 (0)	–––	–––	10 (48)	11 (52)
	CRB–OIB–MORB	21 (100)	–––	–––	19 (90)	1 (5)	1 (5)
C-MVB: Synthesis of all five diagrams of Agrawal et al. (2008)		105 (100)	0 (0)	19 (–––)	75 (71.4)	15 (14.3)	15 (14.3)
Verma and Agrawal (2011); log-ratios of immobile major and trace elements (t2); no figure	IAB–CRB+OIB–MORB	116 (100)	11 (14.9)	40 (54.1)	–––	–––	23 (31.1)
	IAB–CRB–OIB	116 (100)	14 (18.9)	–––	44 (59.5)	16 (21.6)	–––
	IAB–CRB–MORB	116 (100)	10 (13.5)	–––	46 (62.2)	–––	18 (24.3)
	IAB–OIB–MORB	116 (100)	14 (18.9)	–––	–––	22 (29.7)	38 (51.4)
	CRB–OIB–MORB	116 (100)	–––	–––	37 (50)	18 (24.3)	19 (25.7)
C-MVB: Synthesis of all five diagrams of Verma and Agrawal (2011)		370 (100)	49 (13.2)	40 (–––)	155 (41.9)	68 (18.4)	98 (26.5)

§ IAB–island arc basic (or ultrabasic) rock (this is, in fact, the combined island and continental arc setting); CRB–continental rift basic (or ultrabasic) rock; OIB–ocean island basic (or ultrabasic) rock; MORB–mid-ocean ridge basic (or ultrabasic) rock.

Two sets of diagrams for intermediate magmas from the C-MVB indicated a transitional setting of continental arc to collision. In the first set, the total percent probability values were about 32% and 47%, respectively; in the third set they were about 35% and 40% (Table 6). The remaining set showed a transitional within-plate to collision setting with total percent probability values of about 27% and 47%, respectively (Table 6); this set can also be interpreted as indicating a collision setting for the C-MVB intermediate rocks because the value of 27% for the within-plate setting was close to the by-chance probability of 25%. The relatively low percent probability values of 27% to 32% for the within-plate setting and 47% for the collision setting also indicate a complex petrogenetic origin for the C-MVB intermediate magmas.

Three of the four sets of diagrams clearly indicated a continental arc setting for acid magmas from the C-MVB, with total percent probability values of about 69% to 77% (Verma et al., 2013; Table 7). The first set based on log-ratios of major elements (Verma et al., 2012) also suggested an arc setting but the distinction between the island and continental arcs was not clear (Table 7).

Now the question arises of whether the arc setting indicated for the C-MVB acid rocks is a true arc setting or is the consequence of their origin in the underlying crust. Verma SP et al. (2015b) documented the strengths and weaknesses of the discrimination diagrams and suggested that these diagrams should be used in conjunction with the evaluation of petrogenetic processes. Therefore, these contrasting results on the inferred tectonic setting for the three types of magmas from the C-MVB deserve further consideration (Section 6).

5.5.2. Central American Volcanic Arc (CAVA)

This volcanic province undoubtedly represents a subduction-related setting from several other independent lines of evidence (Molnar and Sykes, 1969; Carr et al., 1982, 2007; Burbach et al., 1984; Carr and Rose, 1986; Guzmán-Speziale et al., 2005; Walker et al., 2009).

Table 6. Application of multidimensional diagrams for deciphering tectonic setting of intermediate magmas from the central part of the Mexican Volcanic Belt (C-MVB).

Magma type; figure name; figure number	Figure type §	Total n umber of samples	Number of discriminated samples				
			Arc			Within-plate CR+	Collision
			IA + CA [$\overline{x} \pm s$] (p_{IA+CA}) Θ	IA [$\overline{x} \pm s$] [p_{IA}] Θ	CA [$\overline{x} \pm s$] [p_{CA}] Θ	OI [$\overline{x} \pm s$] [p_{CR+OI}] Θ	Col [$\overline{x} \pm s$] [p_{Col}] Θ
Intermediate; Verma and Verma (2013); log-ratios of all major elements (mint); no figure	IA+CA–CR+ OI–Col	1351	304 [0.679 ± 0.172] (0.3473–0.9785)	––	––	267 [0.711 ± 0.180] (0.3795–0.9908)	780 [0.755 ± 0.148] (0.3599–0.9999)
	IA–CA–CR+OI	1351	––	66 [0.599 ± 0.126] (0.4077–0.9549)	1030 [0.730 ± 0.133] (0.4059–0.9999)	255 [0.732 ± 0.183] (0.3886–0.9968)	––
	IA–CA–Col	1351	––	68 [0.670 ± 0.175] (0.3856–0.9985)	578 [0.632 ± 0.114] (0.3772–0.9454)	––	705 [0.693 ± 0.152] (0.3949–0.9979)
	IA–CR+OI–Col	1351	––	191 [0.676 ± 0.165] (0.3730–0.9745)	––	309 [0.715 ± 0.179] (0.3517–0.9942)	851 [0.816 ± 0.153] (0.3448–1.0000)
	CA–CR+OI–Col	1351	––	––	380 [0.640 ± 0.156] (0.3376–0.9711)	236 [0.685 ± 0.181] (0.3414–0.9998)	735 [0.703 ± 0.137] (0.3496–0.9734)
C-MVB: Diagrams based on log-ratios of major elements	{Σn} {Σprob} [%prob]	6755	{304} {206.2773} [–––]	{325} {214.2816} [5.0%]	{1988} {1360.8785} [31.9%]	{1067} {759.3741} [15.7%]	{3071} {2288.6058} [47.4%]
Intermediate; Verma and Verma (2013); log-ratios of immobile major and trace elements (mtint); no figure		725	114 [0.647 ± 0.146] (0.3485–0.9728)	––	––	200 [0.736 ± 0.174] (0.4099–0.9980)	411 [0.683 ± 0.139] (0.3558–0.9742)
	IA+CA–CR+ OI–Col	725	––	54 [0.590 ± 0.147] (0.3399–0.9096)	334 [0.629 ± 0.144] (0.3791–0.9870)	337 [0.752 ± 0.186] (0.3551–0.9994)	––
	IA–CA–CR+OI	725	––	27 [0.497 ± 0.103] (0.3371–0.7280)	205 [0.569 ± 0.128] (0.3499–0.9744)	––	493 [0.712 ± 0.163] (0.3559–0.9683)
	IA–CA–Col	725	––	90 [0.626 ± 0.140] (0.3676–0.9632)	––	205 [0.724 ± 0.173] (0.3817–0.9985)	430 [0.694 ± 0.133] (0.3418–0.9722)
	IA–CR+OI–Col	725	––	––	182 [0.729 ± 0.167] (0.3921–0.9991)	189 [0.724 ± 0.176] (0.3705–0.9990)	354 [0.723 ± 0.156] (0.3670–0.9922)
	CA–CR+OI–Col	725	114 [0.647 ± 0.146] (0.3485–0.9728)	––	––	200 [0.736 ± 0.174] (0.4099–0.9980)	411 [0.683 ± 0.139] (0.3558–0.9742)
C-MVB: Diagrams based on log-ratios of immobile major and trace elements	{Σn} {Σprob} [%prob]	3625	{114} {73.7275} [–––]	{171} {101.6670} [4.6%]	{721} {459.5937} [20.7%]	{931} {685.8711} [27.4%]	{1688} {1186.1752} [47.3%]
Intermediate; Verma and Verma (2013); log-ratios of immobile trace elements (tint); no figure	IA+CA–CR+ OI–Col	233	50 [0.590 ± 0.138] (0.3942–0.9243)	––	––	63 [0.736 ± 0.177] (0.3584–0.9996)	120 [0.755 ± 0.180] (0.3767– 1.0000)
	IA–CA–CR+OI	233	––	2 [0.484 ± 0.059] (0.4423, 0.5262)	159 [0.679 ± 0.167] (0.3948–0.9985)	72 [0.715 ± 0.143] (0.3840– 1.0000)	––
	IA–CA–Col	233	––	1 (0.4885)	119 [0.620 ± 0.120] (0.3821–0.8979)	––	113 [0.707 ± 0.179] (0.3934–0.9990)
	IA–CR+OI–Col	233	––	35 [0.590 ± 0.118] (0.3946–0.8721)	––	67 [0.748 ± 0.171] (0.3927–0.9988)	131 [0.780 ± 0.177] (0.3923–0.9999)
	CA–CR+OI–Col	233	––	––	111 [0.675 ± 0.137] (0.4265–0.9499)	49 [0.694 ± 0.170] (0.3658–0.9994)	73 [0.715 ± 0.194] (0.3959–0.9995)
C-MVB: Diagrams based on log-ratios of immobile trace elements	{Σn} {Σprob} [%prob]	1165	{50} {29.4989} [–––]	{38} {22.0945} [3.0%]	{389} {256.6613} [34.8%]	{251} {181.9975} [22.3%]	{437} {324.8701} [39.9%]

§ IA–island arc; CR–continental rift; OI–ocean island; Col–collision; $\overline{x} \pm s$ – mean ± standard deviation; {Σn} – total number of samples for the five diagrams; {Σprob} – total probability for a given tectonic setting in all five diagrams; [%prob] – total percent probability value for a given tectonic setting in all five diagrams; Θ (p_{IA+CA}), [p_{IA}], [p_{CA}], [p_{CR+OI}], and [p_{Col}] – probability for the five tectonic fields.

Table 7. Application of multidimensional diagrams for deciphering tectonic setting of acid magmas from the central part of the Mexican Volcanic Belt (C-MVB).

Magma type; figure name	Figure type §	Total number of samples	Number of discriminated samples				
			Arc			Within-plate CR+ OI	Collision Col
			IA+ CA [$\bar{x} \pm s$] (p_{IA+CA}) Θ	IA [$\bar{x} \pm s$] [p_{IA}] Θ	CA [$\bar{x} \pm s$] [p_{CA}] Θ	[$\bar{x} \pm s$] [p_{CR+OI}] Θ	[$\bar{x} \pm s$] [p_{Col}] Θ
Acid; Verma et al. (2012); all major element concentrations (macid)	IA+CA–CR+OI–Col	705	579 [0.920 ± 0.095] (0.4042–0.9961)	––	––	38 [0.702 ± 0.192] (0.3890–0.9768)	88 [0.815 ± 0.155] (0.4136–0.9932)
	IA–CA–CR+OI	705	––	414 [0.647 ± 0.094] (0.4961–0.9044)	211 [0.660 ± 0.128] (0.3506–0.9722)	80 [0.771 ± 0.195] (0.4044– 1.0000)	––
	IA–CA–Col	705	––	366 [0.599 ± 0.084] (0.4470–0.9080)	239 [0.598 ± 0.086] (0.4224–0.8470)	––	100 [0.888 ± 0.142] (0.4901– 1.0000)
	IA–CR+OI–Col	705	––	563 [0.949 ± 0.093] (0.3950–0.9996)	––	44 [0.700 ± 0.129] (0.4856–0.9529)	98 [0.842 ± 0.145] (0.4495–0.9841)
	CA–CR+OI–Col	705	––	––	595 [0.936 ± 0.114] (0.4177–0.9995)	27 [0.677 ± 0.166] (0.4153–0.8999)	83 [0.773 ± 0.141] (0.4309–0.9958)
C-MVB: Diagrams based on all major element concentrations	{Σn} {Σprob} [%prob]	3525	{579} {532.6557} [–––]	{1343} {1021.3676} [46.4%]	{1045} {839.0403} [38.0%]	{189} {137.4377} [4.8%]	{369} {307.1471} [10.8%]
Acid; Verma et al. (2013); log-ratios of all major elements (macid)	IA+CA–CR+OI–Col	705	576 [0.909 ± 0.104] (0.4002–0.9950)	––	––	72 [0.717 ± 0.199] (0.3932–0.9992)	57 [0.728 ± 0.171] (0.3565–0.9956)
	IA–CA–CR+OI	705	––	0 (0)	584 [0.891 ± 0.080] (0.4579–0.9913)	121 [0.915 ± 0.141] (0.4972–0.9999)	––
	IA–CA–Col	705	––	4 [0.548±0.064] (0.4852–0.6366)	602 [0.898 ± 0.076] (0.4435–0.9683)	––	99 [0.897 ± 0.141] (0.4650– 1.0000)
	IA–CR+OI–Col	705	––	420 [0.688±0.154] (0.3504–0.9936)	––	162 [0.648 ± 0.163] (0.3497–0.9990)	123 [0.596 ± 0.169] (0.3451–0.9811)
	CA–CR+OI–Col	705	––	––	582 [0.935±0.107] (0.3715–0.9988)	65 [0.714 ± 0.188] (0.4079–0.9962)	58 [0.701 ± 0.163] (0.3989–0.9955)
C-MVB: Diagrams based on log-ratios of all major elements	{Σn} {Σprob} [%prob]	3525	{576} {523.4817} [–––]	{424} {291.1469} [12.5%]	{1768} {1604.9671} [68.8%]	{420} {313.6001} [10.5%]	{337} {244.2449} [8.2%]
Acid; Verma et al. (2013); log-ratios of immobile major and trace elements (mtacid)	IA+CA–CR+OI–Col	383	308 [0.758±0.124] (0.3824–0.9529)	––	––	30 [0.749 ± 0.184] (0.4677–0.9996)	45 [0.618 ± 0.159] (0.3881–0.9324)
	IA–CA–CR+OI	383	––	5 [0.601 ± 0.073] (0.5116–0.6863)	325 [0.802 ± 0.086] (0.4122–0.9518)	53 [0.906 ± 0.128] (0.4879–0.9992)	––
	IA–CA–Col	383	––	5 [0.571 ± 0.057] (0.5352–0.6709)	317 [0.748 ± 0.078] (0.4709–0.9192)	––	61 [0.844 ± 0.165] (0.4330–0.9991)
	IA–CR+OI–Col	383	––	90 [0.561 ± 0.126] (0.4079–0.9172)	––	33 [0.729±0.183] (0.4218–0.9986)	260 [0.583 ± 0.111] (0.3449–0.9281)
	CA–CR+OI–Col	383	––	––	322 [0.791±0.119] (0.3615–0.9566)	28 [0.753±0.176] (0.5085–0.9994)	33 [0.622 ± 0.143] (0.3723–0.8786)
C-MVB: Diagrams based on log-ratios of immobile major and trace elements	{Σn} {Σprob} [%prob]	1915	{308} {233.3330} [–––]	{100} {56.3449} [5.2%]	{964} {752.2157} [68.8%]	{144} {115.6279} [8.2%]	{399} {251.3386} [17.8%]
Acid; Verma et al. (2013); log-ratios of immobile trace elements (tacid)	IA+CA–CR+OI–Col	174	166 [0.840±0.094] (0.4423–0.9971)	––	––	6 [0.852 ± 0.121] (0.6967–0.9594)	2 [0.534 ± 0.106] (0.4596, 0.6094)
	IA–CA–CR+OI	174	––	4 [0.698 ± 0.171] (0.5600–0.9237)	157 [0.909 ± 0.086] (0.5149–0.9991)	13 [0.950 ± 0.092] (0.6761–1.0000)	––
	IA–CA–Col	174	––	0 (0)	167 [0.839 ± 0.063] (0.5990–0.9998)	––	7 [0.906 ± 0.059] (0.8106–0.9801)
	IA–CR+OI–Col	174	––	35 [0.661 ± 0.152] (0.4171–0.9525)	––	15 [0.768 ± 0.175] (0.5269–0.9899)	124 [0.741 ± 0.150] (0.4614– 1.0000)
	CA–CR+OI–Col	174	––	––	164 [0.934 ± 0.071] (0.5548–0.9990)	6 [0.872 ± 0.101] (0.7462–0.9615)	4 [0.660 ± 0.183] (0.4699–0.8224)
C-MVB: Diagrams based on log-ratios of immobile trace elements	{Σn} {Σprob} [%prob]	870	{166} {139.4569} [–––]	{39} {25.9141} [4.6%]	{488} {436.0769} [77.0%]	{40} {34.2070} [4.6%]	{137} {101.9036} [13.8%]

For explanation of § and Θ, see Table 6.

Table 8. Application of multidimensional diagrams for deciphering tectonic setting of Neogene basic magmas from the Central American Volcanic Arc (CAVA).

Figure reference; figure type; figure no.	Discrimination diagram §	Total no. of samples (%)	Predicted tectonic affinity and number of discriminated samples (%)				
			IAB	CRB+ OIB	CRB	OIB	MORB
Verma et al. (2006); log-ratios of major elements (m2); no figure	IAB–CRB–OIB–MORB	183 (100)	144 (78.7)	––	19 (10.4)	0 (0)	20 (10.9)
	IAB–CRB–OIB	183 (100)	137 (74.9)	––	35 (19.1)	11 (6)	––
	IAB–CRB–MORB	183 (100)	143 (78.1)	––	21 (11.5)	––	19 (10.4)
	IAB–OIB–MORB	183 (100)	149 (81.4)	––	––	14 (7.7)	20 (10.9)
	CRB–OIB–MORB	183 (100)	––	––	139 (76)	0 (0)	44 (24)
CAVA: Synthesis of all five diagrams of Verma et al. (2006)		915 (100)	573 (62.6)	––	214 (23.4)	25 (2.7)	103 (11.3)
Agrawal et al. (2008); log-ratios of immobile trace elements (t1); no figure	IAB–CRB+OIB–MORB	65 (100)	35 (53.8)	4 (6.2)	––	––	26 (40)
	IAB–CRB–OIB	65 (100)	26 (40)	––	26 (40)	13 (20)	––
	IAB–CRB+ MORB	65 (100)	35 (53.8)	––	4 (6.2)	––	26 (40)
	IAB–OIB–MORB	65 (100)	35 (53.8)	––	––	2 (3.1)	28 (43.1)
	CRB–OIB–MORB	65 (100)	––	––	5 (7.7)	0 (0)	60 (92.3)
CAVA: Synthesis of all five diagrams of Agrawal et al. (2008)		325 (100)	131 (40.3)	4 (–––)	38 (11.7)	16 (4.9)	140 (43.1)
Verma and Agrawal (2011); log-ratios of immobile major and trace elements (t2); no figure	IAB–CRB+OIB–MORB	183 (100)	46 (59)	9 (11.5)	––	––	23 (29.5)
	IAB–CRB–OIB	183 (100)	61 (78.2)	––	17 (21.8)	0 (0)	––
	IAB–CRB–MORB	183 (100)	46 (59)	––	9 (11.5)	––	23 (29.5)
	IAB–OIB–MORB	183 (100)	45 (57.7)	––	––	5 (6.4)	28 (35.9)
	CRB–OIB–MORB	183 (100)	––	––	11 (14.1)	0 (0)	67 (85.9)
CAVA: Synthesis of all five diagrams of Verma and Agrawal (2011)		390 (100)	198 (50.8)	9 (–––)	45 (11.5)	6 (1.5)	141 (36.2)

§ IAB–island arc basic (or ultrabasic) rock; CRB–continental rift basic (or ultrabasic) rock; OIB–ocean island basic (or ultrabasic) rock; MORB–mid-ocean ridge basic (or ultrabasic) rock.

Therefore, it should be useful to check the functioning of the multidimensional diagrams for different kinds of rocks from the CAVA.

The basic rocks from the CAVA indicated an arc (Figures 10a–10e; the first set of diagrams with about 63% percent probability; Table 8) or a transitional arc to MORB setting, with about 40% to 43% for arc and 51% to 36% for MORB (Table 8). When the rocks from the front-arc region were separately considered, this set of diagrams suggested an arc setting (results not shown separately in Table 8), because these samples mostly plotted in the arc field (Figures 10a–10d).

All three sets of diagrams for intermediate magmas indicated a continental arc setting for the CAVA with total percent probability values at about 55%, 58%, and 66%, respectively (Table 9).

Finally, all four sets of diagrams available for acid magmas also consistently showed a continental arc setting for the CAVA, because the total percent probability values were high at about 57%, 63%, 64%, and 69%, respectively (Table 10).

Thus, a good functioning of the multidimensional diagrams for all kinds of magmas is clearly established from the CAVA data.

Now, the questions arise as follows: "Why do these diagrams indicate conflicting results for the C-MVB?", and "Can there be different tectonic settings for basic, intermediate, and acid magmas that are closely related in space and time?" or else, "What role does the origin of magmas play in the resolution of these discrepancies?" I will attempt to answer these questions in Section 6.

6. Discussion

If the C-MVB basic magmas were generated in a continental rift setting, they should be similar to other continental rifts or extensional areas and different from continental and island arcs or continental collision zones. The C-MVB intermediate and acid magmas indicated a different tectonic setting than the basic magmas. Intermediate types suggested a transitional arc to collision setting, whereas the acid magmas showed an arc setting. If it is true that the tectonic setting is dependent on the type of magmas, there

Table 9. Application of multidimensional diagrams for deciphering tectonic setting of intermediate magmas from the Central American Volcanic Arc (CAVA).

Magma type; figure name; figure number	Figure type §	Total number of samples	Number of discriminated samples				
			Arc			Within−plate CR+	Collision Col
			IA+ CA [$\overline{x} \pm s$] ($p_{IA+ CA}$) Θ	IA [$\overline{x} \pm s$] [p_{IA}] Θ	CA [$\overline{x} \pm s$] [p_{CA}] Θ	OI [$\overline{x} \pm s$] [$p_{CR+ OI}$] Θ	[$\overline{x} \pm s$] [p_{Col}] Θ
Intermediate; Verma and Verma (2013); log-ratios of all major elements (mint); no figure	IA+CA−CR+OI−Col	498	433 [0.900 ± 0.140] (0.3504–0.9992)	−−−	−−−	21 [0.740 ± 0.168] (0.3820–0.9827)	44 [0.630 ± 0.085] (0.4883–0.8117)
	IA−CA−CR+OI	498	−−−	129 [0.662 ± 0.158] (0.3918–0.9779)	347 [0.644 ± 0.093] (0.3869–0.9938)	22 [0.659 ± 0.180] (0.3922–0.9862)	−−−
	IA−CA−Col	498	−−−	125 [0.667 ± 0.176] (0.3617–0.9915)	358 [0.633 ± 0.104] (0.3622–0.8714)	−−−	15 [0.521 ± 0.109] (0.3545–0.7589)
	IA−CR+OI−Col	498	−−−	415 [0.907 ± 0.131] (0.3977–0.9996)	−−−	25 [0.719 ± 0.186] (0.3627–0.9867)	58 [0.709 ± 0.131] (0.3909–0.9054)
	CA−CR+OI−Col	498	−−−	−−−	427 [0.879 ± 0.151] (0.4113–0.9996)	25 [0.729 ± 0.146] (0.4636–0.9465)	46 [0.6417 ± 0.0996] (0.4585–0.8239)
CAVA: Diagrams based on log-ratios of major elements	{Σn} {Σprob} [%prob]	2490	{433} {389.6590} [−−−]	{669} {545.0745} [36.2%]	{1132} {825.4543} [54.9%]	{93} {66.2545} [3.4%]	{163} {106.2025} [5.5%]
Intermediate; Verma and Verma (2013); log-ratios of immobile major and trace elements (mtint); no figure	IA+CA−CR+OI−Col	725	232	214 [0.907 ± 0.098] (0.3860–0.9962)	−−−	−−−	4 [0.816 ± 0.181] (0.5820–0.9678)
	IA−CA−CR+OI	725	232	−−−	65 [0.682 ± 0.115] (0.5034–0.9932)	163 [0.693 ± 0.080] (0.3803–0.8916)	4 [0.755 ± 0.277] (0.4714–0.9933)
	IA−CA−Col	725	232	−−−	59 [0.655 ± 0.114] (0.4458–0.9723)	159 [0.672 ± 0.091] (0.4200–0.8971)	−−−
	IA−CR+OI−Col	725	232	−−−	209 [0.884 ± 0.087] (0.5176–0.9955)	−−−	5 [0.707 ± 0.228] (0.4608–0.9656)
	CA−CR+OI−Col	725	232	−−−	−−−	216 [0.942 ± 0.100] (0.4270–0.9997)	5 [0.762 ± 0.172] (0.5181–0.9242)
CAVA: Diagrams based on log-ratios of immobile major and trace elements	{Σn} {Σprob} [%prob]	1160	{214} {194.1879} [−−−]	{333} {267.8415} [36.6%]	{538} {423.2965} [57.8%]	{18} {13.6314} [1.5%]	{57} {39.5218} [4.1%]
Intermediate; Verma and Verma (2013); log-ratios of immobile trace elements (tint); no figure	IA+CA−CR+OI−Col	227	213 [0.886±0.095] (0.5140–0.9989)	−−−	−−−	8 [0.741±0.145] (0.5440–0.9136)	6 [0.746±0.118] (0.5776–0.9009)
	IA−CA−CR+OI	227	−−−	51 [0.654 ± 0.137] (0.4357–0.9218)	169 [0.807±0.133] (0.4899–0.9580)	7 [0.730±0.204] (0.4273–0.9468)	−−−
	IA−CA−Col	227	−−−	43 [0.670±0.118] (0.4359–0.9065)	178 [0.790±0.115] (0.4341–0.9233)	−−−	6 [0.693±0.180] (0.5018–0.9903)
	IA−CR+OI−Col	227	−−−	206 [0.742±0.161] (0.4123–0.9982)	−−−	10 [0.732±0.175] (0.4070–0.9439)	11 [0.694±0.125] (0.4774–0.8768)
	CA−CR+OI−Col	227	−−−	−−−	217 [0.929±0.089] (0.4578–0.9993)	6 [0.814±0.122] (0.5903–0.9170)	4 [0.657±0.165] (0.4945–0.8864)
CAVA: Diagrams based on log-ratios of immobile trace elements	{Σn} {Σprob} [%prob]	1135	{213} {188.7361} [−−−]	{300} {214.9189} [29.6%]	{564} {478.6132} [65.9%]	{31} {23.2449} [2.5%]	{27} {18.8996} [2.0%]

§ IA–island arc; CR–continental rift; OI–ocean island; Col–collision; $\overline{x} \pm s$ – mean ± standard deviation; {Σn} – total number of samples for the five diagrams; {Σprob} – total probability for a given tectonic setting in all five diagrams; [%prob] – total percent probability value for a given tectonic setting in all five diagrams; Θ ($p_{IA+ CA}$), [p_{IA}], [p_{CA}], [$p_{CR+ OI}$], and [p_{Col}] – probability for the five tectonic fields.

Table 10. Application of multidimensional diagrams for deciphering tectonic setting of acid magmas from the Central American Volcanic Arc (CAVA).

Magma type; figure name	Figure type §	Total number of samples	Number of discriminated samples				
			Arc			Within−plate CR+ OI [$\overline{x} \pm s$] [$p_{CR+\ OI}$] Θ	Collision Col [$\overline{x} \pm s$] [p_{Col}] Θ
			IA+ CA [$\overline{x} \pm s$] ($p_{IA+\ CA}$) Θ	IA [$\overline{x} \pm s$] [p_{IA}] Θ	CA [$\overline{x} \pm s$] [p_{CA}] Θ		
Acid; Verma et al. (2012); all major element concentrations (macid)	IA+CA−CR+OI−Col	54	48 [0.891 ± 0.099] (0.5432–0.9998)	−−−	−−−	1 (0.4681)	5 [0.560 ± 0.183] (0.3555–0.8448)
	IA−CA−CR+OI	54	−−−	16 [0.706 ± 0.178] (0.4979–0.9955)	37 [0.648 ± 0.131] (0.4605–0.8651)	1 (0.7510)	−−−
	IA−CA−Col	54	−−−	12 [0.784 ± 0.184] (0.4991–0.9899)	39 [0.656 ± 0.096] (0.4969–0.8913)	−−−	3 [0.708 ± 0.063] (0.6404–0.7640)
	IA−CR+OI−Col	54	−−−	44 [0.893 ± 0.150] (0.4354– 1.0000)	−−−	1 (0.3489)	9 [0.686 ± 0.108] (0.5418–0.8864)
	CA−CR+OI−Col	54	−−−	−−−	49 [0.911 ± 0.112] (0.4892– 1.0000)	0 (0)	5 [0.502 ± 0.092] (0.3742–0.5924)
CAVA: Diagrams based on all major element concentrations	{Σn} {Σprob} [%prob]	270	{48} {42.7755} [−−−]	{72} {59.9994} [36.1%]	{125} {94.2048} [56.7%]	{3} {1.5680} [0.8%]	{22} {13.6144} [6.4%]
Acid; Verma et al. (2013); log-ratios of all major elements (macid)	IA+CA−CR+OI−Col	54	44 [0.860 ± 0.107] (0.5712–0.9932)	−−−	−−−	8 [0.633 ± 0.118] (0.3980–0.7812)	2 [0.4727 ± 0.0136] (0.4631, 0.4823)
	IA−CA−CR+OI	54	−−−	8 [0.809 ± 0.197] (0.4324–0.9983)	38 [0.797 ± 0.108] (0.5102–0.9280)	8 [0.815 ± 0.198] (0.5054–0.9937)	−−−
	IA−CA−Col	54	−−−	6 [0.623 ± 0.242] (0.3998–0.9664)	40 [0.833 ± 0.104] (0.4867–0.9483)	−−−	8 [0.691 ± 0.153] (0.4823–0.9379)
	IA−CR+OI−Col	54	−−−	32 [0.692 ± 0.204] (0.4167– 1.0000)	−−−	18 [0.592 ± 0.123] (0.3742–0.7657)	4 [0.504 ± 0.093] (0.3702–0.5857)
	CA−CR+OI−Col	54	−−−	−−−	45 [0.883 ± 0.124] (0.4234–0.9994)	8 [0.618 ± 0.093] (0.4512–0.7515)	1 (0.4246)
CAVA: Diagrams based on log-ratios of all major elements	{Σn} {Σprob} [%prob]	270	{44} {37.8345} [−−−]	{46} {32.3461} [19.6%]	{123} {103.3702} [63.1%]	{42} {27.1790} [13.0%]	{15} {8.9123} [4.3%]
Acid; Verma et al. (2013); log-ratios of immobile major and trace elements (mtacid)	IA+ CA−CR+ OI−Col	28	26 [0.733 ± 0.143] (0.4576–0.9231)	−−−	−−−	0 (0)	2 [0.520 ± 0.062] (0.4767, 0.5639)
	IA−CA−CR+ OI	28	−−−	6 [0.750 ± 0.114] (0.6110–0.8759)	21 [0.755 ± 0.129] (0.4800–0.8853)	1 (0.8502)	−−−
	IA−CA−Col	28	−−−	6 [0.747 ± 0.131] (0.5303–0.8695)	20 [0.700 ± 0.112] (0.4849–0.8709)	−−−	2 [0.628 ± 0.245] (0.4549, 0.8011)
	IA−CR+ OI−Col	28	−−−	9 [0.834 ± 0.159] (0.5074–0.9721)	−−−	2 [0.5005 ± 0.0109] (0.4929, 0.5082)	17 [0.585 ± 0.080] (0.4346–0.6946)
	CA−CR+ OI−Col	28	−−−	−−−	27 [0.761 ± 0.135] (0.4824–0.9353)	1 (0.5702)	0 (0)
CAVA: Diagrams based on log-ratios of immobile major and trace elements	{Σn} {Σprob} [%prob]	140	{26} {19.0614} [−−−]	{21} {16.4920} [21.1%]	{68} {50.3920} [64.4%]	{4} {2.4214} [2.3%]	{21} {12.2346} [12.2%]
Acid; Verma et al. (2013); log-ratios of immobile trace elements (tacid)	IA+CA−CR+OI−Col	5	5 [0.778 ± 0.141] (0.5810–0.9693)	−−−	−−−	0 (0)	0 (0)
	IA−CA−CR+OI	5	−−−	1 (0.9286)	4 [0.911 ± 0.052] (0.8474–0.9719)	0 (0)	−−−
	IA−CA−Col	5	−−−	1 (0.9326)	4 [0.8651 ± 0.0165] (0.8517–0.8891)	−−−	0 (0)
	IA−CR+OI−Col	5	−−−	1 (0.9998)	−−−	2 [0.676 ± 0.304] (0.4610, 0.8908)	2 [0.767 ± 0.261] (0.5822, 0.9510)
	CA−CR+OI−Col	5	−−−	−−−	5 [0.862 ± 0.123] (0.6709–0.9974)	0 (0)	0 (0)
CAVA: Diagrams based on log-ratios of immobile trace elements	{Σn} {Σprob} [%prob]	25	{5} {3.8881} [−−−]	{3} {2.8610} [18%]	{13} {11.4158} [69%]	{2} {1.3518} [6%]	{2} {1.5332} [7%]

For explanation of § and Θ, see Table 6.

should be at least some distinction in space or time for the different magma types. However, all types of magmas from the C-MVB overlap in time because they are all of Neogene-Quaternary (mainly Pliocene to Holocene) age. Their geographical distribution is shown in Figure 11, from which no clear distinction of locations can be observed for the different magma types, neither from the near the trench nor far from the trench areas. Therefore, it is difficult, if not impossible, to attribute the origin of basic, intermediate, and acid rocks to different tectonic settings. Instead of this, it seems more likely that these rock types had drastically different petrogenetic sources, which resulted in rock type-dependent indications from the tectonic discrimination diagrams (Verma, 2015a; Verma SP et al., 2015b). I present and discuss additional quantitative constraints to better understand this complex problem.

6.1. Quantitative treatment of Nb and Ta anomalies in multielement normalized diagrams

To date, the multielement normalized diagrams have generally been used on a simple qualitative basis by identifying, for example, the mere presence or absence of a positive or negative Nb anomaly, without any reference to its size, except by Verma (2006, 2009) who did use a quantitative approach. Such diagrams have been erroneously interpreted by most people who use them qualitatively to infer an arc setting for negative anomalies, irrespective of their size (e.g., Martínez-Serrano et al., 2004). Verma (2006, 2009) indicated the usefulness of such diagrams for basic magmas when quantitative statistical information is derived from them, such as the quantification of Nb anomaly with respect to Ba and La. Thus, these diagrams were rendered as excellent tectonomagmatic indicators.

In these papers (Verma, 2006, 2009), I showed that 1) this anomaly can be negative for basic magmas from both arc and rift tectonic settings, but the size of the anomaly is significantly different for these two settings; 2) the basic or ultrabasic magmas from arcs and continental rift or extension-related settings can be clearly distinguished from the size of the negative Nb anomaly; and 3) the LTVF (Verma, 2006) and C-MVB (Verma, 2009) of southern Mexico are more consistent with a continental rift setting rather than with an arc setting. Therefore, it is worthwhile to extend this kind of work for all kinds of magmas from basic to acid.

Here, I quantitatively use both Nb and Ta anomalies in primitive mantle normalized diagrams, first by defining them as follows:

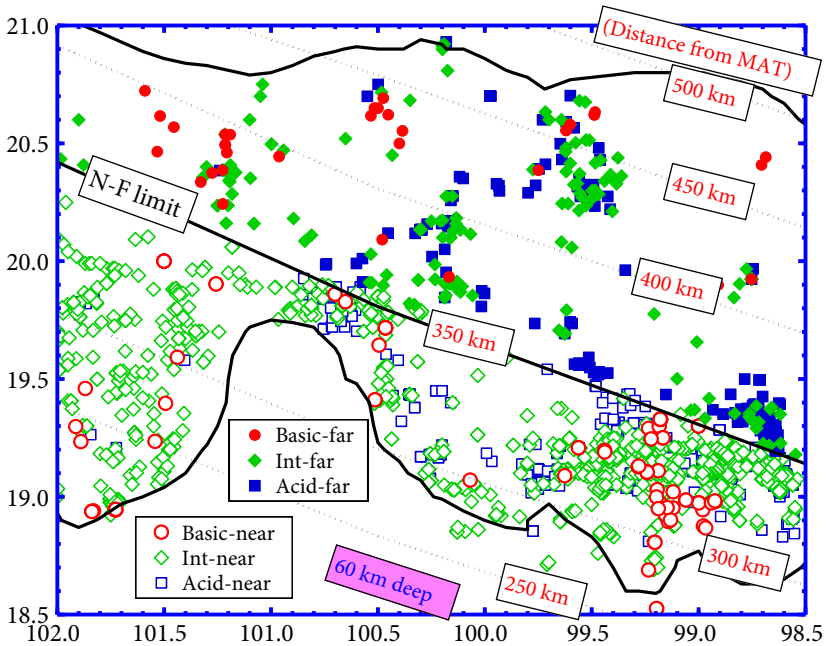

Figure 11. The geographic distribution of different magma types in the C-MVB. The symbols are shown as insets; the numbers 250 to 500 km refer to the horizontal distance from the Middle America Trench (MAT in Figure 1); 60 km deep means that here the subducted slab is about 60 km deep; N-F limit refers to the subdivision used in this work; more information is given in Figure 2.

$$\left\{Nb/Nb^*\right\}_{pm} = \frac{2\cdot(Nb_{sa}/Nb_{pm})}{(Ba_{sa}/Ba_{pm})+(La_{sa}/La_{pm})}, \quad (3)$$

$$\left\{Ta/Ta^*\right\}_{pm} = \frac{2\cdot(Ta_{sa}/Ta_{pm})}{(Ba_{sa}/Ba_{pm})+(La_{sa}/La_{pm})}. \quad (4)$$

Here, for Eq. (3), the element symbols Nb (a high-field strength element – HFSE), Ba (a large ion lithophile element – LILE), and La (a light rare-earth element – LREE) refer to the concentrations of these elements in a sample or normalizing material; the subscript $_{sa}$ stands for the sample and $_{pm}$ for the primitive mantle; and the superscript * refers to the Nb concentration that would result from a smooth pattern for Ba to La on the primitive mantle-normalized multielement diagram (see Figure 7 for an example of such diagrams). Note that on each side of Nb the elements Ba and La are exactly the third nearest neighbors, i.e., at the same distance on both sides in the multielement diagram. This observation makes the simple Eq. (3) applicable for the calculation of the quantitative parameter $\{Nb/Nb^*\}_{pm}$.

The other anomaly parameter $\{Ta/Ta^*\}_{pm}$ of Eq. (4) is defined similarly for Ta, being a HFSE as is Nb. This would not correspond to Figure 7 as presented, but rather for a similar diagram in which Nb and Ta have been interchanged. This is done to make the two quantitative parameters $\{Nb/Nb^*\}_{pm}$ and $\{Ta/Ta^*\}_{pm}$ directly comparable to each other.

Alternative equations can instead be proposed to justify the log-scale on the y-axis, but the interpretation will not change.

The statistical information (mean, standard deviation, no. of samples, and 99% confidence limits of the mean value) for the Nb and Ta anomalies ($\{Nb/Nb^*\}_{pm}$ and $\{Ta/Ta^*\}_{pm}$) is summarized in Table 11. For a smooth curve without any anomaly the value of $\{Nb/Nb^*\}_{pm}$ or $\{Ta/Ta^*\}_{pm}$ will be about 1. When this quantitative estimate is smaller than 1, the anomaly is said to be negative and its size increases as this value decreases. In some cases, the value of the Nb or Ta anomaly can be higher than 1; this anomaly is said to be positive and its size increases as this value increases.

The C-MVB basic magmas from near the trench show a relatively small negative Nb or Ta anomaly. Thus, we have for $\{Nb/Nb^*\}_{pm}$ mean = 0.54, standard deviation = 0.25, no. of samples = 38, and 99% confidence limits of the mean = 0.43–0.65, and for $\{Ta/Ta^*\}_{pm}$ 0.75, 0.16, 30, and 0.67–0.84, respectively (Table 11). The far from the trench C-MVB basic magmas show very similar values for the Nb anomaly, e.g., 99% confidence limit of the mean 0.41–0.66 (Table 11); no data are available for the Ta anomaly for this region.

The C-MVB intermediate and acid magmas show significantly larger negative anomalies; in fact, the size of the anomalies increases (the 99% confidence limits of the mean values decrease) in the sequence basic-intermediate-acid: $\{Nb/Nb^*\}_{pm}$ 0.43–0.66 for basic, 0.20–0.22 for intermediate, and 0.146–0.158 for acid, and $\{Ta/Ta^*\}_{pm}$ 0.67–0.84 for basic, 0.23–0.27 for intermediate, and 0.21–0.23 for acid (Table 11).

Henceforth, I will cite only the 99% confidence limits of the mean, which combines all the other conventional statistical parameters of mean, standard deviation, no. of samples, and Student t (Verma, 2005, 2012a). This parameter is an excellent estimate of the mean value of the population (μ, an unknown parameter) because μ will lie within these limits at 99% probability or confidence used to estimate the confidence limits (e.g., Jensen et al., 1997; Miller and Miller, 2005; Verma, 2005).

The basic magmas from the front-arc region of the CAVA depicted very large Nb and Ta anomalies, with very small values of $\{Nb/Nb^*\}_{pm}$ of 0.11 to 0.15 and $\{Ta/Ta^*\}_{pm}$ of 0.13 to 0.23, respectively (Table 11), much smaller than the C-MVB for both the near and far from the trench regions. On the contrary, the basic magmas from the back-arc region of the CAVA showed significantly higher values of $\{Nb/Nb^*\}_{pm}$ 0.5 to 1.3 and $\{Ta/Ta^*\}_{pm}$ of 0.241 to 0.366, respectively (Table 11) than the front-arc magmas. Thus, the size of these anomalies may well indicate much greater involvement of substance (fluids or melts) from the subducted slab for the front-arc area as compared to the back-arc region of CAVA.

The intermediate and acid magmas from the CAVA also showed large negative anomalies as the basic magmas from the front-arc. In fact, the 99% confidence limits of the mean values overlapped for these rock types as basic-intermediate-acid: $\{Nb/Nb^*\}_{pm}$ 0.11 to 0.15 for basic, 0.103 to 0.113 for intermediate, and 0.083 to 0.127 for acid, and $\{Ta/Ta^*\}_{pm}$ 0.13 to 0.23 for basic, 0.12 to 0.14 for intermediate, and 0.020 to 0.189 for acid (Table 11).

All other arcs, whether continental or island types (underlain by a thick or thin crust, respectively), consistently showed very large and overlapping negative Nb and Ta anomalies for the different magma types from basic to acid (Table 11). This was consistently true for all 22 regions from the Chilean Andes to the Vanuatu arc compiled in this work. The CAVA showed exactly the same behavior as all these other arcs (Table 11). However, none of the arcs showed the relationship of the C-MVB, in which the basic magmas depicted much smaller Nb and Ta anomalies than the intermediate and acid rocks.

Now, if we examine the behavior of these anomalies in continental rifts or extension-related areas or postcollision extensional zones, the basic rocks in most cases showed smaller anomalies than the intermediate and acid rocks.

Table 11. Statistical information on Nb and Ta anomalies (with respect to Ba and La) for basic, intermediate, and acid rocks from Mexico and other areas representing different tectonic settings.

Area	Magma type	Mean ± standard deviation (number of samples) $\bar{x} \pm s$ (n)		99% Confidence limits (CL) of the mean	
		$\{Nb/Nb^*\}_{pm}$	$\{Ta/Ta^*\}_{pm}$	$\{Nb/Nb^*\}_{pm}$	$\{Ta/Ta^*\}_{pm}$
Central Mexican Volcanic Belt (near the trench)	Basic	0.54 ± 0.25 (38)	0.75 ± 0.16 (30)	0.43–0.65	0.67–0.84
Central Mexican Volcanic Belt (far from the trench)	Basic	0.53 ± 0.24 (28)	––	0.41–0.66	––
Central Mexican Volcanic Belt	Intermediate	0.21 ± 0.09 (498)	0.25 ± 0.11 (274)	0.20–0.22	0.23–0.27
Central Mexican Volcanic Belt	Acid	0.152 ± 0.033 (194)	0.22 ± 0.05 (184)	0.146–0.158	0.21–0.23
Continental and island arcs					
Central American Volcanic Arc (front arc)	Basic	0.13 ± 0.06 (59)	0.18 ± 0.11 (34)	0.11–0.15	0.13–0.23
Central American Volcanic Arc (back arc)	Basic	0.9 ± 0.7 (28)	0.304 ± 0.038 (6)	0.5–1.3	0.241–0.366
Central American Volcanic Arc	Intermediate	0.108 ± 0.030 (289)	0.13 ± 0.05 (213)	0.103–0.113	0.12–0.14
	Acid	0.105 ± 0.040 (25)	0.105 ± 0.029 (4)	0.083–0.127	0.020–0.189
Andes (Chile)	Basic	0.20 ± 0.05 (29)	0.147 ± 0.037 (9)	0.17–0.23	0.105–0.189
	Intermediate	0.186 ± 0.041 (125)	0.192 ± 0.043 (65)	0.177–0.196	0.177–0.206
	Acid	0.177 ± 0.031 (49)	0.194 ± 0.034 (41)	0.165–0.189	0.180–0.208
Andes (Peru)	Acid	0.25 ± 0.10 (37)	0.26 ± 0.11 (33)	0.21–0.30	0.21–0.31
Andes (Ecuador)	Basic	0.079 ± 0.009 (7)	––	0.065–0.090	––
	Intermediate	0.113 ± 0.030 (178)	0.101 ± 0.044 (44)	0.107–0.119	0.083–0.119
	Acid	0.106 ± 0.018 (210)	0.17 ± 0.07 (16)	0.103–0.110	0.11–0.22
Andes (Colombia)	Intermediate	0.23 ± 0.05 (11)	0.23 ± 0.12 (12)	0.18–0.28	0.12–0.34
Aleutians	Basic	0.18 ± 0.07 (15)	0.19 ± 0.09 (14)	0.13–0.24	0.12–0.26
	Intermediate	0.162 ± 0.010 (48)	0.212 ± 0.011 (46)	0.158–0.166	0.208–0.216
	Acid	0.23 ± 0.05 (14)	0.29 ± 0.05 (14)	0.19–0.28	0.24–0.33
Barren Island (Indian Ocean)	Basic	0.089 ± 0.010 (18)	0.121 ± 0.013 (13)	0.082–0.096	0.110–0.131
	Intermediate	0.093 ± 0.007 (16)	0.133 ± 0.017 (15)	0.088–0.097	0.120–0.146
Fiji Islands	Basic	0.064 ± 0.037 (5)	0.024 ± 0.010 (11)	––	0.015–0.033
	Intermediate	0.078 ± 0.041 (11)	0.053 ± 0.020 (13)	0.039–0.116	0.036–0.070
Hokkaido (Japan)	Basic	0.31 ± 0.16 (25)	0.27 ± 0.13 (25)	0.23–0.40	0.20–0.35
	Intermediate	0.16 ± 0.11 (48)	0.17 ± 0.010 (47)	0.12–0.20	0.13–0.21
	Acid	0.17 ± 0.07 (67)	0.21 ± 0.09 (67)	0.14–0.19	0.18–0.24
Izu–Bonin	Basic	0.14 ± 0.05 (20)	0.17 ± 0.07 (15)	0.11–0.17	0.11–0.22
	Intermediate	0.090 ± 0.038 (7)	––	0.037–0.143	––
	Acid	0.083 ± 0.016 (8)	0.21 ± 0.07 (11)	0.063–0.103	0.14–0.28
Japan	Basic	0.21 ± 0.08 (29)	0.25 ± 0.12 (22)	0.17–0.25	0.18–0.32
	Intermediate	0.20 ± 0.08 (90)	0.25 ± 0.11 (73)	0.17–0.22	0.21–0.28
	Acid	0.18 ± 0.05 (20)	––	0.15–0.21	––
Indonesia	Basic	0.15 ± 0.05 (27)	0.26 ± 0.13 (23)	0.13–0.17	0.18–0.33
	Intermediate	0.15 ± 0.06 (91)	0.22 ± 0.10 (71)	0.13–0.17	0.19–0.26
	Acid	0.20 ± 0.13 (7)	0.242 ± 0.014 (15)	0.01–0.38	0.231–0.252

Table 11. (Continued.)

Area	Magma type	Mean ± standard deviation (number of samples) $\bar{x} \pm s$ (n) $\{Nb/Nb^*\}_{pm}$	$\{Ta/Ta^*\}_{pm}$	99% Confidence limits (CL) of the mean $\{Nb/Nb^*\}_{pm}$	$\{Ta/Ta^*\}_{pm}$
	Intermediate	0.206 ± 0.036 (148)	0.253 ± 0.028 (116)	0.198–0.214	0.246–0.260
	Acid	0.174 ± 0.035 (18)	0.167 ± 0.039 (41)	0.151–0.198	0.150–0.183
Kamchatka	Basic	0.14 ± 0.06 (54)	0.2 ± 0.10 (58)	0.12–0.17	0.16–0.23
	Intermediate	0.121 ± 0.035 (105)	0.149 ± 0.044 (102)	0.112–0.130	0.137–0.160
	Acid	0.105 ± 0.040 (68)	0.12 ± 0.06 (7)	0.092–0.118	0.02–0.21
Kermadec	Basic	0.086 ± 0.043 (38)	0.24 ± 0.14 (13)	0.067–0.104	0.13–0.36
	Intermediate	0.11 ± 0.05 (21)	0.5 ± 0.5 (6)	0.08–0.14	––
	Acid	0.09 ± 0.05 (44)	0.125 ± 0.007 (13)	0.07–0.11	0.119–0.131
Mariana	Basic	0.07 ± 0.022 (11)	0.106 ± 0.018 (8)	0.054–0.097	0.084–0.129
	Intermediate	0.087 ± 0.022 (58)	0.113 ± 0.018 (53)	0.079–0.094	0.107–0.120
	Acid	0.1024 ± 0.0043 (13)	0.15 ± 0.07 (8)	0.0988–0.1061	0.07–0.24
Philippines (Bicol, Luzon)	Basic	0.18 ± 0.06 (21)	0.19 ± 0.05 (15)	0.14–0.22	0.15–0.23
	Intermediate	0.20 ± 0.09 (50)	0.21 ± 0.06 (24)	0.16–0.23	0.18–0.25
	Acid	0.156 ± 0.013 (4)	0.191 ± 0.021 (6)	0.116–0.191	0.157–0.224
New Hebrides	Basic	0.12 ± 0.06 (24)	0.053 ± 0.018 (9)	0.09–0.16	0.033–0.073
	Intermediate	0.16 ± 0.06 (33)	0.20 ± 0.12 (5)	0.13–0.19	––
	Acid	0.12 ± 0.029 (9)	––	0.088–0.153	––
New Zealand (North Island)	Basic	0.194 ± 0.043 (14)	0.271 ± 0.043 (11)	0.160–0.229	0.230–0.312
	Intermediate	0.19 ± 0.06 (40)	0.42 ± 0.18 (40)	0.17–0.22	0.34–0.49
	Acid				
Ryukyu (Japan)	Basic	0.31 ± 0.10 (8)	0.36 ± 0.09 (8)	0.19–0.44	0.25–0.47
	Intermediate	0.25 ± 0.08 (13)	0.31 ± 0.07 (13)	0.18–0.31	0.24–0.37
	Acid	0.188 ± 0.040 (28)	0.36 ± 0.16 (4	0.167–0.208	0.27–0.44
Taiwan	Basic	––	––	––	––
	Intermediate	0.17 ± 0.08 (5	0.23 ± 0.10 (5)	0.01–0.34	0.02–0.43
	Acid	0.143 ± 0.010 (6)	0.1873 ± 0.0044 (6)	0.127–0.159	0.1800–0.1945
Solomon Islands	Basic	0.088 ± 0.028 (17)	0.102 ± 0.031 (17)	0.069–0.108	0.080–0.124
	Intermediate	0.087 ± 0.042 (33)	0.16 ± 0.08 (28)	0.066–0.107	0.12–0.20
Tongan Islands	Basic	0.13 ± 0.07 (12)	0.36 ± 0.29 (10)	0.06–0.19	0.06–0.66
	Intermediate	0.20 ± 0.08 (29)	0.36 ± 0.26 (27)	0.16–0.25	0.22–0.49
	Acid	0.23 ± 0.05 (7)	0.31 ± 0.05 (6)	0.16–0.30	0.22–0.40
Vanuatu	Basic	0.064 ± 0.026 (69)	0.079 ± 0.033 (32)	0.056–0.073	0.063–0.095
	Intermediate	0.15 ± 0.07 (11)	0.15 ± 0.07 (10)	0.09–0.22	0.08–0.22
Continental rifts or extensional areas, including postcollision extension					
San Luis Potosí (Mexico)	Basic	0.78 ± 0.36 (15)	1.10 ± 0.44 (4)	0.49–1.06	––
	Intermediate	0.19 ± 0.05 (4)	––	0.04–0.33	––
Baja California (Mexico) – Pliocene–Pleistocene	Basic	0.137 ± 0.012 (4)	––	0.102–0.172	––
	Intermediate	0.13 ± 0.05 (32)	––	0.11–0.16	––
Baja California (Mexico) – Miocene	Intermediate	0.126 ± 0.022 (15)	––	0.108–0.143	––
Mogollon–Datil volcanic field, New Mexico (USA)	Basic	0.75 ± 0.27 (13)	0.87 ± 0.32 (9)	0.52–0.98	0.51–1.23
	Intermediate	0.163 ± 0.030 (10)	0.19 ± 0.03 (10)	0.133–0.194	0.15–0.22
NW Cerro del Rio, New Mexico (USA)	Basic	––	0.61 ± 0.05 (5)	––	0.50–0.72
	Intermediate	––	0.46 ± 0.10 (8)	––	0.33–0.58

Table 11. (Continued.)

Area	Magma type	Mean ± standard deviation (number of samples) $\bar{x} \pm s$ (n)		99% Confidence limits (CL) of the mean	
		$\{Nb/Nb^*\}_{pm}$	$\{Ta/Ta^*\}_{pm}$	$\{Nb/Nb^*\}_{pm}$	$\{Ta/Ta^*\}_{pm}$
	Intermediate	0.22 ± 0.10 (7)	––	0.08–0.35	––
Rio Grande rift, New Mexico (USA)	Basic	0.7 ± 0.5 (29)	0.8 ± 0.5 (28)	0.5–1.0	0.5–1.1
	Intermediate	0.21 ± 0.09 (14)	0.21 ± 0.07 (13)	0.13–0.28	0.16–0.27
San Juan volcanic field, Colorado (USA)	Intermediate	0.17 ± 0.08 (26)	––	0.13–0.22	––
	Acid	0.12 ± 0.05 (7)	––	0.06–0.19	––
Hurricane volcanic field, Utah (USA)	Basic	0.60 ± 0.17 (27)	0.66 ± 0.22 (27)	0.51–0.69	0.55–0.78
Santa Rosa Calico volcanic field, Nevada (USA)	Intermediate	0.22 ± 0.07 (12)	0.26 ± 0.10 (8)	0.16–0.28	0.14–0.39
Western USA	Basic	0.61 ± 0.36 (46)	0.38 ± 0.06 (14)	0.47–0.75	0.33–0.42
	Intermediate	0.17 ± 0.06 (10)	––	0.11–0.24	––
Northwest Iran	Basic	0.46 ± 0.10 (14)	0.42 ± 0.08 (8)	0.38–0.55	0.32–0.51
	Intermediate	0.422 ± 0.026 (6)	––	0.379–0.465	––
Eastern Iran	Basic	0.88 ± 0.11 (6)	0.90 ± 0.13 (6)	0.70–1.05	0.68–1.12
	Intermediate	0.70 ± 0.33 (7)	0.8 ± 0.5 (7)	0.24–1.16	0.1–1.4
Western and Northwestern Anatolia (Turkey)	Basic	0.21 ± 0.09 (30)	0.7 ± 0.7 (28)	0.17–0.26	0.4–1.1
	Basic	1.45 ± 0.25 (9)	––	1.17–1.73	––
	Intermediate	0.15 ± 0.06 (37)	0.19 ± 0.07 (37)	0.13–0.18	0.16–0.22
	Acid	0.129 ± 0.027 (17)	0.175 ± 0.038 (16)	0.110–0.148	0.147–0.202
Eastern Anatolia (Turkey)	Basic	0.782 ± 0.014 (20)	0.784 ± 0.038 (20)	0.773–0.791	0.760–0.809
	Acid	0.50 ± 0.13 (25)	0.680 ± 0.017 (24)	0.43–0.58	0.580–0.779
North and Northeast China	Basic	0.78 ± 0.17 (21)	0.49 ± 0.11 (4)	0.67–0.88	0.17–0.80
	Intermediate	0.47 ± 0.09 (8)	0.37 ± 0.09 (5)	0.36–0.57	0.18–0.56
Lhasa terrane (Tibet)	Intermediate	0.24 ± 0.06 (11)	0.263 ± 0.043 (11)	0.18–0.31	0.222–0.304
	Acid	0.232 ± 0.024 (10)	0.284 ± 0.036 (10)	0.207–0.256	0.247–0.322
Central and South Tibet	Basic	0.12 ± 0.06 (5)	0.11 ± 0.06 (5)	––	––
	Intermediate	0.21 ± 0.07 (42)	0.199 ± 0.041 (33)	0.19–0.23	0.179–0.218
	Acid	0.122 ± 0.029 (35)	0.15 ± 0.05 (42)	0.109–0.136	0.13–0.17
NW Africa (Morocco and Mali)	Basic	0.73 ± 0.10 (6)	0.63 ± 0.15 (5)	0.56–0.89	0.32–0.94
	Intermediate	0.72 ± 0.13 (18)	0.73 ± 0.13 (10)	0.64–0.81	0.60–0.87
Djibouti (Africa) – negative anomaly	Basic	0.78 ± 0.13 (9)	––	0.64–0.92	––
Djibouti (Africa) – positive anomaly	Basic	1.6 ± 0.5 (9)	1.7 ± 0.5 (15)	1.1–2.1	1.3–2.1
Ethiopian rift (Africa) – negative anomaly	Basic	0.6 ± 0.17 (14)	0.7 ± 0.5 (14)	0.46–0.74	0.4–1.1
Ethiopian rift (Africa) – positive anomaly	Basic	1.28 ± 0.24 (28)	1.5 ± 0.30 (28)	1.15–1.40	1.30–1.62
Massif Central (France)	Basic	1.49 ± 0.19 (17)	––	1.36–1.62	––
Saudi Arabia	Basic	1.47 ± 0.27 (11)	––	1.21–1.73	––
Continental collision (Cretaceous to Paleogene)					
Central Anatolia	Intermediate	0.224 ± 0.041 (22)	0.28 ± 0.06 (22)	0.195–0.253	0.23–0.32
	Acid	0.211 ± 0.025 (12)	0.27 ± 0.11 (13)	0.189–0.233	0.18–0.37
Western Anatolia	Acid	0.17 ± 0.08 (42)	0.35 ± 0.10 (41)	0.14–0.21	0.31–0.40
Ulubey	Intermediate	0.077 ± 0.012 (27)	0.075 ± 0.027 (27)	0.070–0.084	0.059–0.090
	Acid	0.090 ± 0.006 (10)	0.113 ± 0.010 (10)	0.084–0.097	0.103–0.122
Western Pontides	Acid	0.114 ± 0.009 (36)	0.115 ± 0.015 (32)	0.109–0.118	0.108–0.122
Lesser Caucasus (Azerbaijan)	Basic	0.26 ± 0.06 (5)	0.28 ± 0.05 (5)	0.14–0.38	0.18–0.37
	Intermediate	0.31 ± 0.07 (7)	0.32 ± 0.08 (7)	0.213–0.402	0.21–0.42
	Acid	0.21 ± 0.07 (9)	0.27 ± 0.11 (7)	0.13–0.29	0.12–0.41
Himalayas and Tibet	Basic	0.160 ± 0.039 (4)	0.14 ± 0.05 (4)	0.045–0.276	––
	Intermediate	0.169 ± 0.038 (5)	0.20 ± 0.07 (5)	0.09–0.25	0.05–0.34
	Acid	0.18 ± 0.09 (31)	0.27 ± 0.11 (28)	0.14–0.23	0.21–0.33

It is also instructive to note that most such rift-related areas did show negative Nb and Ta anomalies. Only in some regions of Africa, Saudi Arabia, and Massif Central (France) have positive Nb and Ta anomalies been observed (Table 11). A close examination of the size of negative Nb and Ta anomalies in the C-MVB and most rift or extension-related areas and their interrelationships for basic, intermediate, and acid magmas clearly confirmed that the C-MVB is similar to this group of tectonics and not to arcs.

In the final part of Table 11, the data compiled for different rock types from continental collision zones clearly showed that in terms of the Nb and Ta anomalies, these areas depict a similar behavior as continental or island arcs. These negative anomalies are very large for all rock types (Table 11).

Therefore, it is a misconception or misinterpretation when the presence of negative anomalies is simply attributed to an arc setting. Such anomalies are also the characteristic features of continental collision zones. Furthermore, the negative Nb and Ta anomalies also constitute a widespread feature of most continental rifts as well, but their size is considerably smaller in these zones, especially for basic and ultrabasic rocks. The C-MVB is akin to continental rifts in this sense.

6.2. Quantitative comparison of near and far trench/front and back-arc magmas from the C-MVB and CAVA in terms of subduction-sensitive parameters

Several simple element ratios have traditionally been used to decipher the possible influence of the subducted slab. For example, Tatsumi et al. (1992) used Sr and Nd isotopes and Rb/K and Rb/Zr for understanding across-arc variations in the Izu-Bonin arc. Besides such simple ratios, Verma (2006) demonstrated the use of more complex parameters based on the groupings of LILEs (e.g., K, Rb, Cs, Ba, and Sr), REEs (light REEs La, Ce, Pr, and Nd; HREEs Ho to Lu), and HFSEs (e.g., Ti, P, Hf, Zr, Nb, and Ta) to understand such petrogenetic processes. The middle REE – M-REE from Sm to Tb – were not used but can also be evaluated in future.

Although many more ratio parameters can be constructed, some elements have been traditionally determined less commonly in volcanic rocks, e.g., Cs from the LILE group. In the future, when the multielement analytical techniques, such as inductively coupled plasma mass spectrometry, are more frequently employed, this work can be extended to include other complex ratio parameters.

To better understand the effect of the subducted slab in the origin of C-MVB and CAVA magmas, here I resort to such complex ratio parameters for different types of the near and far from the trench (or front-arc and back-arc) magmas. Thus, to have a larger number of samples from different groups to statistically better represent them, the following six ratio parameters were used.

The "four LILEs to four LREEs" ratio (i.e. the ratio of averaged behavior of K, Rb, Ba, and Sr to the averaged behavior of La, Ce, Pr, and Nd) parameter:

$$\{\text{LILE4/LREE4}\}_E = \frac{\left[(K_{sa}/K_E)+(Rb_{sa}/Rb_E)+(Ba_{sa}/Ba_E)+(Sr_{sa}/Sr_E)\right]/4}{\left[(La_{sa}/La_E)+(Ce_{sa}/Ce_E)+(Pr_{sa}/Pr_E)+(Nd_{sa}/Nd_E)\right]/4}, \quad (5)$$

the "four LILEs to three LREEs" ratio (i.e. the ratio of averaged behavior of K, Rb, Ba, and Sr to the averaged behavior of La, Ce, and Nd) parameter:

$$\{\text{LILE4/LREE3}\}_E = \frac{\left[(K_{sa}/K_E)+(Rb_{sa}/Rb_E)+(Ba_{sa}/Ba_E)+(Sr_{sa}/Sr_E)\right]/4}{\left[(La_{sa}/La_E)+(Ce_{sa}/Ce_E)+(Nd_{sa}/Nd_E)\right]/3}, \quad (6)$$

the "four LILEs to five HREEs" ratio (i.e. the ratio of averaged behavior of K, Rb, Ba, and Sr to the averaged behavior of Ho, Er, Tm, Yb, and Lu) parameter:

$$\{\text{LILE4/HREE5}\}_E = \frac{\left[(K_{sa}/K_E)+(Rb_{sa}/Rb_E)+(Ba_{sa}/Ba_E)+(Sr_{sa}/Sr_E)\right]/4}{\left[(Ho_{sa}/Ho_E)+(Er_{sa}/Er_E)+(Tm_{sa}/Tm_E)+(Yb_{sa}/Yb_E)+(Lu_{sa}/Lu_E)\right]/5}, \quad (7)$$

the "four LILEs to three HREEs" ratio (i.e. the ratio of averaged behavior of K, Rb, Ba, and Sr to the averaged behavior of Er, Yb, and Lu) parameter:

$$\{\text{LILE4/HREE3}\}_E = \frac{\left[(K_{sa}/K_E)+(Rb_{sa}/Rb_E)+(Ba_{sa}/Ba_E)+(Sr_{sa}/Sr_E)\right]/4}{\left[(Er_{sa}/Er_E)+(Yb_{sa}/Yb_E)+(Lu_{sa}/Lu_E)\right]/3}, \quad (8)$$

the "five LILEs to five HREEs" ratio (i.e. the ratio of averaged behavior of K, Rb, Cs, Ba, and Sr to the averaged behavior of Ti, P, Zr, Nb, and Ta) parameter:

$$\{\text{LILE5/HFSE5}\}_E = \frac{\left[(K_{sa}/K_E)+(Rb_{sa}/Rb_E)+(Cs_{sa}/Cs_E)+(Ba_{sa}/Ba_E)+(Sr_{sa}/Sr_E)\right]/5}{\left[(Ti_{sa}/Ti_E)+(P_{sa}/P_E)+(Zr_{sa}/Zr_E)+(Nb_{sa}/Nb_E)+(Ta_{sa}/Ta_E)\right]/5}, \quad (9)$$

and the "four LILEs to four HREEs" ratio (i.e. the ratio of averaged behavior of K, Rb, Ba, and Sr to the averaged behavior of Ti, P, Hf, and Ta) parameter:

$$\{\text{LILE4/HFSE4}\}_E = \frac{\left[(K_{sa}/K_E)+(Rb_{sa}/Rb_E)+(Ba_{sa}/Ba_E)+(Sr_{sa}/Sr_E)\right]/4}{\left[(Ti_{sa}/Ti_E)+(P_{sa}/P_E)+(Hf_{sa}/Hf_E)+(Ta_{sa}/Ta_E)\right]/4}. \quad (10)$$

The subscript $_{sa}$ represents the sample whereas the subscript $_E$ is for the silicate earth values from McDonough and Sun (1995). Any other normalization can equally be used in order to make the multicomponent parameters free from the measurement units. Similarly, instead of the simple arithmetic mean, a more complex geometric mean parameter can be used. Although the actual ratio parameter values will change, the final interpretation should remain practically unchanged.

The results of this quantitative objective comparison for the C-MVB and CAVA are summarized in Table 12. Only the 99% confidence limits of the mean values were tabulated. The first parameter $\{\text{LILE4/LREE4}\}_E$ (Eq. (5)) for basic magmas from the C-MVB and CAVA will be discussed in more detail. This parameter has a range of 1.17–1.47 for the 99% confidence limits of the mean for the near the trench basic rocks (C-MVB-near taken as Group A) and 1.24–1.91 for the far from the trench (C-MVB-far taken as Group B) region (see the first row of data in Table 12). The application of the significance test (Student t) at a strict 99% confidence level showed for its one-sided version that neither of the inequalities "Group A > Group B" or "Group A < Group B" was valid or inferred, i.e. the basic magmas from the near the trench region of the C-MVB did not show higher or lower values of the slab-sensitive parameter $\{\text{LILE4/LREE4}\}_E$ than the far from the trench region.

Similarly, the application of the two-sided version of the t-test at the same 99% confidence level showed that there was no significant difference between the two groups, i.e. "Group A = Group B". If the subducted Cocos plate had contributed in any way (fluids or melts) to the genesis of basic magmas from the C-MVB, the opposite should have been true, i.e. "Group A > Group B", for this particular parameter, which is precisely the case for the CAVA basic rocks.

For this volcanic province, the front-arc magmas (CAVA-front) have 99% confidence limits of 2.80–3.03, whereas the back-arc magmas (CAVA-back) show only values of 1.01–2.30 (see the second row of data in Table 12). Application of one-sided and two-sided versions of the t-test at the strict 99% confidence level showed that "Yes, Group A > Group B" and "Yes, Group A ≠ Group B", respectively. Clearly, the influence of the subducted slab was evidenced from the objective considerations from the t-test because the slab-sensitive parameter $\{\text{LILE4/LREE4}\}_E$ showed significantly higher values (with a 99% confidence level) for the front-arc than the back-arc region.

For basic magmas from the C-MVB, the values of all other slab-sensitive parameters (Eqs. (6)–(10)) did not differ significantly for the near the trench and far from the trench regions (Table 12). For comparison, all these parameters showed statistically significant differences between the two regions of CAVA. In fact, the expected result for the subduction signal of "Yes, Group A > Group B" was true for all the parameters listed in Table 12 for the CAVA.

The inference for intermediate magmas from the C-MVB was also consistently true for most parameters; the exceptions include $\{\text{LILE4/LREE4}\}_E$ for both versions of the t-test and $\{\text{LILE4/LREE4}\}_E$ for the one-sided test (Table 12). On the other hand, for the CAVA intermediate rocks all parameters consistently indicated that the front-arc magmas have higher values of the subduction signal than the back-arc magmas. A comparison of both the near and far trench intermediate magmas from the C-MVB with the CAVA intermediate rocks also indicated that the C-MVB is similar to the CAVA back-arc but different from the CAVA front-arc (results are not tabulated, but the confidence limit values in Table 12 can be easily compared).

The acid magmas from the C-MVB consistently show that all subduction signal parameters from the near the trench region are not significantly higher (or lower), nor significantly different from the far from the trench region (Table 12), ascertaining thus that there is no contribution from the subducted slab in the genesis of these magmas. This is true at a high 99% confidence level. Such a comparison could not be achieved for the CAVA because of the lack of data for acid rocks from the back-arc region.

Table 12. Statistical information of subduction signal for the central part of the Mexican Volcanic Belt (C-MVB) and Central American Volcanic Arc (CAVA).

Parameter	Group A	Group B	99% confidence limit of the mean		Application of one-sided t-test at 99% confidence level	Application of two-sided t-test at 99% confidence level
			Group A	Group B	Group A > or < Group B: yes/no	Group A ≠ Group B: yes/no
Basic magma						
$\{LILE4/LREE4\}_E$	C-MVB–near	C-MVB–far	1.17–1.47	1.24–1.91	No	No significant difference
$\{LILE4/LREE4\}_E$	CAVA–front	CAVA–back	2.80–3.03	1.01–2.30	Yes, Group A > Group B	Yes, Group A ≠ Group B
$\{LILE4/LREE3\}_E$	C-MVB–near	C-MVB–far	1.24–1.39	1.25–1.56	No	No significant difference
$\{LILE4/LREE3\}_E$	CAVA–front	CAVA–back	2.7–3.2	1.46–1.87	Yes, Group A > Group B	Yes, Group A ≠ Group B
$\{LILE4/HREE5\}_E$	C-MVB–near	C-MVB–far	4.9–6.3	4.4–7.5	No	No significant difference
$\{LILE4/HREE5\}_E$	CAVA–front	CAVA–back	7.7–9.2	4.6–7.1	Yes, Group A > Group B	Yes, Group A ≠ Group B
$\{LILE4/HREE3\}_E$	C-MVB–near	C-MVB–far	5.1–6.3	4.4–7.6	No	No significant difference
$\{LILE4/HREE3\}_E$	CAVA–front	CAVA–back	7.8–9.1	5.1–6.8	Yes, Group A > Group B	Yes, Group A ≠ Group B
$\{LILE5/HFSE5\}_E$	C-MVB–near	C-MVB–far	1.54–1.94	––	––	––
$\{LILE5/HFSE5\}_E$	CAVA–front	CAVA–back	4.1–5.7	1.86–3.17	Yes, Group A > Group B	Yes, Group A ≠ Group B
$\{LILE4/HFSE4\}_E$	C-MVB–near	C-MVB–far	1.68–2.01	––	––	––
$\{LILE4/HFSE4\}_E$	CAVA–front	CAVA–back	4.2–5.7	2.39–3.84	Yes, Group A > Group B	Yes, Group A ≠ Group B
Intermediate magma						
$\{LILE4/LREE4\}_E$	C-MVB–near	C-MVB–far	2.1–2.3	2.0–2.6	No	No significant difference
$\{LILE4/LREE4\}_E$	CAVA–front	CAVA–back	2.79–2.89	––	––	––
$\{LILE4/LREE3\}_E$	C-MVB–near	C-MVB–far	2.0–2.1	1.7–2.0	Yes, Group A > Group B	Yes, Group A ≠ Group B
$\{LILE4/LREE3\}_E$	CAVA–front	CAVA–back	2.65–2.72	1.8–2.6	Yes, Group A > Group B	Yes, Group A ≠ Group B
$\{LILE4/HREE5\}_E$	C-MVB–near	C-MVB–far	11.0–12.4	8.6–13.2	No	No significant difference
$\{LILE4/HREE5\}_E$	CAVA–front	CAVA–back	10.0–10.7	7.9–8.0	Yes, Group A > Group B	Yes, Group A ≠ Group B
$\{LILE4/HREE3\}_E$	C-MVB–near	C-MVB–far	11.2–12.5	9.4–13.6	No	No significant difference
$\{LILE4/HREE3\}_E$	CAVA–front	CAVA–back	10.0–10.5	7.9–8.2	Yes, Group A > Group B	Yes, Group A ≠ Group B
$\{LILE5/HFSE5\}_E$	C-MVB–near	C-MVB–far	4.6–5.1	3.8–6.5	Yes, Group A > Group B	No significant difference
$\{LILE5/HFSE5\}_E$	CAVA–front	CAVA–back	5.4–5.8	1.59–4.03	Yes, Group A > Group B	Yes, Group A ≠ Group B
$\{LILE4/HFSE4\}_E$	C-MVB–near	C-MVB–far	4.6–5.1	4.0–6.7	No	No significant difference
$\{LILE4/HFSE4\}_E$	CAVA–front	CAVA–back	6.2–6.7	2.22–4.45	Yes, Group A > Group B	Yes, Group A ≠ Group B
Acid magma						
$\{LILE4/LREE4\}_E$	C-MVB–near	C-MVB–far	3.2–3.4	2.7–3.4	No	No significant difference
$\{LILE4/LREE4\}_E$	CAVA–front	CAVA–back	2.1–7.0	––	––	––
$\{LILE4/LREE3\}_E$	C-MVB–near	C-MVB–far	3.0–3.2	2.7–3.2	No	No significant difference
$\{LILE4/LREE3\}_E$	CAVA–front	CAVA–back	3.4–4.5	––	––	––
$\{LILE4/HREE5\}_E$	C-MVB–near	C-MVB–far	17.6–19.1	16–20	No	No significant difference
$\{LILE4/HREE3\}_E$	C-MVB–near	C-MVB–far	17.8–19.4	15–20	No	No significant difference
$\{LILE4/HREE3\}_E$	CAVA–front	CAVA–back	6–28	––	––	––
$\{LILE5/HFSE5\}_E$	C-MVB–near	C-MVB–far	6.5–7.0	5.5–7.7	No	No significant difference
$\{LILE5/HFSE5\}_E$	CAVA–front	CAVA–back	3.7–16.0	––	––	––
$\{LILE4/HFSE4\}_E$	C-MVB–near	C-MVB–far	6.5–6.9	5.7–7.8	No	No significant difference
$\{LILE4/HFSE4\}_E$	CAVA–front	CAVA–back	4.3–16.0	––	––	––

6.3. Comparison of near and far trench /front and back-arc) magmas from the C-MVB and CAVA in terms of Sr, Nd, and Pb isotopes

The statistics of Sr, Nd, and Pb isotope ratios were also computed for different magma types from the two regions for both provinces. The 99% confidence limits of the mean values for the isotopic ratios are presented in Table 13. These isotopic ratios are sensitive to both the subduction process and crustal contamination; this is especially true for more evolved intermediate and acid magmas. Therefore, they cannot be easily used as clear indicators of the subduction process when the magmas erupt in a continental (about 40 km thick) crust such as beneath the C-MVB and CAVA although they will certainly be more useful in truly island arc settings with a thin crust.

The basic rocks from the near and far from the trench regions of the C-MVB do not show a significant difference in four of the five isotope ratios; only for $^{207}Pb/^{204}Pb$, the near the trench magmas show higher values than the far from the trench magmas (Table 13). Data from both regions of the CAVA are available for only two isotope ratios ($^{87}Sr/^{86}Sr$ and $^{143}Nd/^{144}Nd$); for $^{87}Sr/^{86}Sr$ the front-arc basic magmas have higher values than the back-arc magmas, whereas for $^{143}Nd/^{144}Nd$ both sets of values show no significant difference (Table 13). These results may be consistent with the contribution from the subducted slab in the CAVA because the front-arc basic magmas are shifted towards the subducted slab due to their higher $^{87}Sr/^{86}Sr$ (Figure 8).

For intermediate rocks, the near trench C-MVB and CAVA show lower $^{87}Sr/^{86}Sr$ and higher $^{143}Nd/^{144}Nd$ than the far from the trench (Table 13). The three Pb isotope ratios are lower for the near trench area than the far trench region (Table 13).

Acid magmas can be compared only for the C-MVB. The near trench magmas show lower $^{87}Sr/^{86}Sr$, $^{206}Pb/^{204}Pb$, $^{207}Pb/^{204}Pb$, and $^{208}Pb/^{204}Pb$ but higher $^{143}Nd/^{144}Nd$ than the far from the trench counterpart. These inferences are similar to those for the intermediate rocks. The differences among the isotopic ratios for the C-MVB magmas seem to be opposite to those expected from the involvement of the subducted slab in their genesis.

6.4. Reevaluation of the Nd and Hf isotopes from the C-MVB and CAVA

The C-MVB and CAVA data were compiled from Cai et al. (2014) and Heydolph et al. (2012), respectively. The Cocos plate data were taken from both sources and the CAVA (Guatemalan) crust samples were from Heydolph et al. (2012). A bivariate plot of $^{143}Nd/^{144}Nd$ and $^{176}Hf/^{177}Hf$ is shown in Figure 12. No rocks from the far from the trench area of the C-MVB (Figures 2 and 11) have yet been analyzed for $^{176}Hf/^{177}Hf$. Therefore, only those from the near the trench area of the C-MVB could be plotted.

The intermediate and acid rocks plotted towards lower $^{143}Nd/^{144}Nd$ and $^{176}Hf/^{177}Hf$ values than the C-MVB basic rocks (Figure 12). Cai et al. (2014) argued that the MVB rocks showed a trend towards the mixing curve of oceanic crust and sediments (see their Figure 8a). This curve lies towards the higher values of $^{176}Hf/^{177}Hf$ at any given $^{143}Nd/^{144}Nd$ values but could not be precisely reproduced in the present work because the data plotted by Cai et al. (2014) are still unpublished.

Note that no rock sample from the C-MVB plotted close to either the Cocos MORB compositions (Figure 12) or to the mixing curve of Cocos MORB and sediments (Figure 7a of Cai et al., 2014). On the other hand, the CAVA basic and intermediate rocks did plot close to the Cocos MORB compositions (see CAVA Bas front-arc and Int front-arc; Figure 12).

On the other hand, Cai et al. (2014) downplayed the role of the continental crust (unpublished data from the Mexican crust were plotted in their Figure 7a). They certainly have not analyzed all kinds of C-MVB crust, which makes their interpretation rather biased. I have shown the range of $^{143}Nd/^{144}Nd$ for the C-MVB crust (Table 3) in Figure 12. Unfortunately, the $^{176}Hf/^{177}Hf$ values of these samples have not been reported. I note that the combined $^{143}Nd/^{144}Nd$ and $^{87}Sr/^{86}Sr$ data are more appropriate to explain the origin of the C-MVB rocks (Figure 8) than the limited data so far available for the $^{143}Nd/^{144}Nd$ and $^{176}Hf/^{177}Hf$ plot (Figure 12). If and when the $^{176}Hf/^{177}Hf$ data on more diverse types of crustal rocks from the C-MVB (Table 3) become available, they will extend the range of crustal compositions (Cai et al., 2014; their Figure 7a) and would constitute an "excellent" source and assimilant for the genesis of the acid and

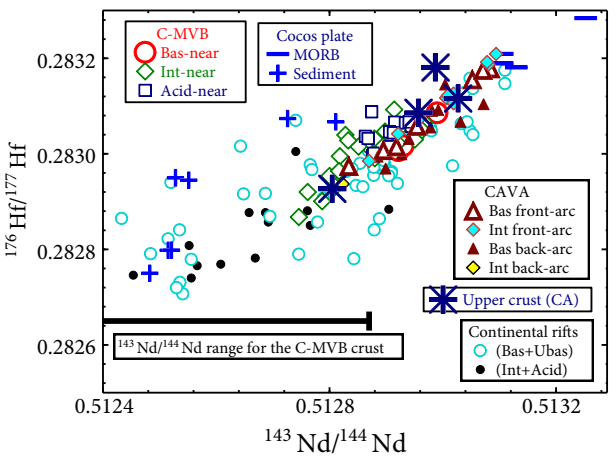

Figure 12. The $^{143}Nd/^{144}Nd$–$^{176}Hf/^{176}Hf$ diagram for the C-MVB and CAVA rocks. The symbols are in insets; the horizontal bar at the bottom left side of the diagram shows the range of $^{143}Nd/^{144}Nd$ measured for the C-MVB crust (Table 3).

Table 13. Statistical information of Sr, Nd, and Pb isotopes for the central part of the Mexican Volcanic Belt (C-MVB) and Central American Volcanic Arc (CAVA).

Parameter	Group A	Group B	99% confidence limit of the mean		Application of one-sided t-test at 99% confidence level	Application of two-sided t-test at 99% confidence level
			Group A	Group B	Group A > or < Group B: yes/no	Group A ≠ Group B: yes/no
Basic magma						
$^{87}Sr/^{86}Sr$	C-MVB–near	C-MVB–far	0.70363–0.70397	0.70355–0.70445	No	No significant difference
$^{87}Sr/^{86}Sr$	CAVA–front	CAVA–back	0.70384–0.70395	0.70311–0.70359	Yes, Group A > Group B	Yes, Group A ≠ Group B
$^{143}Nd/^{144}Nd$	C-MVB–near	C-MVB–far	0.51281–0.51289	0.51274–0.51285	No	No significant difference
$^{143}Nd/^{144}Nd$	CAVA–front	CAVA–back	0.51297–0.51304	0.51292–0.51300	No	No significant difference
$^{206}Pb/^{204}Pb$	C-MVB–near	C-MVB–far	18.694–18.804	18.39–19.21	No	No significant difference
$^{206}Pb/^{204}Pb$	CAVA–front	CAVA–back	18.47–18.98	––	––	––
$^{207}Pb/^{204}Pb$	C-MVB–near	C-MVB–far	15.6013–15.6120	15.5792–15.6195	Yes, Group A > Group B	No significant difference
$^{207}Pb/^{204}Pb$	CAVA–front	CAVA–back	15.525–15.612	––	––	––
$^{208}Pb/^{204}Pb$	C-MVB–near	C-MVB–far	38.492–38.565	38.13–39.06	No	No significant difference
$^{208}Pb/^{204}Pb$	CAVA–front	CAVA–back	38.14–38.73	––	––	––
Intermediate magma						
$^{87}Sr/^{86}Sr$	C-MVB–near	C-MVB–far	0.70393–0.70405	0.70401–0.70433	Yes, Group A < Group B	Yes, Group A ≠ Group B
$^{87}Sr/^{86}Sr$	CAVA–front	CAVA–back	0.70378–0.70383	0.70392–0.70420	Yes, Group A < Group B	Yes, Group A ≠ Group B
$^{143}Nd/^{144}Nd$	C-MVB–near	C-MVB–far	0.51285–0.51288	0.51271–0.51275	Yes, Group A > Group B	Yes, Group A ≠ Group B
$^{143}Nd/^{144}Nd$	CAVA–front	CAVA–back	0.51296–0.51300	0.51282–0.51287	Yes, Group A > Group B	Yes, Group A ≠ Group B
$^{206}Pb/^{204}Pb$	C-MVB–near	C-MVB–far	18.64–18.67	18.61–18.83	Yes, Group A < Group B	Yes, Group A ≠ Group B
$^{206}Pb/^{204}Pb$	CAVA–front	CAVA–back	18.86–18.97	––	––	––
$^{207}Pb/^{204}Pb$	C-MVB–near	C-MVB–far	15.575–15.585	15.575–15.631	Yes, Group A < Group B	Yes, Group A ≠ Group B
$^{207}Pb/^{204}Pb$	CAVA–front	CAVA–back	15.565–15.582	––	––	––
$^{208}Pb/^{204}Pb$	C-MVB–near	C-MVB–far	38.35–38.41	38.32–38.72	Yes, Group A < Group B	Yes, Group A ≠ Group B
$^{208}Pb/^{204}Pb$	CAVA–front	CAVA–back	38.60–38.71	––	––	––
Acid magma						
$^{87}Sr/^{86}Sr$	C-MVB–near	C-MVB–far	0.70389–0.70418	0.70441–0.70471	Yes, Group A < Group B	Yes, significant difference
$^{87}Sr/^{86}Sr$	CAVA–front	CAVA–back	0.70367–0.70421	––	––	––
$^{143}Nd/^{144}Nd$	C-MVB–near	C-MVB–far	0.51282–0.51287	0.51267–0.51273	Yes, Group A > Group B	Yes, Group A ≠ Group B
$^{143}Nd/^{144}Nd$	CAVA–front	CAVA–back	0.51284–0.51304	––	––	––
$^{206}Pb/^{204}Pb$	C-MVB–near	C-MVB–far	18.60–18.66	18.696–18.749	Yes, Group A < Group B	Yes, Group A ≠ Group B
$^{206}Pb/^{204}Pb$	CAVA–front	CAVA–back	––	––	––	––
$^{207}Pb/^{204}Pb$	C-MVB–near	C-MVB–far	15.571–15.592	15.596–15.617	Yes, Group A < Group B	Yes, Group A ≠ Group B
$^{207}Pb/^{204}Pb$	CAVA–front	CAVA–back	––	––	––	––
$^{208}Pb/^{204}Pb$	C-MVB–near	C-MVB–far	38.30–38.42	38.48–38.59	Yes, Group A < Group B	Yes, Group A ≠ Group B
$^{208}Pb/^{204}Pb$	CAVA–front	CAVA–back	––	––	––	––

intermediate C-MVB magmas, respectively. At least one sample of the Guatemalan crust reported by Heydolph et al. (2012) constitutes the appropriate crustal assimilant or source for the C-MVB rocks (Figure 12).

Another strong argument against the inference of Cai et al. (2014) is the present compilation for several continental rifts or extensional areas (Germany from Kolb et al., 2012; New Zealand from Timm et al., 2009; South Korea from Choi et al., 2006; the USA – Basin and Range and other basins from Beard and Johnson, 1997). The C-MVB data are indistinguishable from these extensional area or continental rift data; in fact, some of these compiled rift data plotted beyond the C-MVB data towards lower $^{143}Nd/^{144}Nd$ and $^{176}Hf/^{177}Hf$ (Figure 12).

Similarly, the interpretation of the other bivariate diagrams by Cai et al. (2014) is ambiguous; for evolved magmas these diagrams also cannot distinguish slab input from the continental crust as demonstrated above for their isotope-isotope diagram.

6.5. A new tectono-petrogenetic model

From all the available geological, geophysical, and geochemical evidence, it is clear that the subducted slab does not exist beneath the C-MVB, the mantle wedge is consequently missing, the slab does not and probably cannot contribute to the genesis of the magmas, and the C-MVB is similar to the rift or extension-related areas in all aspects or parameters covered in this work. The rift-like model of Sheth et al. (2000) and asymmetric extension model of Márquez et al. (2001) can be modified as a "symmetric" extension model, with the mantle upwelling taking place at about 20°N latitude. This extensional feature might well represent the continuation of the third arm (the Chapala rift) of the ongoing triple rift system towards the east all along the MVB (Figure 1). The downwelling southern arm of this mantle flow would provide the necessary downward force (and probably the required "lubrication") for the subducted slab to sink into the mantle without any seismicity. It will also forbid the slab to continue to progress towards the MVB volcanic front (Figure 2). The basic magmas can thus originate only in the upper mantle because the subducted slab, being away from the MVB, cannot contribute any substance to their source region. The acid magmas would be largely products of the partial fusion of the older continental crust, for which the required heat would be provided by the mantle upwelling and the formation and uprise of basic magmas from the mantle towards the crust. The intermediate magmas could have a hybrid origin in the underlying mantle and crust.

This is only an outline of a preliminary proposal to explain the origin of the MVB, particularly the C-MVB, and should be worked out in greater detail in a separate paper. For example, the presence of the mantle down-flow towards the north of the MVB will have to be evaluated, and quantitative thermal and petrogenetic constraints would necessarily be required.

Nevertheless, it may be worthwhile to stress the great complexity of the C-MVB in particular and the MVB in general, as has been correctly pointed out by many researchers (e.g., Verma, 1987, 2002, 2009; Verma and Aguilar-Y-Vargas, 1988; Luhr, 1997; Ferrari, 2004; Blatter et al., 2007; Gómez-Tuena et al., 2007b; Torres-Alvarado et al., 2011; Velasco-Tapia and Verma, 2013), but there is no justification to call this volcanic province a volcanic arc (e.g., Chesley et al., 2002). Even worse would be to call a part of the MVB as housing volcanism of the "behind-the-arc" type (Siebert et al., 2002) because, if it were so, then these authors should have specified where the "true" arc-volcanism of the MVB is located in southern Mexico.

The complexity of the MVB might be similar to (or even greater than) that of southern Central America from central Costa Rica to Panama, where unlike Guatemala to northwestern Costa Rica, the geochemistry is not arc-like, and a plethora of different models have been put forth (Defant et al., 1992; Russo and Silver, 1994; Herrstrom et al., 1995; Johnston and Thorkelson, 1997; Harry and Green, 1999; Abratis and Wörner, 2001; Feigenson et al., 2004; Gazel et al., 2009).

Now, if one really wants to change the widely accepted name of the Mexican Volcanic Belt (MVB), or the Trans-Mexican Volcanic Belt (TMVB), as called by numerous researchers (see the references in this work), it should better be called a continental rift. In other words, the Mexican Volcanic Rift might be better nomenclature to represent all its geological, geophysical, geochemical, and plate tectonic characteristics.

I suggest that the scholars studying the MVB become more objective in their work, that they take into account all available scientific arguments to reach unbiased inferences, that they clearly distinguish facts from fiction or evidence from imagination, that they practice a quantitative rather than a qualitative methodology, and that even those practicing a quantitative approach take into account the statistics of experimental data (Verma, 2012a, 2015a). We might thus eventually reach a consensus in our thinking about the origin and evolution of this fascinating geological province in southern Mexico – the Mexican Volcanic Belt housing over 8000 volcanoes.

In summary, a new tectono-petrogenetic model consistent with all available evidence is briefly presented, which is likely to motivate new work on this fascinating geological subprovince of Mexico. Furthermore, I humbly offer this review paper for open debate by the scientific community who may have and like to promote alternative views to those affirmed in this work; such an action is also likely to promote additional work for a better knowledge of this volcanic region. I hope the numerous questions still pending in our knowledge are eventually answered.

7. Conclusions

A review of the geological, geophysical, geochemical, and plate tectonic information clearly indicates the great complexity of the MVB. Overall, the data indicate that the basic and acid rocks from the C-MVB originated in the mantle and continental crust, respectively, whereas the intermediate rocks likely represent a hybrid origin in both mantle and crust. The application of the multidimensional diagrams to rocks from the Central American Volcanic Arc (CAVA; Figure 1) consistently showed an arc setting for all three magma types, confirming thus their good functioning for an expected arc setting. In summary, from the geological, geochemical, and geophysical evidence summarized in this paper and the new, quantitative, robust, objective statistical approach practiced here, one can safely conclude that the tectonic setting of the C-MVB is dominantly related to the ongoing extension. Finally, it appears that the subduction setting for the MVB advocated by numerous workers has resulted probably from subjective, qualitative arguments, which have been shown to fail when the same information compiled in this paper was examined by the quantitative statistics-based methodology. In fact, from quantitative estimates of Nb and Ta anomalies and other complex slab-sensitive parameters, the C-MVB is akin to continental rifts or extension-related areas whereas the CAVA is a classic example of a subduction-related setting.

Acknowledgments

This work was supported by DGAPA-PAPIIT grant IN104813. I thank my colleague K Pandarinath for critically reading an earlier version of this paper. I am also much grateful to the three journal reviewers and the editor handling my manuscript for their appreciation of the work and suggestions for improvement.

References

Abratis M, Wörner G (2001). Ridge collision, slab-window formation, and the flux of Pacific asthenosphere into the Caribbean realm. Geology 29: 127–130.

Absar N, Sreenivas B (2015). Petrology and geochemistry of greywackes of the ~1.6 Ga Middle Aravalli Supergroup, northwest India: evidence for active margin processes. Int Geol Rev 57: 134–158.

Agostini S, Corti G, Doglioni C, Carminati E, Innocenti F, Tonarini S, Manetti P, Di Vincenzo G, Montanari D (2006). Tectonic and magmatic evolution of the active volcanic front in El Salvador: insight into the Berlín and Ahuachapán geothermal areas. Geothermics 35: 368–408.

Agostini S, Doglioni C, Innocenti F, Manetti P, Tonarini S, Savascin MY (2007). The Transition from Subduction-Related to Intraplate Neogene Magmatism in the Western Anatolia and Aegean Area. Cenozoic Volcanism in the Mediterranean Area. Boulder, Colorado, USA: Geological Society of America Special Paper.

Agostini S, Tokçaer M, Savaşçın MY (2010). Volcanic rocks from Foça-Karaburun and Ayvalik-Lesvos grabens (western Anatolia) and their petrogenetic-geodynamic significance. Turk J Earth Sci 19: 157–184.

Agrawal S, Guevara M, Verma SP (2008). Tectonic discrimination of basic and ultrabasic rocks through log-transformed ratios of immobile trace elements. Int Geol Rev 50: 1057–1079.

Aguillón-Robles A, Tristán-González M, Aguirre-Díaz GJ, López-Doncel RA, Bellon H, Martínez-Esparza G (2014). Eocene to Quaternary mafic-intermediate volcanism in San Luis Potosí, central Mexico: the transition from Farallon plate subduction to intra-plate continental magmatism. J Volcanol Geotherm Res 276: 152–172.

Aguillón-Robles A, Tristán-González M, López-Doncel RA, García-Arreola ME, Almaguer-Rodríguez JL, Maury RC (2012). Trace elements geochemistry and origin of volcanic units from the San Luis Potosí and Río Santa María volcanic fields, Mexico: the bearing of ICP-QMS data. Geofís Int 51: 293–308.

Aguirre-Díaz GJ (2001). Recurrent magma mingling in successive ignimbrites from Amealco caldera, central Mexico. Bull Volcanol 63: 238–251.

Aguirre-Díaz GJ, Dubois M, Laureyns J, Schaaf P (2002). Nature and P-T conditions of the crust beneath the central Mexican Volcanic Belt based on a Precambrian crustal xenolith. Int Geol Rev 44: 222–242.

Aguirre-Díaz GJ, López-Martínez M (2009). Geologic evolution of the Donguinyó-Huichapan caldera complex, central Mexican Volcanic Belt, Mexico. J Volcanol Geotherm Res 179: 133–148.

Aguirre-Díaz GJ, McDowell FW (1999). Volcanic evolution of the Amealco caldera, central Mexico. In: Delgado-Granados H, Aguirre-Díaz G, Stock JM, editors. Cenozoic Tectonics and Volcanism of Mexico. Boulder, Colorado, USA: Geological Society of America Special Paper, pp. 1–14.

Agustín-Flores J, Siebe C, Guilbaud MN (2011). Geology and geochemistry of Pelagatos, Cerro del Agua, and Dos Cerros monogenetic volcanoes in the Sierra Chichinautzin Volcanic Field, south of México City. J Volcanol Geotherm Res 201: 143–162.

Aitchison J (1986). The Statistical Analysis of Compositional Data. London, UK: Chapman and Hall.

Akal C (2003). Mineralogy and geochemistry of melilite leucitites, Balçıkhisar, Afyon (Turkey). Turk J Earth Sci 12: 215–239.

Alam MA, Chandrasekharam D, Vaselli O, Capaccioni B, Manetti P, Santo PB (2004). Petrology of the prehistoric lavas and dyke of the Barren Island, Andaman Sea, Indian ocean. Proc Indian Acad Sci (Earth Planet Sci) 113: 715–722.

Alaniz-Álvarez SA, Nieto-Samaniego AF (2007). The Taxco-San Miguel de Allende fault system and the Trans-Mexican Volcanic Belt: two tectonic boundaries in central México active during the Cenozoic, Geology of Mexico. In: Celebrating the Centenary of the Geological Society of Mexico. Boulder, CO, USA: The Geological Society of America, pp. 301–316.

Alaniz-Alvarez SA, Nieto-Samaniego AF, Ferrari L (1998). Effect of strain rate in the distribution of monogenetic and polygenetic volcanism in the Transmexican Volcanic Belt. Geology 26: 591–594.

Aldanmaz E, Pearce JA, Thirlwall MF, Mitchell JG (2000). Petrogenetic evolution of late Cenozoic, post-collision volcanism in western Anatolia, Turkey. J Volcanol Geotherm Res 102: 67–95.

Allan JF (1986). Geology of the northern Colima and Zacoalco grabens, southwest Mexico: Late Cenozoic rifting in the Mexican Volcanic Belt. Geol Soc Am Bull 97: 473–485.

Alvarado GE, Soto GJ, Schmincke HU, Bolge LL, Sumita M (2006). The 1968 andesitic lateral blast eruption at Arenal volcano, Costa Rica. J Volcanol Geotherm Res 157: 9–33.

Anguita F, Verma SP, Márquez A, Vasconcelos FM, López I, Laurrieta A (2001). Circular features in the Trans-Mexican Volcanic Belt. J Volcanol Geotherm Res 107: 265–274.

Arce JL, Cervantes KE, Macías JL, Mora JC (2005). The 12.1 ka Middle Toluca Pumice: A dacitic Plinian–subplinian eruption of Nevado de Toluca in Central Mexico. J Volcanol Geotherm Res 147: 125–143.

Arce JL, Layer PW, Lassiter JC, Benowitz JA, Macías JL, Ramírez-Espinosa J (2013). $^{40}Ar/^{39}Ar$ dating, geochemistry, and isotopic analyses of the Quaternary Chichinautzin volcanic field, south of Mexico City: implications for timing, eruption rate, and distribution of volcanism. Bull Volcanol 75: 1–25.

Arce JL, Macías JL, Vázquez-Selem L (2003). The 10.5 ka Plinian eruption of Nevado de Toluca volcano, Mexico: stratigraphy and hazard implications. Geol Soc Am Bull 115: 230–248.

Arce JL, Macías R, García Palomo A, Capra L, Macías JL, Layer P, Rueda H (2008). Late Pleistocene flank collapse of Zempoala volcano (central Mexico) and the role of fault reactivation. J Volcanol Geotherm Res 177: 944–958.

Armstrong-Altrin JS (2015). Evaluation of two multidimensional discrimination diagrams from beach and deep-sea sediments from the Gulf of Mexico and their application to Precambrian clastic sedimentary rocks. Int Geol Rev 57: 1444–1459.

Avellán DR, Macías JL, Pardo N, Scolamacchia T, Rodriguez D (2012). Stratigraphy, geomorphology, geochemistry and hazard implications of the Nejapa volcanic field, western Managua, Nicaragua. J Volcanol Geotherm Res 213–214: 51–71.

Ayabe M, Takanashi K, Shuto K, Ishimoto H, Kawabata H (2012). Petrology and geochemistry of adakitic dacites and high-MgO andesites, and related calc-alkaline dacites from the Miocene Okoppe volcanic field, N Hokkaido, Japan. J Petrol 53: 547–588.

Bardintzeff JM, Deniel C (1992). Magmatic evolution of Pacaya and Cerro Chiquito volcanological complex, Guatemala. Bull Volcanol 54: 267–283.

Barnett V, Lewis T (1994). Outliers in Statistical Data. Chichester, UK: John Wiley & Sons.

Barrat JA, Jahn BM, Fourcade S, Joron JL (1993). Magma genesis in an ongoing rifting zone: the Tadjoura Gulf (Afar area). Geochim Cosmochim Acta 57: 2291–2302.

Barrat JA, Joron JL, Taylor RN, Fourcade S, Nesbitt RW, Jahn BM (2003). Geochemistry of basalts from Manda Hararo, Ethiopia: LREE-depleted basalts in Central Afar. Lithos 69: 1–13.

Bau M, Knittel U (1993). Significance of slab-derived partial melts and aqueous fluids for the genesis of tholeiitic and calc-alkaline island-arc basalts: evidence from Mt. Arayat, Philippines. Chem Geol 105: 233–251.

Beard BL, Johnson CM (1997). Hafnium isotope evidence for the origin of Cenozoic basaltic lavas from the southwestern United States. J Geophys Res 102: 20149–20178.

Beate B, Monzier M, Spikings R, Cotten J, Silva J, Bourdon E, Eissen JP (2001). Mio-Pliocene adakite generation related to flat subduction in southern Ecuador: the Quimsacocha volcanic center. Earth Planet Sci Lett 192: 561–570.

Beccaluva L, Bianchini G, Natali C, Siena F (2009). Continental flood basalts and mantle plumes: a case study of the northern Ethiopian Plateau. J Petrol 50: 1377–1403.

Bertrand H (1991). The Mesozoic tholeiitic province of northwest Africa: a volcano-tectonic record of the early opening of Central Atlantic. In: Kampunzu AB , Lubala RT, editors. Magmatism in Extensional Structural Settings. Berlin, Germany: Springer, pp. 147–188.

Besch T, Verma SP, Kramm U, Negendank JFW, Tobschall HJ, Emmermann R (1995). Assimilation of sialic crustal material by volcanics of the easternmost extension of the Trans-Mexican Volcanic Belt: evidence from Sr and Nd isotopes. Geofís Int 34: 263–282.

Best MG, Christiansen EH (2001). Igneous Petrology. Waltham, MA, USA: Blackwell Science.

Bevington PR, Robinson DK (2003). Data Reduction and Error Analysis for the Physical Sciences. Boston, MA, USA: McGraw-Hill.

Bindeman IN, Leonov VL, Izbekov PE, Ponomareva VV, Watts KE, Shipley NK, Perepelov AB, Bazanova LI, Jicha BR, Singer BS et al. (2010). Large-volume silicic volcanism in Kamchatka: Ar–Ar and U–Pb ages, isotopic, and geochemical characteristics of major pre-Holocene caldera-forming eruptions. J Volcanol Geotherm Res 189: 57–80.

Bjørnerud MG, Austrheim H (2004). Inhibited eclogite formation: the key to the rapid growth of strong and buoyant Archean continental crust. Geology 32: 765–768.

Blatter DL, Carmichael ISE, Deino AL, Renne PR (2001). Neogene volcanism at the front of the central Mexican volcanic belt: basaltic andesites to dacites, with contemporaneous shoshonites and high-TiO_2 lava. Geol Soc Am Bull 113: 1324–1342.

Blatter DL, Farmer GL, Carmichael ISE (2007). A north-south transect across the Central Mexican Volcanic Belt at ~100°W: spatial distribution, petrological, geochemical, and isotopic characteristics of Quaternary volcanism. J Petrol 48: 901–950.

Blatter DL, Hammersley L (2010). Impact of the Orozco Fracture Zone on the Central Mexican Volcanic Belt. J Volcanol Geotherm Res 197: 67–84.

Bloomfield K (1973). The age and significance of Tenango basalt, central Mexico. Bull Volcanol 37: 586–595.

Bloomfield K (1975). A late-Quaternary monogenetic volcano field in central Mexico. Geol Rundsch 64: 476–497.

Bolge LL, Carr MJ, Feigenson MD, Alvarado GE (2006). Geochemical stratigraphy and magmatic evolution at Arenal volcano, Costa Rica. J Volcanol Geotherm Res 157: 34–48.

Booden MA, Smith IEM, Black PM, Mauk JL (2011). Geochemistry of the Early Miocene volcanic succession of Northland, New Zealand, and implications for the evolution of subduction in the Southwest Pacific. J Volcanol Geotherm Res 199: 25–37.

Bora S, Kumar S (2015). Geochemistry of biotites and host granitoid plutons from the Proterozoic Mahakoshal Belt, central India tectonic zone: implication for nature and tectonic setting of magmatism. Int Geol Rev 57: 1686–1706.

Boudal (1985). Pétrologie d'un grand volcan andésitique mexicain: le Popocatépetl. PhD, Clermont-Ferrand II University, Aubiere, France (in French).

Bouyo MH, Zhao Y, Penaye J, Zhang SH, Njel UO (2015). Neoproterozoic subduction-related metavolcanic and metasedimentary rocks from the Rey Bouba Greenstone Belt of north-central Cameroon in the Central African Fold Belt: new insights into a continental arc geodynamic setting. Precamb Res 261: 40–53.

Brueseke ME, Hart WK (2009). Intermediate composition magma production in an intracontinental setting: Unusual andesites and dacites of the mid-Miocene Santa Rosa–Calico volcanic field, Northern Nevada. J Volcanol Geotherm Res 188: 197–213.

Bryant JA, Yogodzinski GM, Churikova TG (2011). High-Mg# andesitic lavas of the Shisheisky complex, northern Kamchatka: implications for primitive calc-alkaline magmatism. Contrib Mineral Petrol 161: 791–810.

Bryant JA, Yogodzinski GM, Hall ML, Lewicki JL, Bailey DG (2006). Geochemical constraints on the origin of volcanic rocks from the Andean Northern volcanic zone, Ecuador. J Petrol 47: 1147–1175.

Burbach GV, Frohlich C, Pennington WD, Matumoto T (1984). Seismicity and tectonics of the subducted Cocos plate. J Geophys Res 89: 7719–7735.

Cai Y, LaGatta A, Goldstein SL, Langmuir CH, Gómez-Tuena A, Martín-Del Pozzo AL, Carrasco-Núñez G (2014). Hafnium isotope evidence for slab melt contributions in the Central Mexican Volcanic Belt and implications for slab melting in hot and cold slab arcs. Chem Geol 377: 45–55.

Calmus T, Aguillón-Robles A, Maury RC, Bellon H, Benoit M, Cotten J, Bourgois J, Michaud F (2003). Spatial and temporal evolution of basalts and magnesian andesites ("bajaites") from Baja California, Mexico: the role of slab melts. Lithos 66: 77–105.

Calvache VML, Williams SN (1997). Geochemistry and petrology of the Galeras Volcanic Complex, Colombia. J Volcanol Geotherm Res 77: 21–38.

Cameron BI, Walker JA, Carr MJ, Patino LC, Matías O, Feigenson MD (2002). Flux versus decompression melting at stratovolcanoes in southeastern Guatemala. J Volcanol Geotherm Res 119: 21–50.

Camp VE, Roobol MJ, Hooper PR (1991). The Arabian continental alkali basalt province: part II. Evolution of Harrats Khaybar, Ithnayn, and Kura, Kingdom of Saudi Arabia. Geol Soc Am Bull 103: 363–391.

Campos-Enríquez JO, Alatorre-Zamora MA, Keppie JD, Belmonte-Jiménez SI, Ramón-Márquez VM (2014). Interpretation of gravity profiles across the northern Oaxaca terrane, its boundaries and the Tehuacán Valley, southern Mexico. J South Am Earth Sci 56: 396–408.

Campos-Enríquez JO, Alatriste-Vilchis DR, Huizar-Álvarez R, Marines-Campos R, Alatorre-Zamora MA (2003). Subsurface structure of the Tecocomulco sub-basin (northeastern Mexico basin), and its relationship to regional tectonics. Geofís Int 42: 3–24.

Campos-Enríquez JO, Corbo-Camargo F, Arzate-Flores J, Keppie JD, Arango-Galván C, Unsworth M, Belmonte-Jiménez SI (2013). The buried southern continuation of the Oaxaca-Juarez terrane boundary and Oaxaca Fault, southern Mexico: Magnetotelluric constraints. J South Am Earth Sci 42: 62–73.

Campos-Enríquez JO, Sánchez-Zamora O (2000). Crustal structure across southern Mexico inferred from gravity data. J South Am Earth Sci 13: 479–489.

Capra L, Macías JL, Garduño VH (1997). The Zitácuaro Volcanic Complex, Michoacán, Mexico: magmatic and eruptive history of a resurgent caldera. Geofís Int 36: 161–179.

Carmichael ISE, Frey HM, Lange RA, Hall CM (2006). The Pleistocene cinder cones surrounding Volcán Colima, Mexico re-visited: eruption ages and volumes, oxidation states, and sulfur content. Bull Volcanol 68: 407–419.

Carr MJ (1984). Symmetrical and segmented variation of physical and geochemical characteristics of the Central American volcanic front. J Volcanol Geotherm Res 20: 231–252.

Carr MJ, Feigenson MD, Bennett EA (1990). Incompatible element and isotopic evidence for tectonic control of source mixing and melt extraction along the Central American arc. Contrib Mineral Petrol 105: 369–380.

Carr MJ, Rose WI Jr (1986). CENTAM – a data base of Central American volcanic rocks. J Volcanol Geotherm Res 33: 239–240.

Carr MJ, Rose WI, Stoiber RE (1982). Central America. In: Thorpe RS, editor. Andesites. Chichester, UK: John Wiley & Sons, pp. 149–166.

Carr MJ, Saginor I, Alvarado GE, Bolge LL, Lindsay FN, Milidakis K, Turrin BD, Feigenson MD, Swisher CC 3rd (2007). Element fluxes from the volcanic front of Nicaragua and Costa Rica. Geochem Geophys Geosys 8: Q06001.

Cassidy M, Taylor RN, Palmer MR, Cooper RJ, Stenlake C, Trofimovs J (2012). Tracking the magmatic evolution of island arc volcanism: Insights from a high-precision Pb isotope record of Montserrat, Lesser Antilles. Geochem Geophys Geosys 13: 1–19.

Castillo PR, Newhall CG (2004). Geochemical constraints on possible subduction components in lavas of Mayon and Taal volcanoes, southern Luzon, Philippines. J Petrol 45: 1089–1108.

Cathelineau M, Izquierdo G, Vázquez GR, Guevara M (1991). Deep geothermal wells in the Los Azufes (Mexico) caldera: volcanic basement stratigraphy based on major-element analysis. J Volcanol Geotherm Res 47: 149–159.

Cathelineau M, Oliver R, Nieva D (1987). Geochemistry of volcanic series of the Los Azufres geothermal field (Mexico). Geofís Int 26: 273–290.

Cavazos Tovar JG (2006). Magmatismo adakítico en el volcán Tancítaro, Michoacán, México. MSc, Universidad Nacional Autónoma de México, Mexico City, Mexico (in Spanish).

Cervantes P, Wallace PJ (2003). Role of H_2O in subduction-zone magmatism: new insights from melt inclusions in high-Mg basalts from central Mexico. Geology 31: 235–238.

Chadwick J, Perfit M, McInne B, Kamenov G, Plank T (2009). Arc lavas on both sides of a trench: Slab window effects at the Solomon Islands triple junction, SW Pacific. Earth Planet Sci Lett 279: 293–302.

Chadwick JP, Troll VR, Ginibre RG, Morgan D, Gertisser R, Waight TE, Davidson JP (2007). Carbonate assimilation at Merapi Volcano, Java, Indonesia: insights from crystal isotope stratigraphy. J Petrol 48: 1793–1812.

Chan LH, Leeman WP, You CF (1999). Lithium isotopic composition of Central American Volcanic Arc lavas: implications for modification of subarc mantle by slab-derived fluids. Chem Geol 160: 255–280.

Chauvel C, Jahn BM (1984). Nd-Sr isotope and REE geochemistry of alkali basalts from the Massif Central, France. Geochim Cosmochim Acta 48: 93–110.

Chen JL, Xu JF, Wang BD, Kang ZQ, Jie L (2010). Origin of Cenozoic alkaline potassic volcanic rocks at KonglongXiang, Lhasa terrane, Tibetan Plateau: products of partial melting of a mafic lower-crustal source? Chem Geol 273: 286–299.

Chesley J, Ruiz J, Righter K, Ferrari L, Gomez-Tuena A (2002). Source contamination versus assimilation: an example from the Trans-Mexican Volcanic Arc. Earth Planet Sci Lett 195: 211–221.

Chiaradia M, Müntener O, Beate B (2011). Enriched basaltic andesites from mid-crustal fractional crystallization, recharge, and assimilation (Pilavo volcano, Western Cordillera of Ecuador). J Petrol 52: 1107–1141.

Choi AH, Mukasa SB, Kwon ST, Andronikov AV (2006). Sr, Nd, Pb and Hf isotopic compositions of late Cenozoic alkali basalts in South Korea: evidence for mixing between the two dominant asthenospheric mantle domains beneath East Asia. Chem Geol 232: 134–151.

Churikova T, Dorendorf F, Wörner G (2001). Sources and fluids in the mantle wedge below Kamchatka, evidence from across-arc geochemical variation. J Petrol 42: 1567–1593.

Class C, Altherr R, Volker F, Eberz G, McCulloch MT (1994). Geochemistry of Pliocene to Quaternary alkali basalts from the Huri Hills, northern Kenya. Chem Geol 113: 1–22.

Cruz-Huicochea R, Verma SP (2013). New critical values for F and their use in the ANOVA and Fisher's F tests for evaluating geochemical reference material granite G-2 (U.S.A.) and igneous rocks from the Eastern Alkaline Province (Mexico). J Iber Geol 39: 13–30.

D'Atonio M (2008). Reconstrucción de los eventos eruptivos de hace ~28 y ~13 ka asociados el emplazamiento de flujos de bloques y ceniza en el volcán Nevado de Toluca (México). PhD, Universidad Nacional Autónoma de México, Mexico City, Mexico (in Spanish).

Daoud MA, Maury RC, Barrat JA, Taylor RN, Le Gall B, Guillou H, Cotten J, Rolet J (2010). A LREE-depleted component in the Afar plume: further evidence from Quaternary Djibouti basalts. Lithos 114: 327–336.

Davidson J, Wilson M (2011). Differentiation and source processes at Mt Pelée and the Quill; active volcanoes in the Lesser Antilles Arc. J Petrol 52: 1493–1531.

Davidson JP, Ferguson KM, Colucci MT, Dungan MA (1988). The origin and evolution of magmas from the San Pedro-Pellado volcanic complex, S. Chile: multicomponent sources and open system evolution. Contrib Mineral Petrol 100: 429–445.

Davis JM, Hawkesworth CJ (1995). Geochemical and tectonic transitions in the evolution of the Mogollon-Datil volcanic field, New Mexico, U.S.A. Chem Geol 119: 31–53.

Defant MJ, Jackson TE, Drummond MS, De Boer JZ, Bellon H, Feigenson MD, Maury RC, Stewart RH (1992). The geochemistry of young volcanism throughout western Panama and southeastern Costa Rica: an overview. J Geol Soc London 149: 569–579.

Delgado H, Molinero R, Cervantes P, Nieto-Obregón J, Lozano-Santa Cruz R, Macías-González HL, Mendoza-Rosales C, Silva-Romo G (1998). Geology of Xitle volcano in southern Mexico City - a 2000-year-old monogenetic volcano in an urban area. Rev Mex Cienc Geol 15: 115–131.

Demant A (1981). L'axe néo-volcanique transmexicain, étude volcanologique et pétrographique, signification géodynamique. PhD, Université de Droit, d'Economie et des Sciences d'Aix-Marseille, Marseille, France (in French).

DeMets C, Stein S (1990). Present-day kinematics of the Rivera plate and implications for tectonics in southwestern Mexico. J Geophys Res 95: 21931–21948.

DeMets C, Wilson DS (1997). Relative motions of the Pacific, Rivera, North American, and Cocos plates. J Geophys Res 102: 2789–2806.

Díaz-González L, Cruz-Huicochea R (2013). Application of discordancy and significance statistical tests for the comparison of dacitic volcanism from the central part of the Mexican Volcanic Belt. Nova Scient 6: 158–178.

Dilek Y, Imamverdiyev N, Altunkaynak S (2010). Geochemistry and tectonics of Cenozoic volcanism in the Lesser Caucasus (Azerbaijan) and the peri-Arabian region: collision-induced mantle dynamics and its magmatic fingerprint. Int Geol Rev 52: 536–578.

Dobson PF, Mahood GA (1985). Volcanic stratigraphy of the Los Azufres geothermal area, Mexico. J Volcanol Geotherm Res 25: 273–287.

Dorendorf F, Churikova T, Koloskov A, Wörner G (2000). Late Pleistocene to Holocene activity at Bakening volcano and surrounding monogenetic centers (Kamchatka): volcanic geology and geochemical evolution. J Volcanol Geotherm Res 104: 131–151.

Dreher ST, Eichelberger JC, Larsen JF (2005). The petrology and geochemistry of the Aniakchak caldera-forming ignimbrite, Aleutian arc, Alaska. J Petrol 46: 1747–1768.

Duffield WA, Heiken GH, Wohletz KH, Maassen LW, Dengo G, McKee EH, Castañeda O (1992). Geology and geothermal potential of the Tecuamburro volcano area, Guatemala. Geothermics 21: 425–446.

DuFrane SA, Asmerom Y, Mukasa SB, Morris JD, Dreyer BM (2006). Subduction and melting processes inferred from U–series, Sr–Nd–Pb isotope, and trace element data, Bicol and Bataan arcs, Philippines. Geochim Cosmochim Acta 70: 3401–3420.

Duncker KE, Wolff JA, Harmon RS, Leat PT, Dickin AP, Thompson RN (1991). Diverse mantle and crustal components in lavas of the NW Cerros del Rio volcanic field, Rio Grande Rift, New Mexico. Contrib Mineral Petrol 108: 331–345.

Dupuy C, Dostal J, Marcelot G, Bougault H, Joron JL, Treuil M (1982). Geochemistry of basalts from central and southern New Hebrides arc: implication for their source rock composition. Earth Planet Sci Lett 60: 207–225.

Edwards CMH, Menzies MA, Thirlwall MF, Morris JD, Leeman WP, Harmon RS (1994). The transition to potassic alkaline volcanism in island arcs: the Ringgit-Beser complex, east Java, Indonesia. J Petrol 35: 1557–1595.

Eggins SM (1993). Origin and differentiation of picritic arc magmas, Ambae (Aoba), Vanuatu. Contrib Mineral Petrol 114: 79–100.

Ego F, Ansan V (2002). Why is the Central Trans-Mexican Volcanic Belt (102°-99°W) in transtensive deformation? Tectonophysics 359: 189–208.

Egozcue JJ, Pawlowsky-Glahn V, Mateu-Figueras G, Barceló-Vidal C (2003). Isometric logratio transformations for compositional data analysis. Math Geol 35: 279–300.

Elliott T, Plank T, Zindler A, White WM, Bourdon B (1997). Element transport from slab to volcanic front at the Mariana arc. J Geophys Res 102: 14991–15019.

Faure G (1986). Principles of Isotope Geology. New York, NY, USA: Wiley.

Faure G (2001). Origin of Igneous Rocks. The Isotopic Evidence. Berlin, Germany: Springer.

Feigenson MD, Bolge LL, Carr MJ, Herzberg CT (2003). REE, inverse modeling of HSDP2 basalts: Evidence for multiple sources in the Hawaiian plume. Geochem Geophys Geosys 4: 1–25.

Feigenson MD, Carr MJ (1993). The source of Central American lavas: inferences from geochemical inverse modeling. Contrib Mineral Petrol 113: 226–235.

Feigenson MD, Carr MJ, Maharaj SV, Juliano S, Bolge LL (2004). Lead isotope composition of Central American volcanoes: influence of the Galapagos plume. Geochem Geophys Geosys 5: Q06001.

Feineman M, Moriguti T, Yokoyama T, Terui S, Nakamura E (2013). Sediment-enriched adakitic magmas from the Daisen volcanic field, southwest Japan. Geochem Geophys Geosyst 14: 3009–3031.

Ferrari L (2004). Slab detachment control on mafic volcanic pulse and mantle heterogeneity in central Mexico. Geology 32: 77–80.

Ferrari L, Conticelli S, Vaggelli G, Petrone CM, Manetti P (2000). Late Miocene volcanism and intra-arc-tectonics during the early development of the Trans-Mexican Volcanic Belt. Tectonophysics 318: 161–185.

Ferrari L, Garduño VH, Innocenti F, Manetti P, Pasquare G, Vaggelli G (1994). A widespread mafic volcanic unit at the base of the Mexican Volcanic Belt between Guadalajara and Querétaro. Geofís Int 33: 107–123.

Ferrari L, Pasquare G, Tibaldi A (1990). Plio-Quaternary tectonics of the central Mexican Volcanic Belt and some constraints on its rifting mode. Geofís Int 29: 5–18.

Ferrari L, Petrone CM, Francalanci L (2001). Generation of oceanic-island basalt-type volcanism in the western Trans-Mexican volcanic belt by slab rollback, asthenosphere infiltration, and variable flux melting. Geology 29: 507–510.

Ferrari L, Petrone CM, Francalanci L (2002). Reply: "Generation of oceanic-island basalt type volcanism in the western Trans-Mexican volcanic belt by slab rollback, asthenosphere infiltration, and variable flux melting:. Geology 114: 858–859.

Ferrari L, Rosas-Elguera J (1999). Alkalic (ocean-island basalt type) and calc-alkaline volcanism in the Mexican volcanic belt: a case for plume-related magmatism and propagating rifting at an active margin?: comment and reply. Geology 27: 1055–1056.

Feuerbach DL, Smith EI, Walker JD, Tangeman JA (1993). The role of the mantle during crustal extension: constraints from geochemistry of volcanic rocks in the Lake Mead area, Nevada and Arizona. Geol Soc Am Bull 105: 1561–1575.

Finney B, Turner S, Hawkesworth C, Larsen J, Nye C, George R, Bindeman I, Eichelberger J (2008). Magmatic differentiation at an island-arc caldera: Okmok volcano, Aleutian Islands, Alaska. J Petrol 49: 857–884.

Fitton JG, James D, Leeman WP (1991). Basic magmatism associated with Late Cenozoic extension in the western United States: compositional variations in space and time. J Geophys Res 96: 13693–13711.

Frey FA, Gerlach DC, Hickey RL, Lopez-Escobar L, Munizaga-Villavicencio F (1984). Petrogenesis of the Laguna del Maule volcanic complex, Chile (36°S). Contrib Mineral Petrol 88: 133–149.

Frey HM, Lange RA, Hall CM, Delgado-Granados H, Carmichael ISE (2007). A Pliocene ignimbrite flare-up along the Tepic-Zacoalco rift: evidence for the initial stages of rifting between the Jalisco block (Mexico) and North America. Geol Soc Am Bull 119: 49–64.

Gamble JA, Smith IEM, McCulloch MT, Graham IJ, Kokelaar BP (1993). The geochemistry and petrogenesis of basalts from the Taupo volcanic zone and Kermadec Island arc, S.W. Pacific. J Volcanol Geotherm Res 54: 265–290.

Gamble JA, Wright IC, Woodhead JD, McCulloch MT (1995). Arc and back-arc geochemistry in the southern Kermadec arc-Ngatoro basin and offshore Taupo volcanic zone, SW Pacific. In: Smellie JL, editor. Volcanism Associated with Extension at Consuming Plate Margins. London, UK: Geological Society Special Publication, pp. 193–212.

García-Palomo A, Macías JL, Arce JL, Capra L, Garduño VH, Espíndola JM (2002a). Geology of Nevado de Toluca Volcano and Surrounding Areas, Central Mexico. Boulder, CO, USA: Geological Society of America Map and Chart Series MCH089.

García-Palomo A, Macías JL, Garduño VH (2000). Miocene to Recent structural evolution of the Nevado de Toluca volcano region, Central Mexico. Tectonophysics 318: 281–302.

García-Palomo A, Macías JL, Tolson G, Valdez G, Mora JC (2002b). Volcanic stratigraphy and geological evolution of the Apan region, east-central sector of the Trans-Mexican Volcanic Belt. Geofís Int 41: 133–150.

García Tovar GP (2009). Caracterización geologíca, geoquímica e isotópica de las lavas del estratovolcán Telepón, Sierra Nevada, México. MSc, Universidad Nacional Autónoma de México, Mexico City, Mexico (in Spanish).

Garduño-Monroy VH, Spinner J, Ceragioli E (1993). Geological and structural study of the Chapala rift, State of Jalisco, Mexico. Geofís Int 32: 487–499.

Gazel E, Carr MJ, Hoernle K, Feigenson MD, Szymanski D, Hauff F, van den Bogaard P (2009). Galapagos-OIB in southern Central America: mantle refertilization by arc-hot spot interaction. Geochem Geophys Geosys 10: Q02S11.

Gerlach DC, Frey FA, Moreno-Roa H, Lopez-Escobar L (1988). Recent volcanism in the Puyehue-Cordon Caulle region, southern Andes, Chile (40.5°S): petrogenesis of evolved lavas. J Petrol 29: 333–382.

Gertisser R, Keller J (2003). Trace element and Sr, Nd, Pb and O isotope variations in medium-K and high-K volcanic rocks from Merapi volcano, Central Java, Indonesia: evidence for the involvement of subducted sediments in Sunda Arc magma genesis. J Petrol 44: 457–489.

Gibson SA, Thompson RN, Leat PT, Dickin AP, Morrison MA, Hendry GL, Mitchell JG (1992). Asthenosphere-derived magmatism in the Rio Grande rift, western USA: implications for continental break-up. In: Storey BC, Alabaster T, Pankhurst RJ, editors. Magmatism and the Causes of Continental Break-Up. London, UK: Geological Society Special Publication, pp. 61–89.

Gómez-Tuena A, LaGatta AB, Langmuir CH, Goldstein SL, Ortega-Gutiérrez F, Carrasco-Núñez G (2003). Temporal control of subduction magmatism in the eastern Trans-Mexican Volcanic Belt: mantle sources, slab contributions, and crustal contamination. Geochem Geophys Geosys 4: 8912.

Gómez-Tuena A, Langmuir CH, Goldstein SL, Straub SM, Ortega-Gutiérrez F (2007a). Geochemical evidence for slab melting in the Trans-Mexican Volcanic Belt. J Petrol 48: 537–562.

Gómez-Tuena A, Orozco-Esquivel MT, Ferrari L (2007b). Igneous petrogenesis of the Trans-Mexican volcanic belt. In: Geology of Mexico: Celebrating the Centenary of the Geological Society of Mexico. Boulder, CO, USA: Geological Society of America, pp. 129–181.

González Partida E, Torres Rodriguez V, Birkle P (1997). Plio-Pleistocene volcanic history of the Ahuachapan geothermal system, El Salvador: the Concepción de Ataco caldera. Geothermics 26: 555–575.

Grib EN, Leonov VL, Perepelov AB (2009). The Karymskii Volcanic Center: volcanic rock geochemistry. J Volcanol Seismol+ 3: 367–387.

Guilbaud MN, Siebe C, Agustín-Flores J (2009). Eruptive style of the young high-Mg basaltic-andesite Pelagatos scoria cone, southeast of México City. Bull Volcanol 71: 859–880.

Gunn BM, Mooser F (1971). Geochemistry of the volcanics of central Mexico. Bull Volcanol 34: 577–613.

Guzmán-Speziale M, Valdés-González C, Molina E, Gómez JM (2005). Seismic activity along the Central America volcanic arc: is it related to subduction of the Cocos plate? Tectonophysics 400: 241–254.

Haase KM, Worthington TJ, Stoffers P, Garbe-Schönberg D, Wright I (2002). Mantle dynamics, element recycling, and magma genesis beneath the Kermadec arc-Havre Trough. Geochem Geophys Geosys 3: 1071.

Halama R, Boudon G, Villemant B, Joron JL, Le Friant A, Komorowski JC (2006). Pre-eruptive crystallization conditions of mafic and silicic magmas at the Plat Pays volcanic complex, Dominica (Lesser Antilles). J Volcanol Geotherm Res 153: 200–220.

Han BF, Wang SG, Kagami H (1999). Trace element and Nd-Sr isotope constraints on origin of the Chifeng flood basalts, North China. Chem Geol 155: 187–199.

Handley HK, Macpherson CG, Davidson JP, Berlo K, Lowryñ D (2007). Constraining fluid and sediment contributions to subduction-related magmatism in Indonesia: Ijen volcanic complex. J Petrol 48: 1155–1183.

Harris NBW, Ronghua X, Lewis CL, Chengwei J (1988). Plutonic rocks of the 1985 Tibet Geotraverse, Lhasa to Golmud. Philos T R Soc A 327: 145–168.

Harry DL, Green NL (1999). Slab dehydration and basalt petrogenesis in subduction systems involving very young oceanic lithosphere. Chem Geol 160: 309–333.

Hart SR (1984). A large-scale isotope anomaly in the southern hemisphere mantle. Nature 309: 753–757.

Hasenaka T (1992). Chemical compositions of selected samples. In: Aoki K, editor. Subduction Volcanism and Tectonics of Western Mexican Volcanic Belt International Scientific Research Program (No 03041014) Japan-Mexico Co-operative Research. Sendai, Japan: Faculty of Science, Tohoku University, pp. 238–247.

Hazlett RW (1987). Geology of San Cristobal volcanic complex, Nicaragua. J Volcanol Geotherm Res 33: 223–230.

Hergt JM, Woodhead JD (2007). A critical evaluation of recent models for Lau–Tonga arc–backarc basin magmatic evolution. Chem Geol 245: 9–44.

Hernández Rojas J (2007). Reconstrucción de la dinámica eruptiva de la pómez Ezequiel Montes, Qro. MSc, Universidad Nacional Autónoma de México, Mexico City, Mexico (in Spanish).

Herrstrom EA, Reagan MK, Morris JD (1995). Variations in lava composition associated with flow of asthenosphere beneath southern Central America. Geology 23: 617–620.

Heydolph K, Hoernle K, Hauff F, van den Bogaard P, Portnyagin M, Bindeman I, Garbe-Schönberg D (2012). Along and across arc geochemical variations in NW Central America: Evidence for involvement of lithospheric pyroxenite. Geochim Cosmochim Acta 84: 459–491.

Hickey RL, Frey FA, Gerlach DC, Lopez-Escobar L (1986). Multiple sources for basaltic arc rocks from the southern volcanic zone of the Andes (34°-41°S): trace element and isotopic evidence for contributions from subducted oceanic crust, mantle, and continental crust. J Geophys Res 91: 5963–5983.

Hickey-Vargas R, Moreno Roa H, Lopez Escobar L, Frey FA (1989). Geochemical variations in Andean basaltic and silicic lavas from the Villarrica-Lanin volcanic chain (39.5°S): an evaluation of source heterogeneity, fractional crystallization and crustal assimilation. Contrib Mineral Petrol 103: 361–386.

Hidalgo S, Monzier M, Martin H, Chazot G, Eissen JP, Cotten J (2007). Adakitic magmas in the Ecuadorian volcanic front: petrogenesis of the Iliniza volcanic complex (Ecuador). J Volcanol Geotherm Res 159: 366–392.

Hoang N, Itoh JI, Miyagi I (2011). Subduction components in Pleistocene to Recent Kurile arc magmas in NE Hokkaido, Japan. J Volcanol Geotherm Res 200: 255–266.

Hoffer G, Eissen JP, Beate B, Bourdon E, Fornari M, Cotten J (2008). Geochemical and petrological constraints on rear-arc magma genesis processes in Ecuador: the Puyo cones and Mera lavas volcanic formations. J Volcanol Geotherm Res 176: 107–118.

Hofmann AW, Feigenson MD (1983). Case studies on the origin of basalt. I. Theory and reassessment of Grenada basalts. Contrib Mineral Petrol 84: 382–389.

Hofmann AW, Feigenson MD, Raczek I (1984). Case studies on the origin of basalt: III. Petrogenesis of the Mauna Ulu eruption, Kilauea, 1969-1971. Contrib Mineral Petrol 88: 24–35.

Hole MJ, Saunders AD, Marriner GF, Tarney J (1984). Subduction of pelagic sediments: implications for the origin of Ce-anomalous basalts from the Marianas Islands. J Geol Soc London 141: 453–472.

Hoogewerff JA, van Bergen MJ, Vroon PZ, Hertogen J, Wordel R, Sneyers A, Nasution A, Varekamp JC, Moens HLE, Mouchel D (1997). U-series, Sr-Nd-Pb isotope and trace-element systematics across an active island arc-continent collision zone: implications for element transfer at the slab-wedge interface. Geochim Cosmochim Acta 61: 1057–1072.

Hou ZQ, Gao YF, Qu XM, Rui ZY, Mo XX (2004). Origin of adakitic intrusives generated during mid-Miocene east-west extension in southern Tibet. Earth Planet Sci Lett 220: 139–155.

Ilbeyli N, Pearce JA, Thirlwall MF, Mitchell JG (2004). Petrogenesis of collision–related plutonics in Central Anatolia, Turkey. Lithos 72: 163–182.

Izbekov PE, Eichelberger JC, Ivanov BV (2004). The 1996 eruption of Karymsky volcano, Kamchatka: historical record of basaltic replenishment of an andesite reservoir. J Petrol 45: 2325–2345.

Jensen JL, Lake LW, Corbett PWM, Goggin DJ (1997). Statistics for Petroleum Engineers and Geoscientists. Upper Saddle River, NJ, USA: Prentice Hall.

Jiménez Z, Ponce L (1978). Focal mechanism of six large earthquakes in northern Oaxaca, Mexico, for the period 1928-1973. Geofís Int 17: 379–386.

Jödicke H, Jording A, Ferrari L, Arzate J, Mezger K, Rüpke L (2006). Fluid release from subducted Cocos plate and partial melting of the crust deduced from magnetotelluric studies in southern Mexico: implications for the generation of volcanism and subduction dynamics. J Geophys Res 111: B08102.

Johnson CA, Harrison CGA (1989). Tectonics and volcanism in central Mexico: a Landsat thematic mapper perspective. Remote Sens Environ 28: 273–286.

Johnson CA, Harrison CGA (1990). Neotectonics in central Mexico. Phys Earth Planet Inter 64: 187–210.

Johnston ST, Thorkelson DJ (1997). Cocos-Nazca slab window beneath Central America. Earth Planet Sci Lett 146: 465–474.

Jording A, Ferrari L, Arzate J, Jödicke H (2000). Crustal variations and terrane boundaries in southern Mexico as imaged by magnetotelluric transfer functions. Tectonophysics 327: 1–13.

Karsli O, Chen B, Uysal I, Aydin F, Wijbrans JR, Kandemir R (2008). Elemental and Sr-Nd-Pb isotopic geochemistry of the most recent Quaternary volcanism in the Erzincan basin, Eastern Turkey: framework for the evaluation of basalt-lower crust interaction. Lithos 106: 55–70.

Karsli O, Ketenci M, Uysal I, Dokuz A, Aydin F, Chen B, Kandemir R, Wijbrans J (2011). Adakite-like granitoid porphyries in the Eastern Pontides, NE Turkey: potential parental melts and geodynamic implication. Lithos 127: 354–372.

Kaur P, Chaudhri N, Hofmann AW (2015). New evidence for two sharp replacement fronts during albitization of granitoids from northern Aravalli orogen, northwest India. Int Geol Rev 57: 1658–1683.

Kay SM, Kay RW (1994). Aleutian magmas in space and time. In: Plafker G, Berg HC, editors. Geology of North America. Boulder, CO, USA: Geological Society of America, pp. 687–722.

Kay SM, Maksaev V, Moscoso R, Mpodozis C, Nasi C (1987). Probing the evolving Andean lithosphere: mid-late Tertiary magmatism in Chile (29°-30°30'S) over the modern zone of subhorizontal subduction. J Geophys Res 92: 6173–6189.

Kay SM, Mpodozis C, Ramos VA, Munizaga F (1991). Magma source variations for mid-late Tertiary magmatic rocks associated with a shallowing subduction zone and a thickening crust in the central Andes. GSA Special Papers 265: 113–137.

Kempton PD, Fitton JG, Hawkesworth CJ, Ormerod DS (1991). Isotopic and trace element constraints on the composition and evolution of the lithosphere beneath the southwestern United States. J Geophys Res 96: 13713–13735.

Kheirkhah M, Allen MB, Emami M (2009). Quaternary syn-collision magmatism from the Iran/Turkey borderlands. J Volcanol Geotherm Res 182: 1–12.

Kim WH, Clayton RW, Keppie F (2011). Evidence of a collision between the Yucatán block and Mexico in the Miocene. Geophys J Int 187: 989–1000.

Kimura JI, Kent AJR, Rowe MC, Katakuse M, Nakano F, Hacker BR, van Keken PE, Kawabata K, Stern RJ (2010). Origin of cross-chain geochemical variation in Quaternary lavas from the northern Izu arc: using a quantitative mass balance approach to identify mantle sources and mantle wedge processes. Geochem Geophys Geosys 11: 1–24.

Kimura JI, Yoshida T (2006). Contributions of slab fluid, mantle wedge and crust to the origin of Quaternary lavas in the NE Japan arc. J Petrol 47: 2185–2232.

Kolb M, Paulick H, Kirchenbaur M, Münker C (2012). Petrogenesis of mafic to felsic lavas from the Oligocene Siebengebirge volcanic field (Germany): implications for the origin of intracontinental volcanism in Central Europe. J Petrol 53: 2349–2379.

Koloskov AV, Khubunaya SA (2013). New petrological data on the volcanic rocks of the Chichinautzin region: the sources of the magmatic melts and the origin of the Trans-Mexican Volcanic Belt. Russ J Pac Geol 7: 247–261.

Koprubasi N, Aldanmaz E (2004). Geochemical constraints on the petrogenesis of Cenozoic I-type granitoids in Northwest Anatolia, Turkey: evidence for magma generation by lithospheric delamination in a post-collisional setting. Int Geol Rev 46: 705–729.

La Femina PC, Connor CB, Hill BE, Strauch W, Saballos A (2004). Magma-tectonic interactions in Nicaragua: the 1999 seismic swarm and eruption of Cerro Negro volcano. J Volcanol Geotherm Res 137: 187–199.

Lai YM, Song SR, Iizuka Y (2008). Magma mingling in the Tungho area, coastal range of eastern Taiwan. J Volcanol Geotherm Res 178: 608–623.

Larocque ACL, Stimac JA, Siebe C (1998). Metal-residence sites in lavas and tuffs from Volcán Popocatépetl, Mexico: implications for metal mobility in the environment. Environ Geol 33: 197–208.

Lassiter JC, Luhr JF (2001). Osmium abundance and isotope variations in mafic Mexican volcanic rocks: evidence for crustal contamination and constraints on the geochemical behavior of osmium during partial melting and fractional crystallization. Geochem Geophys Geosyst 2: 1027.

Leat PT, Thompson RN, Dickin AP, Morrison MA, Hendry GL (1989). Quaternary volcanism in northwestern Colorado: implications for the roles of asthenosphere and lithosphere in the genesis of continental basalts. J Volcanol Geotherm Res 37: 291–310.

Le Bas MJ (2000). IUGS reclassification of the high-Mg and picritic volcanic rocks. J Petrol 41: 1467–1470.

Le Bas MJ, Le Maitre RW, Streckeisen A, Zanettin B (1986). A chemical classification of volcanic rocks based on the total alkali-silica diagram. J Petrol 27: 745–750.

Lebti PP, Thouret JC, Wörner G, Fornari M (2006). Neogene and Quaternary ignimbrites in the area of Arequipa, southern Peru: stratigraphical and petrological correlations. J Volcanol Geotherm Res 154: 251–275.

Le Maitre RW, Streckeisen A, Zanettin B, Le Bas MJ, Bonin B, Bateman P, Bellieni G, Dudek A, Schmid R, Sorensen H et al. (2002). Igneous Rocks. A Classification and Glossary of Terms: Recommendations of the International Union of Geological Sciences Subcommission of the Systematics of Igneous Rocks. Cambridge, UK: Cambridge University Press.

Lindsay JM, Trumbull RB, Siebel W (2005). Geochemistry and petrogenesis of late Pleistocene to Recent volcanism in southern Dominica, Lesser Antilles. J Volcanol Geotherm Res 148: 253–394.

Luhr JF (1997). Extensional tectonics and the diverse primitive volcanic rocks in the western Mexican Volcanic Belt. Can Min 35: 473–500.

Luhr JF, Allan JF, Carmichael ISE, Nelson SA, Hasenaka T (1989). Primitive calc-alkaline and alkaline rock types from the western Mexican Volcanic Belt. J Geophys Res 94: 4515–4530.

Luhr JF, Carmichael ISE (1985). Jorullo Volcano, Michoacán, México (1759-1774): The earliest stages of fractionation in calc-alkaline magmas. Contrib Mineral Petrol 90: 142–161.

Luhr JF, Haldar D (2006). Barren island volcano (NE Indian Ocean): island-arc high-alumina basalts produced by troctolite contamination. J Volcanol Geotherm Res 149: 177–212.

Luhr JF, Nelson SA, Allan JF, Carmichael ISE (1985). Active rifting in southwestern Mexico: Manifestations of an incipient eastward spreading-ridge jump. Geology 13: 54–57.

Maaløe S (1994). Estimation of the degree of partial melting using concentration ratios. Geochim Cosmochim Acta 58: 2519–2525.

Manea VC, Manea M, Kostoglodov V, Sewell G (2005). Thermo-mechanical model of the mantle wedge in Central Mexican subduction zone and a blob tracing approach for the magma transport. Phys Earth Planet Inter 149: 165–186.

Márquez A, De Ignacio C (2002). Mineralogical and geochemical constraints for the origin and evolution of magmas in Sierra Chichinautzin, Central Mexican Volcanic Belt. Lithos 62: 35–62.

Márquez A, Oyarzun R, de Ignacio C, Doblas M (2001). Southward migration of volcanic activity in the central Mexican Volcanic Belt: asymmetric extension within a two-layer crustal stretching model. J Volcanol Geotherm Res 112: 175–187.

Márquez A, Oyarzun R, Doblas M, Verma SP (1999a). Alkalic (ocean-island basalt type) and calc-alkalic volcanism in the Mexican Volcanic Belt: a case for plume-related magmatism and propagating rifting at an active margin? Geology 27: 51–54.

Márquez A, Oyarzun R, Doblas M, Verma SP (1999b). Reply to Comment by L. Ferrari and J. Rosas Elguera on "Alkalic (ocean basalt type) and calc-alkalic volcanism in the Mexican volcanic belt: a case of plume-related magmatism and propagating rift at an active margin?" Comment and Reply. Geology 27: 1055–1056.

Márquez A, Verma SP, Anguita F, Oyarzun R, Brandle JL (1999c). Tectonics and volcanism of Sierra Chichinautzin: extension at the front of the Central Trans-Mexican Volcanic Belt. J Volcanol Geotherm Res 93: 125–150.

Martin del Pozzo AL (1989). Geoquímica y paleomagnetismo de la Sierra Chichinautzin. PhD, Universidad Nacional Autónoma de México, Mexico City, Mexico (in Spanish).

Martínez-Serrano RG, Schaaf P, Solís-Pichardo G, Hernández-Bernal MS, Hernández-Treviño T, Morales-Contreras JJ, Macías JL (2004). Sr, Nd and Pb isotope and geochemical data from the Quaternary Nevado de Toluca volcano, a source of recent adakitic magmatism, and the Tenango volcanic field, Mexico. J Volcanol Geotherm Res 138: 77–110.

Martynov AY, Kimura JI, Martynov YA, Rybin AV (2010). Geochemistry of late Cenozoic lavas on Kunashir Island, Kurile Arc. Island Arc 19: 86–104.

Mattioli M, Renzulli A, Menna M, Holm PM (2006). Rapid ascent and contamination of magmas through the thick crust of the CVZ (Andes, Ollagüe region): Evidence from a nearly aphyric high-K andesite with skeletal olivines. J Volcanol Geotherm Res 158: 87–105.

McBirney AR (2007). Igneous Petrology. Boston, MA, USA: Jones and Bartlett Publishers.

McBirney AR, Taylor HP, Armstrong RL (1987). Paricutin re-examined: a classical example of crustal assimilation in calc-alkaline magma. Contrib Mineral Petrol 95: 4–20.

McDonough WF, Sun SS (1995). The composition of the Earth. Chem Geol 120: 223–253.

McKenzie D, O'Nions RK (1991). Partial melt distributions from inversion of rare earth element concentrations. J Petrol 32: 1021–1091.

McMillan NJ, Dickin AP, Haag D (2000). Evolution of magma source regions in the Rio Grande rift, southern New Mexico. Geol Soc Am Bull 112: 1582–1593.

Meriggi L, Macías JL, Tommasini S, Capra L, Conticelli S (2008). Heterogeneous magmas of the Quaternary Sierra Chichinautzin volcanic field (central Mexico): the role of an amphibole-bearing mantle and magmatic evolution processes. Rev Mex Cienc Geol 25: 197–216.

Middlemost EAK (1989). Iron oxidation ratios, norms and the classification of volcanic rocks. Chem Geol 77: 19–26.

Miller JN, Miller JC (2005). Statistics and chemometrics for analytical chemistry. Essex, UK: Pearson Prentice Hall.

Mo X, Hou Z, Niu Y, Dong G, Qu X, Zhao Z, Yang Z (2007). Mantle contributions to crustal thickening during continental collision: evidence from Cenozoic igneous rocks in southern Tibet. Lithos 96: 225–242.

Mo X, Niu Y, Dong G, Zhao Z, Hou Z, Zhou S, Ke S (2008). Contribution of syncollisional felsic magmatism to continental crust growth: a case study of the Paleogene Linzizong volcanic succession in southern Tibet. Chem Geol 250: 49–67.

Molnar P, Sykes LR (1969). Tectonics of the Caribbean and Middle America regions from focal mechanisms and seismicity. Geol Soc Am Bull 80: 1639–1684.

Monzier M, Danyushevsky LV, Crawford AJ, Bellon H, Cotten J (1993). High-Mg andesites from the southern termination of the New Hebrides island arc (SW Pacific). J Volcanol Geotherm Res 57: 193–217.

Monzier M, Robin C, Eissen JP, Cotten J (1997). Geochemistry vs. seismo-tectonics along the volcanic New Hebrides Central Chain (Southwest Pacific). J Volcanol Geotherm Res 78: 1–29.

Mooser F, Montiel A, Zuñiga A (1996). Nuevo mapa geológico de las cuencas de México, Toluca y Puebla. Estratigrafía, tectónica y aspectos geotérmicos, 1. Mexico City, Mexico: CFE (in Spanish).

Mora JC, Macías JL, García-Palomo A, Arce JL, Espíndola JM, Manetti P, Vaselli O, Sánchez JM (2004). Petrology and geochemistry of the Tacaná Volcanic complex, Mexico-Guatemala: evidence for the last 40 000 yr of activity. Geofís Int 43: 331–359.

Morán-Zenteno DJ, Cerca M, Keppie JD (2007). The Cenozoic tectonic and magmatic evolution of southwestern México: advances and problems of interpretation. In: Geology of Mexico: Celebrating the Centenary of the Geological Society of Mexico. Boulder, CO, USA: Geological Society of America, pp. 71–91.

Moriguti T, Shibata T, Nakamura E (2004). Lithium, boron and lead isotope and trace element systematics of Quaternary basaltic volcanic rocks in northeastern Japan: mineralogical controls on slab-derived fluid composition. Chem Geol 212: 81–100.

Mukasa SB, Blatter DL, Andronikov AV (2007). Mantle peridotite xenoliths in andesite lava at El Peñon, central Mexican Volcanic Belt: isotopic and trace element evidence for melting and metasomatism in the mantle wedge beneath an active arc. Earth Planet Sci Lett 260: 37–55.

Nakagawa M, Nairn IA, Kobayashi T (1998). The ~10 ka multiple vent pyroclastic eruption sequence at Tongariro Volcanic Centre, Taupo Volcanic Zone, New Zealand: Part 2. Petrological insights into magma storage and transport during regional extension. J Volcanol Geotherm Res 86: 45–65.

Negendank JFW (1972). Volcanics of the Valley of Mexico. Description of some Mexican volcanic rocks with special consideration of the opaques. Part I: petrography of the volcanics. Neues Jb Miner Abh 116: 308–320.

Negendank JFW, Emmermann R, Krawczyk R, Mooser F, Tobschall H, Werle D (1985). Geological and geochemical investigations on the eastern Trans Mexican Volcanic Belt. Geofís Int 24: 477–575.

Nelson SA, Gonzalez-Caver E, Kyser TK (1995). Constraints on the origin of alkaline and calc-alkaline magmas from the Tuxtla Volcanic Field, Veracruz, Mexico. Contrib Mineral Petrol 122: 191–211.

Nixon GT (1988a). Petrology of the younger andesites and dacites of Iztaccíhuatl volcano, Mexico: I. Disequilibrium phenocryst assemblages as indicators of magma chamber processes. J Petrol 29: 213–264.

Nixon GT (1988b). Petrology of the younger andesites and dacites of Iztaccíhuatl volcano, Mexico: II. Chemical stratigraphy, magma mixing, and the composition of basaltic magma influx. J Petrol 29: 265–303.

Nixon GT (1989). The geology of Iztaccíhuatl volcano and adjacent areas of the Sierra Nevada and Valley of Mexico. GSA Special Papers 219: 1–59.

Norini G, Groppelli G, Lagmay AMF, Capra L (2006). Recent left-oblique slip faulting in the central eastern Trans-Mexican volcanic belt: seismic hazard and geodynamic implications. Tectonics 25: TC4012.

Nye CJ, Reid MR (1986). Geochemistry of primary and least fractionated lavas from Okmok volcano, central Aleutians: implications for arc magma genesis. J Geophys Res 91: 10271–10287.

Ohba T, Matsuoka K, Kimura Y, Ishikawa H, Fujimaki H (2009). Deep crystallization differentiation of arc tholeiite basalt magmas from Northern Honshu arc, Japan. J Petrol 50: 1025–1046.

Ormerod DS, Rogers NW, Hawkesworth CJ (1991). Melting in the lithospheric mantle: inverse modelling of alkali-olivine basalts from the Big Pine volcanic field, California. Contrib Mineral Petrol 108: 305–317.

Ortega-Gutiérrez F, Elías-Herrera M, Dávalos-Elizondo MG (2008). On the nature and role of the lower crust in the volcanic front of the Trans-Mexican Volcanic Belt and its fore-arc region, southern and central Mexico. Rev Mex Cienc Geol 25: 346–364.

Pacheco JF, Singh SK (1998). Source parameters of two moderate Mexican earthquakes estimated from a single-station, near-source recording, and from MT inversion of regional data: a comparison of the results. Geofís Int 37: 95–102.

Pacheco JF, Singh SK (2010). Seismicity and state of stress in Guerrero segment of the Mexican subduction zone. J Geophys Res 115: B01303.

Pandarinath K (2014a). Tectonomagmatic origin of Precambrian rocks of Mexico and Argentina inferred from multi-dimensional discriminant-function based discrimination diagrams. J South Am Earth Sci 56: 464–484.

Pandarinath K (2014b). Testing of the recently developed tectonomagmatic discrimination diagrams from hydrothermally altered igneous rocks of 7 geothermal fields. Turk J Earth Sci 23: 412–426.

Pandarinath K, Verma SK (2013). Application of four sets of tectonomagmatic discriminant function based diagrams to basic rocks from northwest Mexico. J Iber Geol 39: 181–195.

Pang KN, Chung SL, Zarrinkoub MH, Mohammadi SS, Yang HM, Chu CH, Lee HY, Lo CH (2012). Age, geochemical characteristics and petrogenesis of Late Cenozoic intraplate alkali basalts in the Lut–Sistan region, eastern Iran. Chem Geol 306–307: 40–53.

Parat F, Dungan MA, Lipman PW (2005). Contemporaneous trachyandesitic and calc-alkaline volcanism of the Huerto andesite, San Juan Volcanic Field, Colorado, USA. J Petrol 46: 859–891.

Pardo M, Suárez G (1993). Step subduction geometry of the Rivera plate beneath the Jalisco block in Western Mexico. J Geophys Res 20: 2391–2394.

Pardo M, Suárez G (1995). Shape of the subducted Rivera and Cocos plates in southern Mexico: Seismic and tectonic implications. J Geophys Res 100: 12357–12373.

Pardo N, Avellán DR, Macías JL, Scolamacchia T, Rodríguez D (2008). The ~1245 yr BP Asososca maar: new advances on recent volcanic stratigraphy of Managua (Nicaragua) and hazard implications. J Volcanol Geotherm Res 176: 493–512.

Patino LC, Carr MJ, Feigenson MD (1997). Cross-arc geochemical variations in volcanic fields in Honduras C.A.: progressive changes in source with distance from the volcanic front. Contrib Mineral Petrol 129: 341–351.

Patino LC, Carr MJ, Feigenson MD (2000). Local and regional variations in Central American arc lavas controlled by variations in subducted sediment input. Contrib Mineral Petrol 138: 265–283.

Peate DW, Pearce JA, Hawkesworth CJ, Colley H, Edwards CMH, Hirose K (1997). Geochemical variations in Vanuatu arc lavas: the role of subducted material and a variable mantle wedge composition. J Petrol 38: 1331–1358.

Pérez RJ, Pal S, Terrell DJ, Urrutia FJ, López MM (1979). Preliminary report on the analysis of some "in-house" geochemical reference samples from Mexico. Geofís Int 18: 197–209.

Pérez-Campos X, Kim Y, Husker A, Davis PM, Clayton RW, Iglesias A, Pacheco JF, Singh SK, Manea VC, Gurnis M (2008). Horizontal subduction and truncation of the Cocos plate beneath central Mexico. Geophys Res Lett 35: L18303.

Petterson MG, Haldane MI, Smith DJ, Billy D, Jordan NJ (2011). Geochemistry and petrogenesis of the Gallego Volcanic field, Solomon Islands, SW Pacific and geotectonic implications. Lithos 125: 915–927.

Pradal E, Robin C (1994). Long-lived magmatic phases at Los Azufres volcanic center, Mexico. J Volcanol Geotherm Res 63: 201–215.

Rahman MS, Mondal MEA (2015). Evolution of continental crust of the Aravalli craton, NW India, during the Neoarchaean–Palaeoproterozoic: evidence from geochemistry of granitoids. Int Geol Rev 57: 1510–1525.

Ramos VA, Folguera A (2009). Andean flat-slab subduction through time. In: Murphy JB, Keppie JD, Hynes AJ, editors. Ancient Orogens and Modern Analogues. London, UK: Geological Society of London Special Publications, pp. 31–54.

Raos AM, Crawford AJ (2004). Basalts from the Efate Island group, central section of the Vanuatu arc, SW Pacific: geochemistry and petrogenesis. J Volcanol Geotherm Res 134: 35–64.

Robin C (1984). Le Volcan Popocatépetl (Mexique): structure, evolution pétrologique et risques. Bull Volcanol 47: 1–23 (in French).

Robin C, Eissen JP, Samaniego P, Martin H, Hall M, Cotten J (2009). Evolution of the late Pleistocene Mojanda-Fuya Fuya volcanic complex (Ecuador), by progressive adakitic involvement in mantle magma sources. Bull Volcanol 71: 233–258.

Rodríguez C, Sellés D, Dungan M, Langmuir C, Leeman W (2007). Adakitic dacites formed by intracrustal crystal fractionation of water-rich parent magmas at Nevado de Longaví volcano (36.2°S; Andean southern volcanic zone, central Chile). J Petrol 18: 2033–2061.

Rogers NW, Setterfield TN (1994). Potassium and incompatible-element enrichment in shoshonitic lavas from the Tavua volcano, Fiji. Chem Geol 118: 43–62.

Rollinson HR (1993). Using Geochemical Data: Evaluation, Presentation, Interpretation. Essex, UK: Longman Scientific Technical.

Romick JD, Perfit MR, Swanson SE, Shuster RD (1990). Magmatism in the eastern Aleutian arc: temporal characteristic of igneous activity on Akutan Island. Contrib Mineral Petrol 104: 700–721.

Rotolo SG, Castorina F (1998). Transition from mildly-tholeiitic to calc-alkaline suite: the case of Chicontepec volcanic centre, El Salvador, Central America. J Volcanol Geotherm Res 86: 117–136.

Rueda H, Macías JL, Arce JL, Gardner JE, Layer PW (2013). The ~ 31 ka rhyolitic Plinian to sub-Plinian eruption of Tlaloc Volcano, Sierra Nevada, central Mexico. J Volcanol Geotherm Res 252: 73–91.

Russo RM, Silver PG (1994). Trench parallel flow beneath the Nazca plate from seismic anisotropy. Science 263: 1105–1111.

Ryder CH, Gill JB, Tepley F 3rd, Ramos F, Reagan M (2006). Closed-to open-system differentiation at Arenal volcano (1968-2003). J Volcanol Geotherm Res 157: 75–93.

Sakuyama M, Nesbitt RW (1986). Geochemistry of the Quaternary volcanic rocks of the Northeast Japan arc. J Volcanol Geotherm Res 29: 413–450.

Samaniego P, Le Pennec JL, Robin C, Hidalgo S (2011). Petrological analysis of the pre-eruptive magmatic process prior to the 2006 explosive eruptions at Tungurahua volcano (Ecuador). J Volcanol Geotherm Res 199: 69–84.

Samaniego P, Martin H, Monzier M, Robin C, Fornari M, Eissen JP, Cotten J (2005). Temporal evolution of magmatism in the northern volcanic zone of the Andes: the geology and petrology of Cayambe volcanic complex (Ecuador). J Petrol 46: 2225–2252.

Schaaf P, Stimac J, Siebe C, Macías JL (2005). Geochemical evidence for mantle origin and crustal processes in volcanic rocks from Popocatépetl and surrounding monogenetic volcanoes, central Mexico. J Petrol 46: 1243–1282.

Schuth S, Rohrbach A, Münker C, Ballhaus C, Garbe-Schönberg D, Qopoto C (2004). Geochemical constraints on the petrogenesis of arc picrites and basalts, New Georgia group, Solomon Islands. Contrib Mineral Petrol 148: 288–304.

Sendjaja YA, Kimura JI, Sunardi E (2009). Across-arc geochemical variation of Quaternary lavas in west Java, Indonesia: mass-balance elucidation using arc basalt simulator model. Island Arc 18: 201–224.

Sheth HC (2008). Do major oxide tectonic discrimination diagrams work? Evaluating new log-ratio and discriminant-analysis-based diagrams with Indian Ocean mafic volcanics and Asian ophiolites. Terra Nova 20: 229–236.

Sheth HC, Torres-Alvarado IS, Verma SP (2000). Beyond subduction and plumes: a unified tectonic-petrogenetic model for the Mexican Volcanic Belt. Int Geol Rev 42: 1116–1132.

Sheth HC, Torres-Alvarado IS, Verma SP (2002). What is the "calc-alkaline rock series"? Int Geol Rev 44: 686–701.

Shinjo R, Woodhead JD, Hergt JM (2000). Geochemical variation within the northern Ryukyu: magma source compositions and geodynamic implications. Contrib Mineral Petrol 140: 263–282.

Shukuno H, Tamura Y, Tani K, Chang Q, Suzuki T, Fiske RS (2006). Origin of silicic magmas and the compositional gap at Sumisu submarine caldera, Izu-Bonin arc, Japan. J Volcanol Geotherm Res 156: 187–216.

Siebe C, Rodríguez-Lara V, Schaaf P, Abrams M (2004). Geochemistry, Sr-Nd isotope composition, and tectonic setting of Holocene Pelado, Guespalapa and Chichinautzin scoria cones, south of Mexico City. J Volcanol Geotherm Res 130: 197–226.

Siebe C, Schaaf P, Urrutia-Fucugauchi J (1999). Mammoth bones embedded in a late Plesitocene lahar from Popocatépetl volcano, near Tocuila, central México. Geol Soc Am Bull 111: 1550–1562.

Siebert L, Carrasco-Núñez G (2002). Late-Pleistocene to precolumbian behind-the-arc mafic volcanism in the eastern Mexican Volcanic Belt; implications for future hazards. J Volcanol Geotherm Res 115: 179–205.

Silva Mora L (1988). Algunos aspectos de los basaltos y andesitas cuaternarias de Michoacán Oriental. Rev Inst Geol UNAM 7: 89–96 (in Spanish).

Singer BS, Smith KE, Jicha BR, Beard BL, Johnson CM, Rogers NW (2011). Tracking open-system differentiation during growth of Santa María volcano, Guatemala. J Petrol 52: 2335–2363.

Singh SK, Ordaz M, Pacheco JF, Alcántara L, Iglesias A, Alcocer S, García D, Pérez-Campos X, Valdes C, Almora D (2007). A report on the Atoyac, Mexico, earthquake of 13 April 2007 (M 5.9). Seismol Res Lett 78: 635–648.

Singh SK, Pardo M (1993). Geometry of the Benioff zone and state of stress in the overriding plate in central Mexico. Geophys Res Lett 20: 1483–1486.

Singh SK, Ponce L, Nishenko SP (1985). The great Jalisco, Mexico earthquakes of 1932: subduction of the Rivera plate. Bull Seismol Soc Am 75: 1301–1313.

Smith EI, Sánchez A, Walker JD, Wang K (1999). Geochemistry of mafic magmas in the Hurricane Volcanic Field, Utah: implications of small- and large-scale chemical variability of the lithospheric mantle. J Geol 107: 433–448.

Smith IEM, Stewart RB, Price RC (2003). The petrology of a large intra-oceanic silicic eruption: the Sandy Bay tephra, Kermadec arc, southwest Pacific. J Volcanol Geotherm Res 124: 173–194.

Smith IEM, Worthington TJ, Price RC, Stewart RB, Maas R (2006). Petrogenesis of dacite in an oceanic subduction environment: Raoul Island, Kermadec arc. J Volcanol Geotherm Res 156: 252–265.

Smith TE, Thirlwall M, Holm PE, Harris MJ (2004). Petrogenesis of orthopyroxene- and amphibole-bearing andesites, Mustique, Grenadine Islands, Lesser Antilles arc: isotope, trace element and physical constraints. Island Arc 13: 73–94.

Srivastava RK, Samal AK, Gautam GC (2015). Geochemical characteristics and petrogenesis of four Palaeoproterozoic mafic dike swarms and associated large igneous provinces from the eastern Dharwar craton, India. Int Geol Rev 57: 1460–1482.

Stolz AJ, Varne R, Davies GR, Wheller GE, Fodon JD (1990). Magma source components in an arc-continent collision zone: the Flores-Lembata sector, Sunda arc, Indonesia. Contrib Mineral Petrol 105: 585–601.

Straub SM, LaGatta AB, Martin-Del Pozzo AL, Langmuir CH (2008). Evidence from high-Ni olivines for a hybridized peridotite/pyroxenite source for orogenic andesites from the central Mexican Volcanic Belt. Geochem Geophys Geosys 9: Q03007.

Straub SM, Martin-Del Pozzo AL (2001). The significance of phenocryst diversity in tephra from recent eruptions at Popocatépetl volcano (central Mexico). Contrib Mineral Petrol 140: 487–510.

Suarez G, Singh SK (1986). Tectonic interpretation of the Trans-Mexican Volcanic Belt—discussion. Tectonophysics 127: 155–160.

Sun SS, McDonough WF (1989). Chemical and isotopic systematics of oceanic basalts: implications for mantle composition and processes. In: Saunders AD, Norry MJ, editors. Magmatism in the Ocean Basins. London, UK: Geological Society Special Publication, pp. 313–345.

Sussman D (1985). Apoyo caldera, Nicaragua: a major Quaternary silicic eruptive center. J Volcanol Geotherm Res 24: 249–282.

Suter M, Carrillo Martínez M, López Martínez M, Farrar E (1995a). The Aljibes half-graben - active extension at the boundary between the Trans-Mexican Volcanic Belt and the basin and range province, Mexico. Geol Soc Am Bull 107: 627–641.

Suter M, López Martínez M, Quintero Legorreta O, Carrillo Martínez M (2001). Quaternary intra-arc extension in the central Trans-Mexican Volcanic Belt. Geol Soc Am Bull 113: 693–703.

Suter M, Quintero O, Johnson CA (1992). Active faults and state of stress in the central part of the Trans-Mexican Volcanic Belt, Mexico. 1. The Venta de Bravo fault. J Geophys Res 97: 11983–11993.

Suter M, Quintero-Legorreta O, López-Martínez M, Aguirre-Díaz G, Farrar E (1995b). The Acambay graben: active intraarc extension in the Trans-Mexican Volcanic Belt, Mexico. Tectonics 14: 1245–1262.

Swinamer RT (1989). The geomorphology, petrography, geochemistry and petrogenesis of the volcanic rocks in the Sierra del Chichinautzin, Mexico. MSc, Queen's University, Kingston, ON, Canada.

Takanashi K, Shuto K, Sato M (2011). Origin of Late Paleogene to Neogene basalts and associated coeval felsic volcanic rocks in southwest Hokkaido, northern NE Japan arc: constraints from Sr and Nd isotopes and major- and trace-element chemistry. Lithos 125: 368–392.

Tamura Y, Tani K, Ishizuka O, Chang Q, Shukuno H, Fiske RS (2005). Are arc basalts dry, wet, or both? Evidence from the Sumisu caldera volcano, Izu–Bonin arc, Japan. J Petrol 46: 1769–1803.

Tamura Y, Yuhara M, Ishii T, Irino N, Shukuno H (2003). Andesites and dacites from Daisen volcano, Japan: partial-to-total remelting of an andesite magma body. J Petrol 44: 2243–2260.

Tatsumi Y, Murasaki M, Arsadi EM, Nohda S (1991). Geochemistry of Quaternary lavas from NE Sulawesi: transfer of subduction components into the mantle wedge. Contrib Mineral Petrol 107: 137–149.

Tatsumi Y, Murasaki M, Nohda S (1992). Across-arc variation of lava chemistry in the Izu-Bonin arc: identification of subduction components. J Volcanol Geotherm Res 49: 179–190.

Tatsumi Y, Takahashi T, Hirahara Y, Chang Q, Miyazaki T, Kimura JI, Ban M, Sakayori A (2008). New insights into andesite genesis: the role of mantle-derived calc-alkalic and crust-derived tholeiitic melts in magma differentiation beneath Zao volcano, NE Japan. J Petrol 49: 1971–2008.

Temizel I, Arslan M, Ruffet G, Peucat JJ (2012). Petrochemistry, geochronology and Sr-Nd isotopic systematics of the Tertiary collisional and post-collisional volcanic rocks from the Ulubey (Ordu) area, eastern Pontide, NE Turkey: implications for extension-related origin and mantle source characteristics. Lithos 128: 126–147.

Tera F, Brown L, Morris J, Sacks IS, Klein J, Middleton R (1986). Sediment incorporation in island-arc magmas: inferences from ^{10}Be. Geochim Cosmochim Acta 50: 535–550.

Thirlwall MF, Graham AM (1984). Evolution of high-Ca, high-Sr C-series basalts from Grenada, Lesser Antilles: the effects of intra-crustal contamination. J Geol Soc London 141: 427–445.

Thirlwall MF, Graham AM, Arculus RJ, Harmon RS, Macpherson CG (1996). Resolution of the effects of crustal assimilation, sediment subduction, and fluid transport in island arc magmas: Pb-Sr-Nd-O isotope geochemistry of Grenada, Lesser Antilles. Geochim Cosmochim Acta 60: 4785–4810.

Timm C, Hoernle K, Bogaard PVD, Bindeman I, Weaver S (2009). Geochemical evolution of intraplate volcanism at Banks Peninsula, New Zealand: interaction between asthenospheric and lithospheric melts. J Petrol 50: 989–1023.

Tormey DR, Hickey-Vargas R, Frey FA, López-Escobar L (1991). Recent lavas from the Andean volcanic front (33 to 42°S); interpretations of along-arc compositional variations. In: Harmon RS , Rapela CW, editors. Andean Magmatism and Its Tectonic Setting. Boulder, CO, USA: Geological Society of America Special Paper, pp. 57–77.

Torres-Alvarado IS, Smith AD, Castillo-Roman J (2011). Sr, Nd and Pb isotopic and geochemical constraints for the origin of magmas in Popocatépetl volcano (central Mexico) and their relationship with the adjacent volcanic fields. Int Geol Rev 53: 84–115.

Torres-Alvarado IS, Verma SP (2003). Discussion and reply: Neogene volcanism at the front of the central Mexican Volcanic Belt: basaltic andesites to dacites, with contemporaneous shoshonites and high-TiO_2 lava. Geol Soc Am Bull 115: 1020–1024.

Torres-Alvarado IS, Verma SP, Palacios-Berruete H, Guevara M, González-Castillo OY (2003). DC_Base: a database system to manage Nernst distribution coefficients and its application to partial melting modeling. Comput Geosci 29: 1191–1198.

Torres-Alvarado IS, Verma SP, Velasco-Tapia F (2002). Comment: "Generation of oceanic-island basalt type volcanism in the western Trans-Mexican volcanic belt by slab rollback, asthenosphere infiltration, and variable flux melting". Geology 30: 857–858.

Trumbull RB, Wittenbrink R, Hahne K, Emmermann R, Büsch W, Gerstenberger H, Siebel W (1999). Evidence for Late Miocene to Recent contamination of arc andesites by crustal melts in the Chilean Andes (25-26°S) and its geodynamic implications. J South Am Earth Sci 12: 135–155.

Turner S, Foden J (2001). U, Th and Ra disequilibria, Sr, Nd and Pb isotope and trace element variations in Sunda arc lavas: predominance of a subducted sediment component. Contrib Mineral Petrol 142: 43–57.

Turner S, Hawkesworth C, Liu J, Rogers N, Kelley S, Calsteren PV (1993). Timing of Tibetan uplift constrained by analysis of volcanic rocks. Nature 364: 50–54.

Turner S, Hawkesworth CJ, Calsteren PV, Heath E, Macdonald R, Black S (1996). U-series isotopes and destructive plate margin magma genesis in the Lesser Antilles. Earth Planet Sci Lett 142: 191–207.

UNAM and CENAPRED Seismology Group (1995). The Milpa Alta earthquake of January 21, 1995. Geofís Int 34: 355–362.

van Bergen MJ, Vroon PZ, Varekamp JC, Poorter RPE (1992). The origin of the potassic rock suite from Batu Tara volcano (East Sunda arc, Indonesia). Lithos 28: 261–282.

Varol E, Alpaslan M (2012). Quaternary basaltic volcanism reflecting heterogeneous mixture of two mafic melts: Gölova basaltic rocks, Southern Anatolia, Turkey. Geochem Int 50: 63–73.

Velasco-Tapia F (2014). Multivariate analysis, mass balance techniques, and statistical tests as tools in igneous petrology: application to the Sierra de las Cruces Volcanic Range (Mexican Volcanic Belt). The Scientific World Journal 2014: 793236.

Velasco-Tapia F, Rodríguez-Saavedra P, Márquez A, Navarro de León I, De Ignacio C, Marroquín Guerra SG, Quintanilla-Garza J, Rangel-Álvarez OM (2013). Mineralogical and geochemical evidence of magma mingling/mixing in the Sierra de Las Cruces volcanic range, Mexican Volcanic Belt. J Iber Geol 39: 147–166.

Velasco-Tapia F, Verma SP (2001a). Estado actual de la investigación geoquímica en el campo monogenético de la Sierra de Chichinautzin: análisis de información y perspectivas. Rev Mex Cienc Geol 18: 1–36 (in Spanish).

Velasco-Tapia F, Verma SP (2001b). First partial melting inversion model for a rift-related origin of the Sierra de Chichinautzin volcanic field, central Mexican Volcanic Belt. Int Geol Rev 43: 788–817.

Velasco-Tapia F, Verma SP (2013). Magmatic processes at the volcanic front of Central Mexican Volcanic Belt: Sierra de Chichinautzin volcanic field (Mexico). Turk J Earth Sci 22: 32–60.

Vergara M, López-Escobar L, Cancino A, Levi B (1991). The Pichidangui formation; Some geochemical characteristics and tectonic implications of the Triassic marine volcanism in central Chile (31°55' to 32°20'S). GSA Special Papers 265: 93–98.

Vergara M, López-Escobar L, Palma JL, Hickey-Vargas R, Roeschmann C (2004). Late Tertiary volcanic episodes in the area of the city of Santiago de Chile: new geochronological and geochemical data. J South Am Earth Sci 17: 227–238.

Verma SK, Oliveira EP (2013). Application of multi-dimensional discrimination diagrams and probability calculations to Paleoproterozoic acid rocks from Brazilian cratons and provinces to infer tectonic settings. J South Am Earth Sci 45: 117–146.

Verma SK, Oliveira EP (2015). Tectonic setting of basic igneous and metaigneous rocks of Borborema Province, Brazil using multi-dimensional geochemical discrimination diagrams. J South Am Earth Sci 58: 309–317.

Verma SK, Oliveira EP, Verma SP (2015). Plate tectonic settings for Precambrian basic rocks from Brazil by multi-dimensional tectonomagmatic discrimination diagrams and their limitations. Int Geol Rev 57: 1564–1579.

Verma SK, Pandarinath K, Verma SP (2012). Statistical evaluation of tectonomagmatic discrimination diagrams for granitic rocks and proposal of new discriminant-function-based multi-dimensional diagrams for acid rocks. Int Geol Rev 54: 325–347.

Verma SK, Verma SP (2013). Identification of Archaean plate tectonic processes from multidimensional discrimination diagrams and probability calculations. Int Geol Rev 55: 225–248.

Verma SP (1983). Magma genesis and chamber processes at Los Humeros caldera, Mexico - Nd and Sr isotope data. Nature 301: 52–55.

Verma SP (1987). Mexican Volcanic Belt: present state of knowledge and unsolved problems. Geofís Int 26: 309–340.

Verma SP (1991a). Determination of thirteen rare-earth elements by high-performance liquid chromatography in thirty and of K, Rb, Cs, Sr and Ba by isotope dilution mass spectrometry in eighteen international geochemical reference samples. Geostand Newslett 15: 129–134.

Verma SP (1991b). Usefulness of liquid chromatography for determination of thirteen rare-earth elements in rocks and minerals. Lanth Actin Res 3: 237–257.

Verma SP (1992). Seawater alteration effects on REE, K, Rb, Cs, Sr, U, Th, Pb, and Sr- Nd-Pb isotope systematics of mid-ocean ridge basalt. Geochem J 26: 159–177.

Verma SP (1999). Geochemistry of evolved magmas and their relationship to subduction-unrelated mafic volcanism at the volcanic front of the central Mexican Volcanic Belt. J Volcanol Geotherm Res 93: 151–171.

Verma SP (2000a). Geochemistry of the subducting Cocos plate and the origin of subduction-unrelated mafic volcanism at the volcanic front of the central Mexican Volcanic Belt. In: Delgado-Granados H, Aguirre-Díaz G, Stock JM, Editors, Cenozoic Tectonics and Volcanism of Mexico. Boulder, CO, USA: Geological Society of America, pp. 195–222.

Verma SP (2000b). Geochemical evidence for a lithospheric source for magmas from Los Humeros caldera, Puebla, Mexico. Chem Geol 164: 35–60.

Verma SP (2001a). Geochemical evidence for a lithospheric source for magmas from Acoculco caldera, Eastern Mexican Volcanic Belt. Int Geol Rev 43: 31–51.

Verma SP (2001b). Geochemical and Sr-Nd-Pb isotopic evidence for a combined assimilation and fractional crystallisation process for volcanic rocks from the Huichapan caldera, Hidalgo, Mexico. Lithos 56: 141–164.

Verma SP (2001c). Geochemical evidence for a rift-related origin of bimodal volcanism at Meseta Río San Juan, North-Central Mexican volcanic belt. Int Geol Rev 43: 475–493.

Verma SP (2002). Absence of Cocos plate subduction-related basic volcanism in southern Mexico: a unique case on Earth? Geology 30: 1095–1098.

Verma SP (2003). Geochemical and Sr-Nd isotopic evidence for a rift-related origin of magmas in Tizayuca volcanic field, Central Mexican Volcanic Belt. J Geol Soc India 61: 257–276.

Verma SP (2004). Solely extension-related origin of the eastern to west-central Mexican Volcanic Belt (Mexico) from partial melting inversion model. Current Science 86: 713–719.

Verma SP (2005). Estadística Básica para el Manejo de Datos Experimentales: Aplicación en la Geoquímica (Geoquimiometría). Mexico City, Mexico: Universidad Nacional Autónoma de México (in Spanish).

Verma SP (2006). Extension-related origin of magmas from a garnet-bearing source in the Los Tuxtlas volcanic field, Mexico. Int J Earth Sci 95: 871–901.

Verma SP (2009). Continental rift setting for the central part of the Mexican Volcanic Belt: a statistical approach. Open Geology Journal 3: 8–29.

Verma SP (2010). Statistical evaluation of bivariate, ternary and discriminant function tectonomagmatic discrimination diagrams. Turk J Earth Sci 19: 185–238.

Verma SP (2012a). Geochemometrics. Rev Mex Cienc Geol 29: 276–298.

Verma SP (2012b). Application of multi-dimensional discrimination diagrams and probability calculations to acid rocks from Portugal and Spain. Comunicações Geológicas 99: 79–93.

Verma SP (2013). Application of 50 multi-dimensional discrimination diagrams and significance tests to decipher compositional similarities and differences between Hawaiian and Icelandic volcanism. Int Geol Rev 55: 1553–1572.

Verma SP (2015a). Origin, evolution, and tectonic setting of the eastern part of the Mexican Volcanic Belt and comparison with the Central American Volcanic Arc from conventional multielement normalised and new multidimensional discrimination diagrams and discordancy and significance tests. Turk J Earth Sci 24: 111–164.

Verma SP (2015b). Monte Carlo comparison of conventional ternary diagrams with new log-ratio bivariate diagrams and an example of tectonic discrimination. Geochem J 49: 393–412.

Verma SP, Agrawal S (2011). New tectonic discrimination diagrams for basic and ultrabasic volcanic rocks through log-transformed ratios of high field strength elements and implications for petrogenetic processes. Rev Mex Cienc Geol 28: 24–44.

Verma SP, Aguilar-Y-Vargas VH (1988). Bulk chemical composition of magmas in the Mexican Volcanic Belt (Mexico) and inapplicability of generalized arc-models. Chem Erde 48: 203–221.

Verma SP, Armstrong-Altrin JS (2013). New multi-dimensional diagrams for tectonic discrimination of siliciclastic sediments and their application to Precambrian basins. Chem Geol 355: 117–133.

Verma SP, Besch T, Guevara M, Schulz-Dobrich B (1992). Determination of twelve trace elements in twenty-seven and ten major elements in twenty-three geochemical reference samples by X-Ray fluorescence spectrometry. Geostand Newslett 16: 301–309.

Verma SP, Carrasco-Núñez G (2003). Reappraisal of the geology and geochemistry of Volcán Zamorano, central Mexico: implications for discriminating the Sierra Madre Occidental and Mexican Volcanic Belt provinces. Int Geol Rev 45: 724–752.

Verma SP, Carrasco-Núñez G, Milán M (1991). Geology and geochemistry of Amealco caldera, Qro., Mexico. J Volcanol Geotherm Res 47: 105–127.

Verma SP, Cruz-Huicochea R (2013). Alternative approach for precise and accurate Student´s t critical values and application in geosciences. J Iber Geol 39: 31–56.

Verma SP, Cruz-Huicochea R, Díaz-González L (2013a). Univariate data analysis system: deciphering mean compositions of island and continental arc magmas, and influence of underlying crust. Int Geol Rev 55: 1922–1940.

Verma SP, Cruz-Huicochea R, Díaz-González L, Vema SK (2015a). A new computer program TecDIA for multidimensional tectonic discrimination of intermediate and acid magmas and its application to the Bohemian Massif, Czech Republic. J Geosci (in press).

Verma SP, Díaz-González L (2012). Application of the discordant outlier detection and separation system in the geosciences. Int Geol Rev 54: 593–614.

Verma SP, Guevara M, Agrawal S (2006). Discriminating four tectonic settings: five new geochemical diagrams for basic and ultrabasic volcanic rocks based on log-ratio transformation of major-element data. J Earth Syst Sci 115: 485–528.

Verma SP, Guevara M, Besch T, Schulz-Dobrich B (1993b). Elementos traza y mayores en muestras internacionales de referencia geoquímica por espectrometría de rayos-X. Geofís Int 32: 311–319.

Verma SP, Hasenaka T (2004). Sr, Nd, and Pb isotopic and trace element geochemical contraints for a veined-mantle source of magmas in the Michoacán-Guanajuato volcanic field, west-central Mexican Volcanic Belt. Geochem J 38: 43–65.

Verma SP, Luhr JF (2010). Sr, Nd, and Pb isotopic evidence for the origin and evolution of the Cántaro-Colima Volcanic Chain, Western Mexican Volcanic Belt. J Volcanol Geotherm Res 197: 33–51.

Verma SP, Nelson SA (1989). Isotopic and trace element constraints on the origin and evolution of alkaline and calc-alkaline magmas in the northwestern Mexican Volcanic Belt. J Geophys Res 94: 4531–4544.

Verma SP, Pandarinath K, Verma SK, Agrawal S (2013b). Fifteen new discriminant-function-based multi-dimensional robust diagrams for acid rocks and their application to Precambrian rocks. Lithos 168-169: 113–123.

Verma SP, Quiroz-Ruiz A (2008). Critical values for 33 discordancy test variants for outliers in normal samples of very large sizes from 1,000 to 30,000 and evaluation of different regression models for the interpolation of critical values. Rev Mex Cienc Geol 25: 369–381.

Verma SP, Quiroz-Ruiz A (2011). Corrigendum to Critical values for 22 discordancy test variants for outliers in normal samples up to sizes 100, and applications in science and engineering [Rev. Mex. Cienc. Geol., 23 (2006), 302-319]. Rev Mex Cienc Geol 28: 202.

Verma SP, Quiroz-Ruiz A, Díaz-González L (2008). Critical values for 33 discordancy test variants for outliers in normal samples up to sizes 1000, and applications in quality control in Earth Sciences. Rev Mex Cienc Geol 25: 82–96.

Verma SP, Rivera-Gómez MA (2013a). New computer program TecD for tectonomagmatic discrimination from discriminant function diagrams for basic and ultrabasic magmas and its application to ancient rocks. J Iber Geol 39: 167–179.

Verma SP, Rivera-Gómez MA (2013b). Computer programs for the classification and nomenclature of igneous rocks. Episodes 36: 115–124.

Verma SP, Salazar-V A, Negendank JFW, Milán M, Navarro-L I, Besch T (1993a). Características petrográficas y geoquímicas de elementos mayores del campo volcánico de Los Tuxtlas, Veracruz, México. Geofís Int 32: 237–248 (in Spanish).

Verma SP, Torres-Alvarado IS, Satir M, Dobson PF (2005). Hydrothermal alteration effects in geochemistry and Sr, Nd, Pb, and O isotopes of magmas from the Los Azufres geothermal field (Mexico): a statistical approach. Geochem J 39: 141–163.

Verma SP, Torres-Alvarado IS, Sotelo-Rodríguez ZT (2002). SINCLAS: Standard igneous norm and volcanic rock classification system. Comput Geosci 28: 711–715.

Verma SP, Torres-Alvarado IS, Velasco-Tapia F (2003). A revised CIPW norm. Schweiz Miner Petrog Mitteil 83: 197–216.

Verma SP, Verma SK (2013). First 15 probability-based multi-dimensional discrimination diagrams for intermediate magmas and their robustness against post-emplacement compositional changes and petrogenetic processes. Turk J Earth Sci 22: 931–995.

Verma SP, Verma SK, Oliveira EP (2015b). Application of 55 multi-dimensional tectonomagmatic discrimination diagrams to Precambrian belts. Int Geol Rev 57: 1363–1386.

Verma SP, Verma SK, Pandarinath K, Rivera-Gómez MA (2011). Evaluation of recent tectonomagmatic discrimination diagrams and their application to the origin of basic magmas in Southern Mexico and Central America. Pure Appl Geophys 168: 1501–1525.

Vezzoli L, Tibaldi A, Renzulli A, Menna M, Flude S (2008). Faulting-assisted lateral collapses and influence on shallow magma feeding system at Ollague volcano (Central Volcanic Zone, Chile-Bolivia Andes). J Volcanol Geotherm Res 171: 137–159.

von Huene R (1989). The Middle America convergent plate boundary, Guatemala. In: Winterer EL, Hussong DM , Decker RW, editors. The Eastern Pacific Ocean and Hawaii. Boulder, CO, USA: Geological Society of America, pp. 535–550.

Wade JA, Plank T, Stern RJ, Tollstrup DL, Gill JB, O'Leary JC, Eiler JM, Moore RB, Woodhead JD, Trusdell F et al. (2005). The May 2003 eruption of Anatahan volcano, Mariana Islands: geochemical evolution of a silicic island-arc volcano. J Volcanol Geotherm Res 146: 139–170.

Walker JA, Carr MJ, Feigenson MD, Kalamarides RI (1990). The petrogenetic significance of interstratified high- and low-Ti basalts in central Nicaragua. J Petrol 31: 1141–1164.

Walker JA, Patino LC, Cameron BI, Carr MJ (2000). Petrogenetic insights provided by compositional transects across the Central American arc: southeastern Guatemala and Honduras. J Geophys Res 105: 18949–18963.

Walker JA, Patino LC, Carr MJ, Feigenson MD (2001). Slab control over HFSE depletions in central Nicaragua. Earth Planet Sci Lett 192: 533–543.

Walker JA, Teipel AP, Ryan JG, Syracuse E (2009). Light elements and Li isotopes across the northern portion of the Central American subduction zone. Geochem Geophys Geosys 10: 1–23.

Wallace PJ, Carmichael ISE (1999). Quaternary volcanism near the Valley of Mexico: implications for subduction zone magmatism and the effects of crustal thickness variations on primitive magma compositions. Contrib Mineral Petrol 135: 291–314.

Wassmer P, Geissert D, De Fraipont N, Enríquez-Fernandez E (2004). Morphological evolution of la Concepción Valley by huge mass movements on plateau edges in the Eastern part of the Mexican Volcanic Belt (Xalapa, Veracruz, Mexico). Acta Vulcanol 16: 125–132.

Witter JB, Kress VC, Newhall CG (2005). Volcán Popocatépetl, Mexico. Petrology, magma mixing, and immediate sources of volatiles for the 1994—Present eruption. J Petrol 46: 2337–2366.

Woodhead JD (1988). The origin of geochemical variations in Mariana lavas: a general model for petrogenesis in intra-oceanic island arcs. J Petrol 29: 805–830.

Yang T, Grand SP, Wilson DS, Guzman-Speziale M, Gomez-Gonzalez JM, Dominguez-Reyes T, Ni J (2009). Seismic structure beneath the Rivera subduction zone from finite-frequency seismic tomography. J Geophys Res 114: B01302.

Zaid SM (2015a). Geochemistry of sandstones from the Pliocene Gabir Formation, north Marsa Alam, Red Sea, Egypt: Implication for provenance, weathering and tectonic setting. J Afr Earth Sci 102: 1–17.

Zaid SM (2015b). Integrated petrographic, mineralogical, and geochemical study of the Late Cretaceous-Early Tertiary Dakhla shales, Quseir–Nile Valley Province, central Egypt: implications for source area weathering, provenance, and tectonic setting. Arabian Journal of Geosciences (in press).

Zaid SM, Elbadry O, Ramadan Z, Mohamed M (2015). Petrography and geochemistry of Pharaonic sandstone monuments in Tall San Al Hagr, Al Sharqiya Governorate, Egypt: implications for provenance and tectonic setting. Turk J Earth Sci 24: 344–364.

Zaid SM, Gahtani FA (2015). Provenance, diagenesis, tectonic setting, and geochemistry of Hawkesbury Sandstone (Middle Triassic), southern Sydney Basin, Australia. Turk J Earth Sci 24: 72–98.

Zellmer GF, Hawkesworth CJ, Sparks RSJ, Thomas LE, Harford CL, Brewer TS, Loughlin SC (2003). Geochemical evolution of the Soufrière Hills volcano, Montserrat, Lesser Antilles volcanic arc. J Petrol 44: 1349–1374.

Zhang M, Suddaby P, Thompson RN, Thirlwall MF, Menzies MA (1995). Potassic volcanic rocks in NE China: geochemical constraints on mantle source and magma genesis. J Petrol 36: 1275–1303.

Zhao Z, Mo X, Dilek Y, Niu Y, DePaolo DJ, Robinson P, Zhu D, Sun C, Dong G, Zhou S et al. (2009). Geochemical and Sr-Nd-O isotopic compositions of the post-collisional ultrapotassic magmatism in SW Tibet: Petrogenesis and implications for India intra-continental subduction beneath southern Tibet. Lithos 113: 190–212.

Zheng YC, Hou ZQ, Li QY, Sun QZ, Liang W, Fu Q, Li W, Huang KX (2012). Origin of Late Oligocene adakitic intrusives in the southeastern Lhasa terrane: evidence from in situ zircon U–Pb dating, Hf–O isotopes, and whole-rock geochemistry. Lithos 148: 296–311.

Zhidan Z, Xuanxue M, Shuangquan Z, Tieying G, Su Z, Guochen D, Yong W (2001). Post-collisional magmatism in Wuyu basin, central Tibet: evidence for recycling of subducted Tethyan oceanic crust. Science in China (Series D) 44: 27–34.